PREDICTING THE TIME RELATED GENERATION OF ACID ROCK DRAINAGE FROM MINE WASTE: A COPPER CASE STUDY

NATHAN N SIMUNIKA

DECEMBER 2013

Dissertation in fulfilment of the degree of Master of Science in Chemical Engineering

"I know the meaning of plagiarism and declare that all the work in this document, save for that which is properly acknowledged, is my own"

6th May 2014

Synopsis

The mining and beneficiation of coal and hard rock ores generates large volumes of sulphidic waste that may oxidise in the presence of oxygen and result in the generation of acid rock drainage (ARD). In order to effectively manage the long term effects of ARD, there is a need to reliably quantify the associated impacts and how these impacts evolve with time. Traditional laboratory-scale tests only provide a partial picture of ARD generation, and their extrapolation to full-scale deposits is highly uncertain and controversial. This has prompted the development of mathematical models which take into account the governing chemical reaction and physical transport mechanisms. Whilst the accurate and reliable quantification of the time-related ARD profiles requires rigorous mechanistic modeling of both the (bio) chemical reaction and physical transport mechanisms under non-ideal flow conditions, advanced models are complex and only suitable for site-specific studies and operational decision-making contexts. However, in the early stage screening of waste for potential environmental impacts, simple geochemical mass transport models such as PHREEQC can be used. PHREEQC V.2 has capabilities to simulate a wide range of processes that include equilibrium controlled reactions, kinetically controlled reactions and 1-D advective-dispersion transport, and has been used in a wide range of geochemical applications. However, despite its capabilities, little has been published on its applications to ARD prediction. This study focused on the development and application of a PHREEQC based predictive modeling tool, suitable for the early or screening evaluation of the potential long-term ARD risks associated with sulphidic waste deposits.

The research methodology was essentially conducted in four stages namely, model development, model calibration, model validation and model sensitivity analysis. Model development entailed identification of controlling mechanisms and influencing parameters, collection of model input data and extension of the input database. This was based on a comprehensive review and assessment of the chemical, physical and biological mechanisms governing ARD generation from a typical copper sulphide waste, as well as the modelling philosophy, relevant assumptions, limitations and input requirements of the PHREEQC code. Key chemical reactions identified and incorporated into the model included oxidation of sulphide minerals, acid dissolution of carbonate and silicate minerals, and the formation of secondary sulphate, hydroxysulphate and oxyhydroxide precipitates. Due to the limitations of PHREEQC code, simplifying assumptions were made to represent some of the physical transport processes. More specifically, transport was assumed to occur only in 1-D while oxygen and carbon dioxide were assumed to be dissolved in the aqueous phase.

Furthermore, heat was assumed to be distributed uniformly and the catalytic effect of microorganisms on iron and sulphur oxidation was accounted for by assuming a highly oxidising environment in the column. These processes were combined and formulated into a modelling framework using the basic language program imbedded in the input file of PHREEQC code. Subsequent model calibration and validation steps were based on datasets obtained from a laboratory-scale column bioleaching experimental program carried out on low grade copper sulfide ore over the period 2004 to 2006 through the Australian Minerals Industry Research Association (AMIRA project P768A). In the P768A study, columns (0.5 and 1.5 m in height, and containing approximately 4kg and 36kg of crushed ore respectively) were operated in a recycle mode at a feed pH of 1.5 and temperature of 40^{o}C for periods of between 80 and 273 days. Although specifically designed for simulating a heap bioleach process for copper recovery, the leach scenario can be correlated with ARD generation from a waste rock pile under worse case conditions i.e. conditions which promote microbial activity and sulphide oxidation. Model calibration was conducted to address uncertainties associated with the accuracy and reliability of key model input data, specifically mineral surface areas and nature of the precipitating secondary minerals. Model validation was subsequently carried out to assess its predictive capability, using an independent dataset. Finally, model sensitivity analysis was conducted to assess the sensitivity of the model output to changes in key model input parameters, namely pyrite content, calcite content and liquid flow velocity.

Generally, a good correlation was observed between the simulated and measured data, which can be partly attributed to the recycling of the leach solution during the column leach experiments. Some discrepancies were, however, observed in the early leach stages, and have been attributed to the rapid dissolution of fines and metal oxides (on mineral surfaces) during acid agglomeration of the ore prior to column leaching. Under the specific test conditions investigated, leachate quality was found to be controlled by both kinetic and equilibrium reaction mechanisms. In particular, the formation of secondary precipitates, jarosite and gypsum, was found to have a significant effect on pH and soluble concentrations of calcium, iron and, to a lesser extent, potassium. Kinetically-controlled acid dissolution of calcite was found to result in an increase in pH in the early leach stages. After depletion of the calcite, slow dissolution of biotite and K-feldspar buffered the pH at a constant value of approximately 2.

In conclusion, this study has shown that equilibrium, kinetic and 1-D transport processes can be combined into a PHREEQC-based modeling framework to simulate the main geochemical processes governing the generation of ARD in mine waste.

Such a model can provide reasonably accurate estimates of the time-related concentration profiles of key elements under continuous flow through conditions, as well as identify the controlling geochemical processes and parameters. This information is particularly useful in the screening assessment of waste streams and in the identification and preliminary evaluation of potential ARD mitigation options. Further developmental studies are recommended to improve the quality (both in terms of availability and accuracy) of the input data, establish the reliability and certainty of the model outputs, and to expand application to other waste types and leach scenarios.

Acknowledgements

My first gratitude goes to my primary supervisor, Dr Jennifer Lee Broadhurst for granting me the opportunity to study under her supervision. I am deeply grateful for her patience, guidance, support and motivation throughout this study. Special thanks go to my co-supervisor Associate Professor Jochen Petersen for insight and advice, particularly in the modelling aspects of this work. I am also deeply grateful to Professor Sue Harrison, for her interest in this work and insightful comments and suggestions during the different stages of this project. I would also like to thank her for providing the datasets used in the modelling study.

I would like to extend my gratitude to the following people;

- Professor J-P Franzidis for his encouragement and for funding the project through the Minerals to Metal and South African Research Chair Initiatives.
- Mymoena van der Fort, for taking care of the administrative matters and for making my stay comfortable.
- Members of the Acid rock drainage (ARD) and BioMineral 2- Transport and leaching (BM2) discussion groups with whom I interacted during the course of my studies. I am grateful for the valuable discussions that helped me to understand and appreciate the bigger picture of my work.
- To all the students and staff in the Department of Chemical Engineering with whom I interacted throughout the course of my study. To the members of Goodwood and Mowbray Baptist churches for providing me a spiritual home during my stay in Cape Town. To both my immediate and extended family for their constant support, love and encouragement throughout this study.
- Lastly but not the least, to God almighty for granting me good health and strength during the period of this study.

This work is based on the research supported by the South African Research Chairs Initiative of the Department of Science and Technology and National Research Foundation of South Africa. Any opinion, finding and conclusion or recommendation expressed in this material is that of the authors and the NRF does not accept any liability in this regard.

Table of contents

List of figures

List of tables

Glossary

List of abbreviations used in this work

ABA	Acid base accounting – static test method for determining ARD potential
AF	Acid forming
ARD	Acid rock drainage–contaminated acidic leachate from oxidation of sulphide minerals, refers to acid mine drainage (AMD) when it is associated with mine discharge.
EPS	Extracellular polymeric substance: Organic polymer of microbial origin is frequently responsible for binding cells and other particulate materials together (cohesion) and to the substratum (adhesion)
Fe (II)	Ferrous iron – iron in 2nd oxidation state
Fe (III)	Ferric iron – iron in 3rd oxidation state
Fe^{2+}	Free ferrous ions in solution
Fe^{3+}	Free ferric ions in solution
LD	Longitudinal dispersivity
NAF	Non-acid forming
NAG	Net acid generation – a static test method for determining AMD potential
PAF	Potentially acid forming
PLS	Pregnant leach solution
ROM	Run-of-mine – Mined ore of a size that can be processed without further crushing
SCE	Sequential chemical extraction
TD	Transverse dispersivity
XRD	X-ray diffraction – Mineralogical analysis technique

1 INTRODUCTION

The mining industry is of great importance to the economy of the world and much of the progress and development in the world today could not have been attained without mineral and metal products. However, the mining and beneficiation of coal and hard rock ores also results in the generation of large volume waste streams for example waste rock from mining and tailings from milling and flotation processes (Blowes et al., 2003b; Lottermoser, 2007), which may pose a long-term threat to the local environment through metal mobilisation. Mine wastes containing sulphide minerals are particularly problematic as these minerals oxidise in the presence of oxygen and water resulting in the generation of acid rock drainage (ARD). Acid rock drainage is characterised by acidic pH, elevated concentrations of metals and dissolved salts and has the potential to cause prolonged pollution of local water resources.

Acid rock drainage prediction allows for the advance planning of disposal practices and selection of the most suitable mineral processing technology long before the mining operations begin. In addition more informed decisions with regard to acid rock drainage management can be made if the risks are identified at an early stage of a project. This study entails the development and application of a generic predictive modelling tool suitable for the early or screening evaluation of the potential long-term ARD risks associated with the disposal of sulphide wastes.

1.1 Background and motivation

1.1.1 Acid rock drainage: sources, impacts and management

Acid rock drainage (ARD) is defined as the acidic pH drainage water generated by chemical and microbiological reactions that occur simultaneously when sulphide minerals are exposed to oxygen and water (Lottermoser, 2007). Although acid rock drainage can occur wherever sulphide bearing minerals are excavated and exposed to atmospheric oxygen, it is most commonly associated with the mining and processing of coal and sulphide-bearing hard rock ores (Price, 2009). The potential sources of ARD in the mining industry are open pit mine sites, underground workings, ore stockpiles and beneficiation wastes that include waste rock piles, tailing dams and heap leach pads (Coastech Research, 1991; Bernhard, 2005). Acid rock drainage may migrate as runoff or seepage over a prolonged period of time (up to hundreds of years) from mine waste deposits, creating an extensive contamination plume (Price, 2009).

The high acidity and elevated concentration of metals and dissolved salts in ARD water negatively impacts the surface water, aquatic life, soil sediments and ground water (Lottermoser, 2007; Price, 2009). The most common sulphide bearing mineral in mine waste is pyrite (FeS_2), although small quantities of chalcopyrite ($CuFeS_2$) and other metal sulphide minerals have also been reported (Bernhard, 2005). Potential sources of acid rock drainage from base metal sulphide ore beneficiation are illustrated diagrammatically in Figure 1.

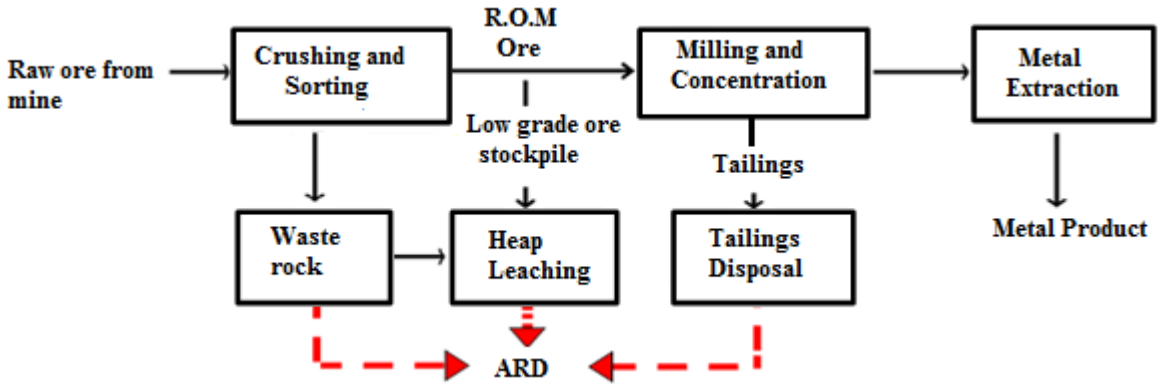

Figure 1: Generic block flow diagram indicating potential sources of ARD from hard rock sulphide ore beneficiation processes (Broadhurst et al., 2007; Hesketh, 2010)

Traditionally, the management of ARD has relied on end-of-pipe treatment techniques which are aimed at preventing the dispersion of ARD into the environment. Processes for ARD treatment can be divided into "passive" and "active" treatment techniques. Active treatment, such as neutralisation in stirred tanks, involves routine reagent addition and regular maintenance, while passive treatment, such as wetlands, only requires occasional maintenance (Bernhard, 2005).

Although treatment strategies may still be required as a temporary or permanent measure to prevent off-site contamination by ARD from historical operations, recent trends are towards preventative approaches which are aimed at minimising or avoiding ARD generation. In practice, preventative approaches for solid wastes mainly entail the application of disposal and management strategies that are aimed at avoiding exposure of sulphide minerals to oxygen and water, and include backfilling, blending and co-disposal and the use of covers and seals (Dorricott & Grice, 2002; Benzaazoua et al., 2004; Maddocks et al., 2009). While these techniques can minimise the effects of ARD in the short term, they do not completely remove the risk of ARD formation, and their ability to effectively mitigate ARD over the long term and provide a "walk-away" status is yet to be proven. A walk-away situation is commonly referred to as one which delivers a maintenance free, self-sustaining site which complies with acceptable environmental standards over the long-term without further interventions (Broadhurst et al., 2007).

These concerns have prompted the development of processes such as paste rock and tailings desulphurisation which are aimed at generating benign wastes through pre-disposal treatment. (Benzaazoua et al., 2004; Hesketh, 2010; Kazadi Mbamba, 2011). Justification for the selection and implementation of ARD mitigation processes that are effective over the long-term requires that likely ARD impacts are reliably and accurately quantified. As emphasised by Broadhurst et al. (2007), "*without a reliable estimate of the time-related release and characteristics of ARD from a waste under typical disposal conditions, there can be no meaningful plan to mitigate or manage the adverse effects.*"

1.1.2 ARD prediction approaches

As pointed out by Broadhurst et al. (2007) and Hansen et al. (2008), forecasting likely environmental impacts such as ARD, despite its importance, is extremely challenging. This is largely due to the vast number of inter-related mechanisms and factors (chemical, biological and physical) governing the time-related ARD concentration profiles (Perkins et al., 1995; Lefebvre et al., 2001a; Broadhurst et al., 2007; INAP, 2009; Price, 2009). Furthermore, the generation of ARD from solid wastes can be extremely prolonged (hundreds and even thousands of years) and there is often a long lag time between solid waste disposal and the generation of ARD (Price, 2009).

The traditional approach to the prediction of ARD from solid waste is through the use of static and kinetic laboratory scale leach tests (Smart et al., 2002; INAP, 2009; Price, 2009). Static tests, such as the acid base accounting (ABA) and the net acid generation (NAG) tests, provide an estimate of the likely acid generating potential of a solid over geological time, but do not give information on the rates of acid generation from the waste. These tests are, however, relatively rapid and are commonly used as screening tests to classify wastes as non-acid forming (NAF), acid forming (AF) or potentially acid forming (PAF) in accordance with universally accepted criteria. The commonly used laboratory scale kinetic tests include column leach, humidity cell and biological shake flask tests (US EPA, 1994; Stewart et al., 2006; Price, 2009; INAP, 2009; Hesketh, 2010). Unlike static tests, kinetic tests can provide information on the weathering rates and the lag period for the onset of acid generation. However, these tests tend to be difficult to set-up and run and can be extremely time-consuming, sometimes requiring years to produce meaningful results (INAP, 2009). Furthermore, the ability of laboratory-scale kinetic tests to realistically simulate field conditions, and hence the direct extrapolation of test results to full-scale deposits, is highly uncertain and controversial (Perkins et al., 1995; Maest et al., 2005; Jambor et al., 2006; Broadhurst et al., 2007; National Research Council, 2007).

The shortcomings and uncertainties associated with laboratory-scale tests has prompted the development of mathematical models which can predict the time-related concentration profiles of leachates, such as ARD, from solid waste deposits, on the basis of the governing chemical reaction and physical transport mechanisms (Perkins et al., 1995; Mayer et al., 2003; Hansen, 2004; Maest et al., 2005; Department of Water Affairs and Forestry, 2008). There are a number of commercial and developmental predictive models available which vary quite significantly in terms of their strengths, limitations and input data requirements (see discussion in section 1.1.3 below). In general, the selection and application of suitable predictive models rely on the ability to simplify the complexities involved, without unduly impacting on accuracy and reliability of model outcomes (Broadhurst et al., 2007). It is also important that cognisance is taken of the decision-making context and associated data quality requirements. While the accurate and reliable quantification of the time-related ARD profiles requires rigorous mechanistic modelling of both the (bio) chemical reaction and physical transport mechanisms under non-ideal flow conditions, these advanced models are complex and data-intensive. As such, they are better suited to site-specific studies and operational decision-making contexts. On the other hand, a number of authors (Kosson et al., 2002; Van der Sloot & Dijkstra, 2004; Broadhurst et al., 2007) have indicated that reasonable estimates of the time-related pH and concentration profiles could be derived through the judicious application of simple mass transport models, in conjunction with knowledge of the reaction mechanisms controlling the mobility of key contaminants and bulk liquid flows. Such estimates are deemed suitable for first-order predictions, consistent with early or screening evaluations of environmental impacts. In the generic protocol proposed by Broadhurst et al. (2007) and represented diagrammatically in Figure 2, simple predictive models can also be used to guide the selection and design of more extensive laboratory-scale tests for the derivation of waste and/or site specific data, as may be deemed necessary.

1.1.3 Quantitative ARD predictive models

A number of predictive models have been developed for predicting time-related leachate quality from solid waste, many specific for ARD (see for example reviews by Evangelou, 1995; Perkins et al., 1995; Crawford, 1999; Mayer et al., 2003; Hansen, 2004; Maest et al., 2005; Department of Water Affairs and Forestry, 2008). While some of these models are in public domain others are only available commercially. On the other hand, some have not been commercialised and are available only at the institution at which they were developed. Examples of non-commercialised models used include models developed by Petersen (1998) and Hansen (2004).

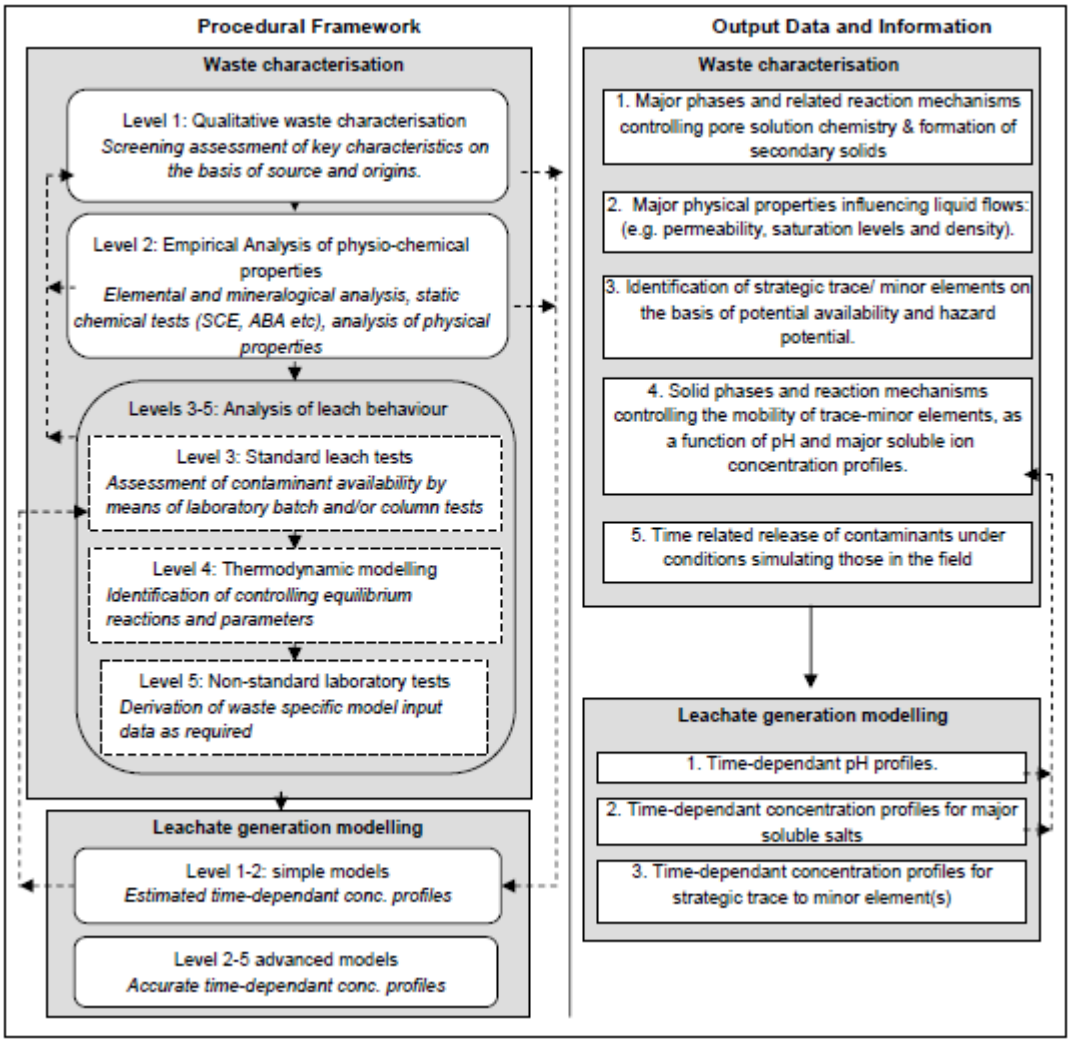

Figure 2: Systematic procedural framework and outcomes for waste characterisation and leachate generation predictions (Broadhurst et al., 2007)

ARD prediction models (and computer codes) are generally divided into geochemical, empirical, engineering and hybrid as indicated in Table 1. In general, geochemical models are classified as either geochemical reaction or coupled transport and reaction models, depending on their transport capabilities. Geochemical reaction computer codes such as MINTEQA2 (Allison et al., 1990) have capabilities to calculate chemical speciation, mass balance and mass transfer. These computer codes do not have transport capabilities (Crawford, 1999). On the other hand, coupled transport and reaction computer codes such as PHREEQC (Parkhurst & Appelo, 1999) incorporate both geochemical reactions and transport of constituents in the saturated media usually in 1-D and in some rare cases in 2-D or 3-D. As the name entails, geochemical models have a strong emphasis on geochemical processes (Crawford, 1999).

Table 1: Examples of commercial models used for prediction of ARD (adapted from Maest et al., 2005)

Category	Name of code	Modelled processes	Reference
GEOCHEMICAL	PHREEQC V.2	Geochemical speciation,1D transport, equilibrium and kinetic reactions	Parkhurst & Appelo (1999)
	MINTEQ	Geochemical speciation and equilibrium reactions	Allison et al., (1990)
	WATEQ4F V.2	Same as MINTEQ	Ball & Nordstrom, (1991) And database updates
	STEQDYQL	Steady-state flow, geochemical speciation, ion exchange, adsorption and kinetic reactions	Furrer et al., (1989, 1990)
	Geochemist's workbench	Same as PHREEQC V.2	http://www.gwb.com
ENGINEERING AND EMPIRICAL	PYROX	Pyrite oxidation by oxygen diffusion	Wunderly et al., 1995
	MINTOX	2D, gas diffusion, sulphide oxidation and transport	Gerke et al., (1998)
	FIDHELM	2D,pyrite oxidation by oxygen diffusion and convection	Pantelis & Ritchie, 1991; Pantelis, 1993; Kuo & Ritchie, 1999
	TOUGH AMD	Oxygen diffusion and convection, heat generation and transfer, unsaturated water flow and solute transport.	Lefebvre & Gélinas, (1995), Lefebvre et al., (2002)
	TOUGHREAC & TOUGH2-CHEM	Acid generation and buffering reactions in unsaturated media, kinetics.	Scharer et al., (1994)
	CRUNCH	Simulate release and attenuation of acid rock drainage in the unsaturated zone	Steefel,(2000)
HYBRID	MIN3P	Steady-state and transient flow, variably saturated, equilibrium reactions, kinetic reactions, microbially mediated reactions, gas and advective-dispersive transport	Mayer et al., 2002
	SULFIDOX	Kinetic and equilibrium controlled reactions, heat generation and transport of air and water.	www.ansto.gov.au./sulfide /sulfidox.html
	POLYMIN	1D or 2D, oxygen diffusion, geochemical speciation and advective-dispersive mass transport.	Molson et al., 2005

Empirical and engineering models are based on prior knowledge of the process and do not generally consider causal mechanisms. Particularly, empirical models are based on observed trends while engineering models only consider key processes believed to influence the system. These key processes are described using systems of equations and simplifying assumptions. The major shortcoming of these models is that their predictive capabilities depend on how much is known about the processes involved (Perkins et al., 1995; Hansen, 2004). Thus, empirical and engineering models are more suitable for site and/or sample specific cases, as well as the detailed design or later decision making stages of a project.

Hybrid models are designed to bridge the gap between geochemical models on the one hand, and empirical and engineering models on the other. These models have a rigorous treatment of geochemical and physical processes governing the generation of ARD (Mayer et al., 2003; Hansen, 2004). Like the geochemical models, hybrid models, take into account the causal mechanisms in their predictive properties. Some hybrid models such as MIN3P can handle a wide range of processes in variably saturated media (Mayer et al., 2003). These models have capabilities to simulate general equilibrium reactions, kinetically controlled reactions and physical transport processes in one, two or three dimensions (Mayer et al., 2002). Generally, hybrid models have a high degree of predictive accuracy (Mayer et al., 2003; Hansen, 2004). However, these models are generally data intensive and complex. This makes them difficult to validate or refute. Furthermore, the interpretation of their results requires specialised skills. As in the case of empirical and engineering models, these models are more suitable for site specific studies (Maest et al., 2005; Nordstrom, 2005).

Although both hybrid and geochemical mass transport models can be used in early stage project decision making (Williamson & Eary, 2006), geochemical models are generally less data intensive and more user friendly. Despite the fact that their transport capability is often limited to one spatial dimension (saturated media), these models can be reliable and accurate if the major input parameters and assumptions are well defined and understood (Maest et al., 2005; Broadhurst et al., 2007). Geochemical mass transport models can predict concentration profiles while providing valuable information pertaining to the controlling mechanisms which assist in waste management decision-making (Maest et al., 2005; Nordstrom, 2005; Department of Water Affairs and Forestry, 2008).

One of the most well established and widely used geochemical mass transport computer codes is PHREEQC, which has a wide range of capabilities that include geochemical modelling, chemical reaction and mass transport modelling (Parkhurst & Appelo, 1999).

The acronym PHREEQC represents pH (pH), redox (RE), equilibrium (EQ) and the language in which the program is written (C) (Snynder & Carline, 2003). PHREEQC is easy to use, well documented, readily available and highly flexible (Parkhurst & Appelo, 1999). PHREEQC is based on its precursor PHREEQE. PHREEQE was developed by the United States Geological Survey (USGS) and had capabilities for speciation and mass transfer calculations. PHREEQE was widely used until the development of PHREEQC V.1 (Parkhurst, 1995). PHREEQC V.1 retained all the capabilities of PHREEQE while incorporating new capabilities, the major ones being inverse modelling and one-dimensional advection transport. The capabilities of PHREEQC V.1 were extended further with the development of PHREEQC V.2 (Parkhurst & Appelo, 1999). Some of the capabilities included in PHREEQC V.2 that were not incorporated in the earlier versions are kinetic reactions, dispersion and diffusion transport processes. PHREEQC V.2 (referred to as PHREEQC in this dissertation) has continued to evolve with regular updates and reviews.

PHREEQC has mainly been used as a geochemical speciation code for calculation of saturation states and distribution of phases in natural and contaminated waters (Banwart & Malmstrom, 2001; Croxford et al., 2004; Kedziorek et al., 2008). In addition, PHREEQC has also been used to determine reactions responsible for the observed changes in subsurface and underground water quality (Schneider et al., 2002; Abreham, 2007; Lenk & Wisotzky, 2011; Vijayan & Noosai, 2012). In this way, PHREEQC has been used as a tool in the mitigation of water contamination. The chemical reaction capabilities of PHREEQC have also been extensively used to simulate a wide range of biotic and abiotic chemical reactions such as leaching of municipal, industrial and radioactive wastes (Cheryl et al., 2005; Tiruta-Barna, 2008). More recently, PHREEQC has been used to simulate the kinetic dissolution of carbon bearing primary basalt minerals and the subsequent capture and storage of carbon dioxide in secondary carbonate minerals (Van Pham et al., 2012; Talman et al., 2013). Degradation of organic matter has also been simulated using PHREEQC (Holch, 2008; Kedziorek et al., 2008). Other applications of the PHREEQC code include the simulation of one dimensional advective transport processes and diffusion in dual porosity media, and the study of the evolution and transport of nutrients and contaminants in soil (Brown et al., 1999; Geberetsadike, 2004; Lipson et al., 2007; Lenk & Wisotzky, 2011; Havik, 2012; Pettena et al., 2013).

In contrast, published studies of PHREEQC application on ARD prediction are limited to date (Nicholson et al., 2003; Williamson & Eary, 2006). Nicholson et al. (2003) used PHREEQC to simulate transport and chemical reaction processes in a waste rock pile. The reaction rates were described using first order kinetic rates based on element release rates in the kinetic experiments.

Consequently, the predictive capability of the model was based on the accuracy of the experimental data and did not consider the causal mechanisms. Furthermore, the model was not validated against any meaningful experimental dataset. Williamson and Eary (2006) used PHREEQC to determine the acid neutralisation capacity of silicates in ARD environments. Their model comprised equilibrium and kinetic reactions. These investigators used standard rate laws and constants from literature to describe the kinetic and equilibrium reactions. With the exception of ore mineralogy, all the model input parameters were obtained from literature. However, the model did not consider the transport of constituents and pyrite was assumed to be oxidised by dissolved oxygen only. Although the model gave insight into the neutralisation capacity of silicate minerals, its predictive capability in terms of leachate drainage quality in a flow-through scenario was not verified.

1.2 Problem statement

Accurate and reliable prediction of the time-related ARD profiles requires the use of mathematical models which take into account the governing chemical reaction and physical transport mechanisms. Rigorous predictive models are, however, both complicated and resource intensive, and warranted only in the case of detailed site-specific predictive studies. Geochemical reaction models coupled with simple mass transport, such as PHREEQC, offer a potential alternative for reliably estimating ARD profiles in the screening environmental assessment stage. Application of these models in predicting the generation of ARD from solid wastes and especially validation against independent data sets has, however, been limited to date.

1.3 Project objectives

The first objective of this project is to build-up a better understanding of the key parameters and mechanisms governing the generation of ARD at mine waste deposit. The second objective is to investigate the capabilities of PHREEQC geochemical code in a column scenario, with a view of assessing its suitability for screening of waste for ARD potential in early stage project decision making. This project seeks to answer the following key questions:

(1) What are the key waste characteristics and mechanisms governing the generation and quality of ARD from solid mine wastes?
(2) To what extent can the mechanisms identified in (1) be incorporated in a PHREEQC based model?
(3) What are the main input parameters required in a PHREEQC based model?

(4) What are the effects of key variables on the accuracy and reliability of the model for simulating ARD profiles in a flow-through scenario?
(5) Under what conditions can PHREEQC code be used for ARD prediction?

1.4 Dissertation scope and structure

This project entails the setting up of a geochemical mass transport model that incorporates chemical reactions and one dimensional (1-D) mass transport of constituents. The model is developed using the public domain PHREEQC code. Prior to model development, a detailed review and assessment of the main mechanisms governing ARD is undertaken. In the second place, the modelling capabilities, underpinning assumptions and simplifications of PHREEQC code are reviewed. The modelling methodology is demonstrated on a low grade copper sulphide ore as a proxy of a copper waste rock. As no experiments were carried out in this study, all the case study data are obtained from the Australian Minerals Industry Research Association (AMIRA) “Improving Heap Bioleaching” P768A project (Watling, 2006). The AMIRA project data was generated from laboratory-scale column leaching experiments conducted on low grade copper sulphide ore. Although the case study was designed to determine the rate and extent of copper extraction in a heap bioleaching scenario under highly acidic conditions, similarities can be drawn between the case study conditions and microbial catalysed ARD generation under highly acidic conditions.

Chapter 1 introduces the project, states the problem statement and defines the project objectives and scope. Chapter 2 is divided into two parts. The first part reviews the relevant literature pertaining to the mechanisms governing the generation of acid rock drainage i.e. chemical reactions and physical transport processes. The second part of the literature review discusses the modelling philosophy, capabilities and limitations of PHREEQC code. Chapter 3 outlines the research methodology, which comprised data collection, model development, model calibration, model validation and model sensitivity analysis. Chapter 4 presents and discusses the results from the model simulations. Finally, Chapter 5 presents the major findings of the study, limitations and future research needs in the light of this work. The summary of the dissertation structure is outlined Figure 3 below.

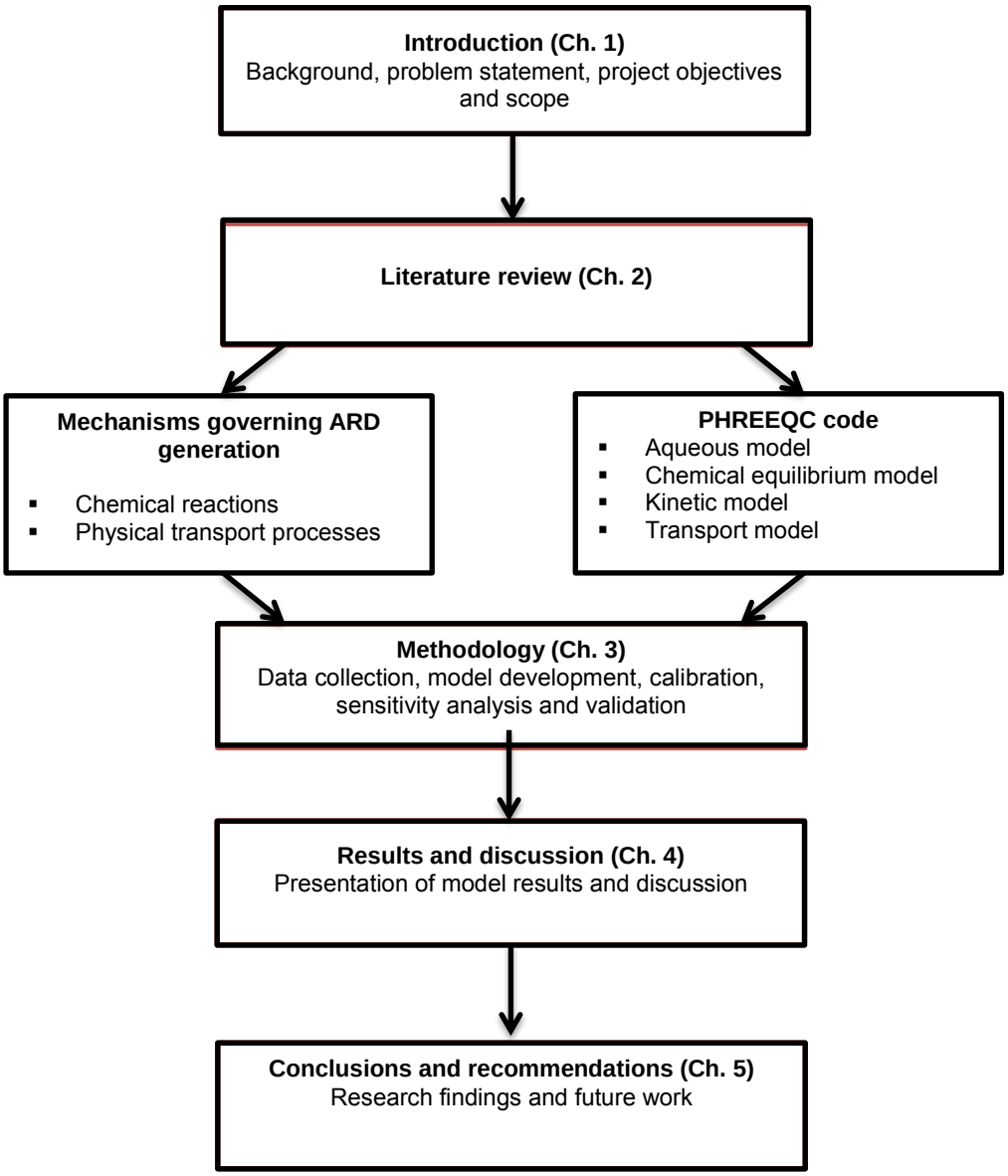

Figure 3: Schematic outline of the dissertation structure

2 LITERATURE REVIEW

A detailed literature review was carried out in order to address the first three research questions, namely (1) identification of the main mechanisms governing the generation of ARD at mine waste, (2) the extent to which these mechanisms can be incorporated into the PHREEQC based model, and (3) the main input parameters into the model. Firstly, the main mechanisms governing the generation of ARD at mine waste are identified through the literature review of the main chemical reactions and physical transport processes in sections 2.1 and 2.2 respectively. Secondly, the main model input parameters to PHREEQC based model and the extent to which the key processes are incorporated into the model are addressed in section 2.3 through an in-depth review of the literature on the modelling philosophy, main input parameters, key assumptions and limitations of PHREEQC code. Lastly, the main findings from the literature review are summarised in section 2.4 and used as a basis to address the remaining key research questions through model development and application in Chapter 3.

2.1 Chemical reactions in sulphidic mine wastes

Sulphide minerals are present in the same ore bodies associated with most of the copper mining activities. The oxidation of these sulphide minerals in their ore bodies is slow due to lack of access to oxidants and thus poses very little threat to the environment (Bernhard, 2005). However, the mining and processing of these ores accelerates the oxidation of sulphide minerals by exposing them to air and water. The oxidation of sulphide minerals generates acid rock drainage that migrates and contaminates the surrounding environment (Lottermoser, 2007). The oxidation of sulphide minerals and the subsequent generation of acid rock drainage are governed by a complex network of chemical reactions and physical transport processes (Perkins et al., 1995). In order to effectively predict the generation of ARD from copper sulphide waste, there is a need to understand the main mechanisms governing its generation.

The main chemical reactions governing the generation of ARD in mine wastes can be divided into three categories on the basis of their sequence of occurrence, namely primary, secondary and tertiary reactions. Primary reactions involve the oxidation of sulphide minerals and the dissolution of carbonate and aluminosilicate minerals. Secondary reactions involve adsorption and secondary minerals precipitation reactions while tertiary reactions involve the dissolution and transformation of precipitated secondary minerals (Perkins et al., 1995; Bernhard, 2005).

In the case of ARD generating wastes, chemical reactions are often also classified according to their effect on pH of the leachate i.e. as acid producing or acid neutralising reactions. The main acid producing reactions involve the oxidation of sulphide minerals, and the precipitation of Al^{3+} and Fe^{3+} bearing oxyhydroxides and hydroxysulphate phases. Depending on the pH conditions, acid is also produced through the dissolution of Al^{3+} and Fe^{3+} bearing hydroxysulphate phases (Elwood Madden et al., 2012). Acid neutralising reactions involve the dissolution of carbonate and aluminosilicate minerals and the dissolution of Al^{3+} and Fe^{3+} bearing oxyhydroxide minerals. Other reactions that can have a significant effect on the quality of leachate from mine wastes include the precipitation of salts (such as gypsum) and adsorption reactions. Adsorption involves the transfer of trace metal ions from the solution to solid surfaces (Lottermoser, 2007). Although this process neither generates nor neutralises acid, it can have a significant effect on the concentration of trace metals in solution (Herbert, 1996). Generally, adsorption of trace metals depends on pH, metal concentration and presence of complexing ligands (Jurjovec et al., 2002; Lottermoser, 2007). The chemical reactions of key significance in terms of the acid generating behaviour of copper sulphide wastes are discussed further in sub-sections 2.1.1 to 2.1.5 below. Adsorption reactions have been specifically excluded, as they are unlikely to occur to a significant extent at the relatively low pH conditions (pH<3) of relevance to this study. Although the chemical reactions discussed in the next sections are relevant to all ARD generating waste, the focus will specifically be on copper sulphide waste which is the focus of the case study application.

2.1.1 Oxidative dissolution of sulphide minerals

Acid rock drainage is generated by the oxidation of sulphide minerals in the presence of oxygen and water. Pyrite is the most common of the sulphide minerals and is closely associated with copper ore deposits (Blowes et al., 2003b; Lottermoser, 2007). Because of its major role in the generation of acid rock drainage, the oxidation mechanisms of pyrite have been the focus of many studies (Davis & Ritchie, 1986; Williamson & Rimistidt, 1994; Evangelou & Zhang, 1995; Garcia et al., 1996; Gunsinger et al., 2006). The oxidation of pyrite occurs when the pyrite mineral is exposed to water and oxygen. This may take place in the presence or absence of microorganisms (abiotic) (Garcia et al., 1996; Nordstrom & Alpers, 1999b). In the abiotic oxidation process, oxygen directly oxidises pyrite according to the reaction represented by Equation 1.

$$FeS_{2(s)} + \frac{7}{2}O_{2(g)} + H_2O_{(l)} \rightarrow Fe^{2+}{}_{(aq)} + 2SO_4^{2-}{}_{(aq)} + 2H^{+}{}_{(aq)} \quad 1$$

However, it is generally agreed that pyrite oxidation is mainly accomplished by the indirect oxidation mechanism (Davis & Ritchie, 1986; Evangelou & Zhang, 1995; Blowes et al.,

2003b; Price, 2009). In the indirect mechanism, the oxidation of pyrite is carried out by both oxygen and ferric iron (Fe^{3+}). These reactions occur in three interconnected steps.

The sequence of reactions describing the indirect oxidation of pyrite is initiated by Equation 1 and propagated by Equations 2 and 3.

$$Fe^{2+}{}_{(aq)} + \frac{1}{4}O_{2(g)} + H^{+}{}_{(aq)} \rightarrow Fe^{3+}{}_{(aq)} + \frac{1}{2}H_2O_{(l)} \quad 2$$

$$FeS_{2(s)} + 14Fe^{3+}{}_{(aq)} + 8H_2O_{(l)} \rightarrow 15Fe^{2+}{}_{(aq)} + 2SO_4^{2-}{}_{(aq)} + 16H^{+}{}_{(aq)} \quad 3$$

The first step in the indirect mechanism involves the oxidation of pyrite by dissolved oxygen at circumneutral pH according to Equation 1. Although pyrite can be oxidised by ferric iron at circumneutral pH, the low solubility of ferric iron at high pH makes this reaction mechanism insignificant (Bernhard, 2005). The second step in the indirect mechanism involves the oxidation of ferrous iron (Fe^{2+}) to ferric iron (Fe^{3+}) by oxygen according to Equation 2. This reaction produces more ferric iron (Fe^{3+}) that eventually becomes the main oxidant of pyrite in the third step when the pH drops to about 4.5 or lower (INAP, 2009). The oxidation of pyrite by ferric iron is reported to be in the range of 2 to 3 orders of magnitude faster than the oxidation by dissolved oxygen (INAP, 2009). As a consequence, this reaction generates more acid (hydrogen ions), dissolved sulphate and ferrous iron (Lottermoser, 2007). The reaction involving the oxidation of ferrous iron to ferric iron and that involving the oxidation of pyrite by ferric iron (Equations 2 and 3) form a continuing cycle of Fe^{2+} conversion to Fe^{3+} and the subsequent oxidation of pyrite by Fe^{3+} to produce Fe^{2+} (Lottermoser, 2007). These reactions continue indefinitely unless either the pH is significantly raised or the oxygen supply to the oxidation site is stopped (Lottermoser, 2007). The main role of oxygen in the indirect oxidation of pyrite is to oxidise ferrous to ferric iron that in turn becomes the main oxidant for pyrite. At lower pH, the oxidation of ferrous iron by oxygen is slow, thus the oxidation of ferrous to ferric iron (Equation 3) becomes the rate limiting reaction to ARD generation (Nordstrom & Alpers, 1999b; INAP, 2009).

However at low pH levels, microbial organisms catalyse the oxidation of sulphide minerals (Coastech Research, 1991). For instance, iron oxidising microorganisms such as *Acidithiobacillus ferrooxidans* catalyse the oxidation of ferrous to ferric iron which in turn becomes the main oxidant for pyrite (Coastech Research, 1991). Likewise, sulphur oxidising microorganisms catalyse sulphur species to sulphate. These catalysed reactions produce acid at a much faster rate. However, the activities of these microorganisms are generally pH and temperature dependent, for example most iron and sulphur oxidising microorganisms have optimal activity at lower pH (<3.5) and above ambient temperature conditions

(Coastech Research, 1991; Garcia et al., 2001; Lottermoser, 2007). Hence, they do not contribute significantly to pyrite oxidation at neutral to alkaline conditions.

Figure 4 below indicates the role of iron and sulphur oxidising microbial organisms in the oxidative dissolution of pyrite (FeS_2) by bacteria.

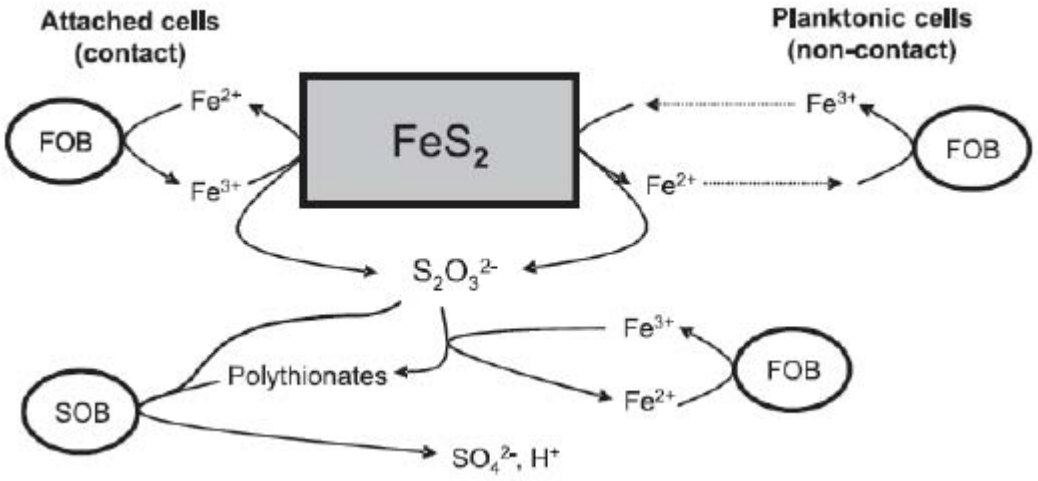

Figure 4: Schematic of pyrite oxidation by acidophilic bacteria (FOB, iron-oxidising prokaryotes; SOB, sulphur-oxidising prokaryotes) (Bryan, 2006)

Pyrite often occurs in association with other sulphide minerals in ore bodies. Some of the common sulphide minerals that are associated with pyrite are shown in Table 2 below together with their acid producing reaction mechanisms.

Table 2: Common acid generating sulphide minerals (Plumlee, 1999)

Mineral	Oxidation by oxygen	Oxidation by ferric ion
Pyrite	generates acid	generates acid
Pyrrhotite	generates acid	generates acid
Arsenopyrite	generates acid	generates acid
Chalcopyrite	do not generate acid	generates acid
Pentlandite	do not generate acid	generates acid
Sphalerite	do not generate acid	generates acid
Galena	do not generate acid	generates acid

With the exception of pyrite and pyrrhotite, the overall net acid produced by the reactions involving these minerals may be low due to the consumption of acid by other reaction mechanisms. As an example, the acid generating oxidative dissolution of chalcopyrite common in acidic and highly oxidising ARD and heap leaching environments is shown in Equation 4.

$$CuFeS_2 + 16Fe^{3+} + 8H_2O \rightarrow 17Fe^{2+} + Cu^{2+} + 2SO_4^{2-} + 16H^+ \quad 4$$

Alternatively, chalcopyrite dissolution can also occur by non-oxidative according to Equation 5.

$$CuFeS_2 + 4H^+ \rightarrow Cu^{2+} + Fe^{2+} + 2H_2S \quad (5)$$

The ferrous iron generated by Equations 4 and 5 can be oxidised to ferric iron in the acidic conditions according to Equation 6 below.

$$Fe^{2+} + \frac{1}{4}O_2 + H^+ \rightarrow Fe^{3+} + H_2O \quad (6)$$

As shown above, some of the acid generated by the oxidative dissolution of chalcopyrite by Equation 4 will be consumed by reactions 5 and 6. In this way, the net acid production by chalcopyrite dissolution is reduced.

2.1.2 Acid dissolution of carbonate minerals

The acid generated by the oxidation of sulphide minerals is mostly neutralised by carbonate minerals. Their rapid dissolution rates make them the most effective acid neutralising minerals if present in abundance (Lottermoser, 2007). The dissolution rates of carbonates are in the range of 10^{-8} to 10^{-5} moles m^{-2} s^{-1} with the more soluble carbonates dissolving faster than the less soluble ones (Perkins et al., 1995; Lottermoser, 2007). Of the carbonate minerals, calcite is the most soluble while siderite is the least soluble (Holland & Turekian, 2005). The dissolution reactions involving carbonates are generally considered to be kinetically controlled with rates increasing with a decrease in pH (Jurjovec et al., 2002). The dissolution of carbonate minerals reduces the acidity of the solution by forming complexes with dissolved hydrogen ion (Lottermoser, 2007). The main carbonate minerals present in copper sulphide mine wastes are calcite, dolomite and siderite (Banwart & Malmstrom, 2001). The acid neutralising dissolution reactions of these minerals are represented by Equations 7 to 11.

Calcite dissolution

$$CaCO_3 + 2H^+ \rightarrow Ca^{2+} + H_2CO_3 \ (pH < 6) \quad (7)$$

$$CaCO_3 + H^+ \rightarrow Ca^{2+} + HCO_3^- \quad (6.5 < pH < 10) \quad (8)$$

Dolomite dissolution

$$CaMg(CO_3)_2 + 4H^+ \rightarrow Ca^{2+} + Mg^{2+} + 2H_2CO_3 \quad (pH < 6) \quad (9)$$

$$CaMg(CO_3)_2 + 2H^+ \rightarrow Ca^{2+} + Mg^{2+} + 2HCO_3^- \quad (6.5 < pH < 10) \qquad 10$$

Siderite dissolution

$$FeCO_3 + H^+ \leftrightarrow Fe^{2+} + HCO_3^- \qquad 11$$

Although siderite can be an acid neutralising mineral at low pH conditions, it does not generally result in net acid neutralisation under the oxidising conditions commonly associated with sulphidic mine wastes. This is due to the oxidation of ferrous iron and subsequent formation of ferric hydroxide, in accordance with the reaction in Equation 12.

$$4Fe(CO_3) + O_2 + 10H_2O \leftrightarrow 4HCO_3^- + 4Fe(OH)_3 + 4H^+ \qquad 12$$

Secondary precipitation reactions and their effect on pH are discussed further in sub-section 2.1.4.

2.1.3 Acid dissolution of aluminosilicate minerals

Aluminosilicates are the most abundant minerals in mine wastes (Stewart et al., 2006). The weathering of these minerals is the main source of metal cations and anions. Like carbonate minerals, the weathering rates of aluminosilicate minerals are also pH dependent with rates generally increasing with decreasing pH (Jurjovec et al., 2002). However, their dependence on pH differs from one mineral to another. Aluminosilicate minerals can be divided into four main categories depending on their weathering rates namely; fast weathering, intermediate weathering, slow weathering and very slow weathering (Perkins et al., 1995; Jambor & Blowes, 1998; Lottermoser, 2007). In the absence of carbonates, the fast weathering aluminosilicates are the most important acid neutralising minerals in mine wastes (Stromberg & Banwart, 1994; Banwart & Malmstrom, 2001; Linklater et al., 2005). However, under low pH conditions, the intermediate and the slow weathering aluminosilicate minerals can also become important neutralisation minerals due to increased weathering rates (Palandri & Kharaka, 2004; Brantley et al., 2008). These categories are shown in Table 3 below.

Table 3: Reaction rates of carbonate and aluminosilicate minerals (Perkins et al., 1995)

Category	Typical mineral	Reaction rates (moles $m^{-2}s^{-1}$)
Fast dissolving	Carbonates (calcite, aragonite, dolomite, magnesite, brucite).	10^{-8} to 10^{-5}
Fast weathering	Feldspar (anorthite),olivine (forsterite), pyroxenes (diopside, hedenbergite, jadeite, spodumene, bronzite) wollastonite, chlorites,garnets,epidotes,nepheline, leucite.	$10^{-10.5}$ to 10^{-9}
Intermediate weathering	Pyroxenes(enstatite, augite), amphiboles (tremolite,actinolite,hornblende,glaucophane anthophyllite), serpentine(chrysotile), mica(biotite), chlorite,talc, hypersthene	10^{-12} to $10^{-10.5}$
Slow weathering	Feldspar (albite, oligoclase, labradorite),clay (kaolinite,vermiculite,montmorillinite)	10^{-13} to 10^{-12}
Very slow weathering	Feldspar (K-feldspar),mica (muscovite)	10^{-14} to 10^{-13}
Inert minerals	Rutile, zircon, quartz	10^{-16} to 10^{-14}

Aluminosilicate minerals neutralise acid by consuming the hydrogen ion from the solution. The weathering reactions of aluminosilicate minerals common in copper sulphide waste are shown in Table 4 below.

Table 4: Primary weathering reactions of some of the aluminosilicate minerals common in copper sulphide waste

Fast weathering	
Plagioclase (anorthite)	$CaAl_2Si_2O_8 + 8H^+ \rightarrow Ca^{2+} + 2Al^{3+} + 2H_4SiO_4$
Diopside	$CaMgSi_2O_6 + 4H^+ + 2H_2O \rightarrow Ca^{2+} + Mg^{2+} + 2H_4SiO_4$
Forsterite	$Mg_2SiO_4 + 4H^+ \rightarrow 2Mg^{2+} + H_4SiO_4$
Intermediate weathering	
Biotite	$KMg_{1.5}Fe_{1.5}AlSi_3O_{10}(OH)_2 + 10H^+ \rightarrow K^+ + Al^{3+} + 1.5Mg^{2+} + 1.5Fe^{2+} + 3H_4SiO_4$
Chlorite	$Al_2Si_2O_5(OH)_4 + 6H^+ \rightarrow 2Al^{3+} + 2H_4SiO_4 + H_2O$
Tremolite	$Ca_2Mg_5Si_8O_{22}(OH)_2 + 14H^+ + 8H_2O \rightarrow 2Ca^{2+} + 5Mg^{2+} + 8H_4SiO_4$
Slow weathering	
Kaolinite	$2Al_2Si_2O_5(OH)_4 + 3H_2SO_4 \rightarrow 2Al^{3+} + 2SiO_2(aq) + 3SO_4^{2-} + 5H_2O$
Albite	$NaAlSi_3O_8 + 4H_2O + 4H^+ \rightarrow Na^+ + Al^{3+} + 3H_4SiO_4$
Very slow weathering	
Muscovite	$KAl_2[AlSi_3O_{10}](OH)_2 + 10H^+ \rightarrow K^+ + 3Al^{3+} + 3H_4SiO_4$
K-feldspar	$KAlSi_3O_8 + 4H_2O + 4H^+ \rightarrow K^+ + Al^{3+} + 3H_4SiO_4$

As in the case of siderite, the effectiveness of aluminosilicate minerals as acid neutralisers is reduced if their dissolution is followed by precipitation of Al^{3+} and Fe^{3+} oxyhydroxides (Perkins et al., 1995; Bernhard, 2005; INAP, 2009). The precipitation of these minerals reduces the acid neutralisation capacity of carbonate and aluminosilicate minerals by releasing the acid back into the solution (Perkins et al., 1995).

These reactions are discussed in more detail in the next section (see section 2.1.4). Furthermore, the precipitation of secondary minerals may form coatings on surfaces of primary carbonate and aluminosilicate minerals. This reduces the reactivity of these minerals and hence their capacity to neutralise acid (Perkins et al., 1995; Jurjovec et al., 2002).

2.1.4 Precipitation of secondary minerals

As can be seen from the discussions in the previous section, the dissolution of primary sulphide, carbonate and aluminosilicate minerals increases the concentration of ions in the solution (see reactions in Equations 1, 3, 4 and Table 4). The interaction of these ions within the solution result in the precipitation of a wide range of secondary minerals that include sulphates, silicates, carbonates, oxyhydroxides and hydroxysulphates (Bernhard, 2005; Lottermoser, 2007). The precipitation of these minerals generally depends on many factors that include pH-Eh conditions, availability of key elements and temperature (Perkins et al., 1995; Bernhard, 2005). Precipitation reactions are generally considered to be equilibrium controlled, although some can be kinetically controlled due to slow precipitation rates (Elwood Madden et al., 2012). While the precipitation of some salts such as gypsum has no effect on the pH of the solution, the precipitation of hydroxysulphates and oxyhydroxides, produces acid by releasing the hydrogen ion into solution (Bernhard, 2005; Lottermoser, 2007).

Ferric iron and aluminium ions form a number of hydroxysulphates and oxyhydroxides compounds due to their abundance in mine waste. The nature and extent of precipitate formation depends on pH, solute concentration levels and, to a lesser extent, temperature (Nordstrom & Alpers, 1999a; Jambor et al., 2000). Generally, hydroxysulphates form at low pH and high sulphate concentrations while oxyhydroxides tend to form at low sulphate concentrations and weakly acidic to alkaline pH conditions (pH>3.5) (Lottermoser, 2007). The main iron hydroxysulphate precipitates that form in copper sulphide mine waste are jarosite and schwertmannite while the main oxyhydroxides are ferrihydrite and goethite. Jarosite is commonly formed at acidic pH values (1-3) and high sulphate concentrations (3000-4000 ppm or higher).

Jarosite has the general formula of $MFe_3(OH)_6(SO_4)_2$, where M = K^+, Na^+, H_3O^+, Ag^+ and NH_4^+. The type of jarosite that forms generally depends on the dominant cation in solution and the relative stability of the jarosite form. K-jarosite is the most thermodynamically stable and common form, and will precipitate preferentially to other jarosite compounds in the presence of dissolved potassium (Elwood Madden et al., 2012). The precipitation of jarosite is usually a slow process with equilibrium attained only after 80 to 125 days at ambient temperatures (Elwood Madden et al., 2012).

However, at higher temperatures (60 to 100 ºC), the precipitation rate of jarosite has been reported to significantly increase (Dutrizac, 2008). At higher pH values (pH>3.5), jarosite becomes metastable and transform to schwertmannite and other oxyhydroxide phases. Schwertmannite is the preferred phase in the pH range 3-4 at sulphate concentrations in the range of 1000-3000 ppm, while the oxyhydroxides, goethite, and ferrihydrite are the preferred phases at lower sulphate concentrations (<1000) and/or higher pH values (pH>3.5). Schwertmannite has a general formula of $Fe_8O_8(OH)_{8-2x}(SO_4)_x.nH_2O$ ($1 \leq x \leq 1.75$) or $Fe_{16}O_{16}(OH)y(SO_4)z.nH_2O$ ($16-y=2z$ and $2 \leq z \leq 2.5$) (Yu et al., 2001; Murad & Rojik, 2004; Gitari, 2006). Ferrihydrite or amorphous ferric hydroxide forms under non-equilibrium conditions and is converted to the more crystalline and less soluble goethite (α-FeOOH) upon ageing. At room temperature, the ageing process is relatively slow and takes several weeks to a number of years, depending on the conditions. At 80ºC to 130ºC conversion is rapid, while the presence of sulphate anions tends to slow down the conversion rate. A review of the literature has indicated that in most aged tailings ferrihydrite and goethite are found to co-exist (Nordstrom & Alpers, 1999a; Jambor et al., 2000).

As mentioned earlier, aluminium bearing hydroxysulphate and oxyhydroxides also form in mine waste with the most important hydroxysulphates being jurbanite, alunite and to a lesser extent basaluminite and the most important oxyhydroxides being Al-hydroxides ($Al(OH)_3(a)$), gibbsite, boehmite (γ-AlOOH) and diapsore (α-AlOOH) (Espana, 2003). Like their iron hydroxysulphates counterparts, aluminium hydroxysulphates also form at low pH and high sulphate concentrations. Of the aluminium hydroxysulphate, jurbanite is the most common and the most thermodynamically stable aluminium hydroxysulphate phase. The formation of aluminium hydroxysulphates is favoured by high sulphate concentrations (SO_4^{2-}>5000mg/L) (Gitari, 2006). Jurbanite ($AlOHSO_4.5H_2O$) forms in acidic conditions (0-3.5) while other hydroxysulphates such as alunite ($KAl_3(OH)_6(SO4)_2$) and basaluminite ($Al_4(OH)_{10}SO_4.5H_2O$) form at a weakly acidic pH (3.5-5.5 and 4.5-5 respectively) (Espana, 2003). At high pH values, basalunite and alunite become metastable and easily transform to more stable phases. For instance, a rise in pH to about 5.5 causes alunite to transform to gibbsite $Al(OH)_3$. Gibbsite is the most stable oxyhydroxide phase and is formed from either the transformation of hydroxysulphate minerals or crystallisation of Al-hydroxides ($Al(OH)_3(a)$) (Nordstrom & Alpers, 1999a; Jambor et al., 2000). Other oxyhydroxides minerals that are likely to form in mine waste include boehmite (γ-AlOOH) and diapsore (α-AlOOH). Generally, oxyhydroxides form at weakly acidic to alkaline pH conditions (4-11) and low sulphate concentrations (SO_4^{2-}<2500mg/L) (Gitari, 2006; Lottermoser, 2007). Table 5 below shows the main conditions under which iron and aluminium hydroxysulphate and oxyhydroxides form.

Table 5: Formation of hydroxysulphates and oxyhydroxides (Espana, 2003; Murad & Rojik, 2004)

Mineral	Formula	pH range	Sulphate concentration (mg L^{-1})
Iron oxyhydroxides/hydroxysulphates			
Jarosite	$KFe_3(SO_4)_2(OH)_6$	1 - 3	>3000
Schwertmannite	$Fe_8O_8(OH)_6SO_4$	3 - 4.5	1000-3000
Ferrihydrite	$Fe(OH)_3$	pH > 5	<1000
Aluminium oxyhydroxides/hydroxysulphate			
Jurbanite	$AlOHSO_4.5H_20$	0<pH<3.5	>5000
Alunite	$KAl_3(OH)_6(SO4)_2$	3.5 – 5.5	>5000
Basalunite	$Al_4(OH)_{10}SO_4.5H_20$	4.5 - 5	>5000
Gibbsite	$Al(OH)_3$	4.0-11	< 2500

In addition to the production of acid due to the formation of iron and aluminium bearing oxyhydroxides and hydroxysulphates, acid is also produced due to the formation of secondary silicate minerals (Perkins et al., 1995). Although the primary dissolution of aluminosilicates can result in the formation of other secondary clay minerals such as montmorillinite ($Al_2Si_4O_{10}(OH)_4$) and illite, kaolinite($Al_2Si_2O_5(OH)_4$) is the most stable and common secondary product arising from the weathering of aluminosilicates in natural environments. Its formation relative to other clay minerals is furthermore favoured by an acid environment (<pH 4) with free drainage, with montmorillinite only forming under more alkaline conditions (pH> 5) (Perkins et al., 1995; Nordstrom & Alpers, 1999a). Acid producing precipitation reactions commonly associated with copper sulphide waste are shown in Table 6 below.

Table 6: Examples of acid generating precipitation reactions common in copper sulphide waste.

Mineral	Precipitation reaction	Log k*
Ferrihydrite	$Fe^{3+}{}_{(aq)} + 3H_2O_{(l)} \leftrightarrow Fe(OH)_{3(s)} + 3H^+{}_{(aq)}$	3.0 - 5.0
Goethite	$Fe^{3+}{}_{(aq)} + 2H_2O_{(l)} \leftrightarrow FeOOH_{(s)} + 3H^+{}_{(aq)}$	-1.0
Hematite	$2Fe^{3+} + 3H_2O \leftrightarrow Fe_2O_3 + 6H^+$	-4.008
Schwertmannite	$8Fe^{3+} + SO_4^{2-} + 14H_2O \leftrightarrow Fe_8O_8(OH)_6SO_4 + 22H^+$ $16Fe^{3+} + 3SO_4^{2-} + 26H_2O \leftrightarrow Fe_{16}O_{16}(OH)_{10}(SO)_3 + 42H^+$	-18.0
Jarosite	$3Fe^{3+} + K + 2SO_4^{2-} + 6H_2O \leftrightarrow KFe_3(SO_4)_2(OH)_6 + 6H^+$	-9.21
Gibbsite	$Al^{3+} + 3H_2O \leftrightarrow Al(OH)_3 + 3H^+$	8.11
Jurbanite	$Al^{3+} + SO_4^{2-} + H_2O \leftrightarrow AlOHSO_4 + H^+$	-3.23
Alunite	$K^+ + 3Al^{3+} + 2SO_4^{2-} + 6H_2O \leftrightarrow KAl_3(SO_4)_2(OH)_6 + 6H^+$	-1.4
Kaolinite	$Al^{3+} + H_4SiO_4 + \frac{1}{2}H_2O \leftrightarrow 3H^+ + \frac{1}{2}Al_2Si_2O_5(OH)_4$	7.435

*All log k values are obtained from PHREEQC default database except the log k values for ferrihydrite, jurbanite and schwertmannite that were obtained from Holland and Turekian (2005), Wateq4f.dat dataset and Bigham et al (1996) respectively.

As shown in section 2.1.2, the dissolution of iron bearing carbonate and silicate minerals such as siderite, biotite and chlorite increases the concentration of dissolved iron resulting in the precipitation of ferric oxyhydroxides such as ferrihydrite. This also increases the acidity of the effluent.

2.1.5 Transformation and re-dissolution of secondary minerals

The transformation and dissolution of secondary minerals are important geochemical processes because of their effects on pH and concentration of dissolved ions over the long term. The most important of these reactions are the transformation and dissolution of hydroxysulphates which results in acid production and the dissolution of oxyhydroxides which results in acid consumption or neutralisation. The rates and extents of transformation and dissolution reaction are mainly driven by pH although other factors such as morphology, temperature, crystal size and order also play a role (Schwertmann, 1991). The transformation and dissolution rate also depends on the precipitate chemistry. The dissolution rate of goethite, for example, decreases as the Al substitution increases (Schwertmann, 1991; Bernhard, 2005). The two main classes of transformation and re-dissolution reactions are discussed in further detail below.

Re-dissolution and transformation of hydroxysulphate reactions (acid forming)

As mentioned in the previous section, the iron and aluminium hydroxysulphates that form at high sulphate concentration and low pH conditions are metastable and tend to transform to more stable phases when they come in contact with high pH solution (4<pH). Transformation reactions involving iron and aluminium hydroxysulphates are acid generating. Some of the common acid producing phase transformation reactions that occur in copper sulphide waste are presented in Table 7 below.

Table 7: Iron and aluminium hydroxysulphate transformation reactions common in copper sulphide waste

Mineral	Transformation reactions	New phase
Ferric bearing hydroxysulphates		
K-jarosite	$KFe_3(SO_4)_2(OH)_6 \leftrightarrow 3FeO(OH) + K^+ + 2SO_4^{2-} + 3H^+$	Goethite
	$KFe_3(SO_4)_2(OH)_6 + 3H_2O \leftrightarrow 3Fe(OH)_{3(S)} + K^+ + 2SO_4^{2-} + 3H^+$	Ferrihydrite
Schwertmannite	$Fe_{16}O_{16}(OH)_{10}(SO_4)_3 + 6H_2O \leftrightarrow 16FeO(OH) + 3SO_4^{2-} + 6H^+$	Goethite
	$Fe_8O_8(OH)_6(SO_4) + 2H_2O \leftrightarrow 8FeO(OH) + SO_4^{2-} + 2H^+$	Goethite
Aluminium bearing hydroxysulphates		
Jurbanite	$Al(SO_4)(OH).5H_2O_{(s)} \leftrightarrow Al(OH)_{3(s)} + 3H_2O_{(l)} + SO_{4(s)}^{2-} + H_{(aq)}^+$	Gibbsite
Alunite	$KAl_3(SO_4)_2(OH)_{6(s)} + 3H_2O_{(l)} \leftrightarrow K_{(aq)}^+ + 3Al(OH)_{3(s)} + 2SO_{4(aq)}^{2-} + 3H_{(aq)}^+$	Gibbsite

As shown in Table 7, the type of the reaction products and the amount of acid generated depends on the type of the transforming mineral. Generally, the transformation of ferric hydroxysulphate results in the formation of ferric oxyhydroxides, such as goethite and ferrihydrite, while the transformation of aluminium hydroxysulphate results in the formation of aluminium oxyhydroxides, mainly gibbsite (Bernhard, 2005).

Transformation reactions are generally slow processes due to the low solubility of hydroxysulphate in solution. As such, they can be described as being kinetically controlled (Lottermoser, 2007). Because of their slow transformation rates, they become the main source of acidity long after the depletion of primary sulphide minerals (Lottermoser, 2007).

Acid neutralisation by re-dissolution of oxyhydroxides

The second type of re-dissolution reaction involves the re-dissolution of iron and aluminium bearing oxyhydroxide at low pH (pH<3.5). Like carbonates and aluminosilicate minerals, the dissolution of these minerals result in an increase in pH and dissolved ion concentrations. Generally, oxyhydroxides dissolve faster than most of the aluminosilicates (Bernhard, 2005). As a result, the dissolution of oxyhydroxides can become an important acid neutralisation process in copper sulphide waste, particularly after the depletion of carbonate minerals. The dissolution reactions of some of the iron and aluminium oxyhydroxides commonly associated with copper sulphide waste are shown in Table 8 below.

Table 8: Acid neutralising by dissolution of iron and aluminium oxyhydroxide reactions

Mineral	Dissolution reaction	Log k
Aluminium hydroxides		
Gibbsite	$Al(OH)_{3(s)} + 3H^{+}_{(aq)} \leftrightarrow Al^{3+}_{(aq)} + 3H_2O_{(l)}$	7.94
Boehmite	$AlOOH_{(s)} + 3H^{+}_{(aq)} \leftrightarrow Al^{3+}_{(aq)} + 2H_2O_{(l)}$	7.83
	Ferric hydroxides	
Ferrihydrite	$Fe(OH)_{3(s)} + 3H^{+}_{(aq)} \leftrightarrow Fe^{3+}_{(aq)} + 3H_2O_{(l)}$	3.0 to 5.0
Goethite	$FeOOH_{(s)} + 3H^{+}_{(aq)} \leftrightarrow Fe^{3+}_{(aq)} + 2H_2O_{(l)}$	-1.0
Hematite	$Fe_2O_{3\,(s)} + 6H^{+}_{(aq)} \leftrightarrow 2Fe^{3+}_{(aq)} + 3H_2O_{(l)}$	-4.008

Like hydroxysulphates, the stability of these oxyhydroxides depends on pH. However, in contrast to the hydroxysulphates, oxyhydroxides become more unstable and tend to dissolve easily at low pH conditions (pH<4) (Holland & Turekian, 2005).

2.2 Physical transport processes

As previously discussed, acid rock drainage generation is governed by a complex network of chemical reactions and physical transport processes. This section focuses on the main physical transport processes that govern the generation of ARD namely bulk fluid transport, solute transport, microbial transport and attachment, heat and oxygen transport.

2.2.1 Bulk fluid flow

Sulphide waste from mining and beneficiation of hard rock ores are deposited as dry coarse-grained (waste rock) and wet fine-grained material (mill tailings). They are generally composed of solid porous particles with different saturation levels. Generally, waste rocks are partially water saturated with voids between the particles filled by both liquid and air (Perkins et al., 1995). Typical moisture content in waste rock is less than 10% by volume with less than 0.1 litres per kg of waste rock (Jones, 1995; Nicholson et al., 2003). Mill tailings on the other hand are deposited as slurry and remain fully saturated with water during the operation of the mine due to the continued disposal of fresh wet mill tailings (Garcia et al., 2005). The saturation of the slurry depends on the construction of the pond or dump, as well as the recharge into such a structure (Jones, 1995).

Typical ratios of pore water to solids are in the range of 10/1 to 20/1 l/kg (Jones, 1995). However, when mining operations cease, the level of water saturation reduces and the mill tailings eventually become partially saturated. However, due to changes in the climatic conditions, all waste deposits are typically subjected to wetting and drying cycles resulting in different levels of water saturation. Generally, water enters the waste deposit through infiltration by rain water and seasonal runoff (for example melt water from snow in cold countries). However, during the dry season, significant amount of moisture is lost through evaporation and drainage at the base of the deposit (Perkins et al., 1995). The reduction in the moisture content causes the gas to occupy the pore spaces initially occupied by water. This increases the gas content (oxygen) in the waste deposits which in turn increases the rate of oxidation of sulphide minerals. A waste deposit can be described as a porous media and thus the bulk flow of liquid in a saturated or unsaturated waste deposit is commonly described by Darcy's law as:

$$v_D = \frac{Q}{A} = -K\frac{dh}{dx} \qquad 13$$

where v_D is the specific discharge describing the flow through a bed at macroscopic and microscopic level and K is the hydraulic conductivity. The value of K depends on the characteristics of the material i.e. high for coarse grained material and low for fine-grained

and densely packed material. The term dh/dx is the hydraulic gradient usually expressed in terms of gradient of fluid potential which is the change in mechanical energy per unit mass of fluid as a result of flow. The fluid potential increases with height and is mathematically expressed as:

$$\varphi = gh \qquad 14$$

where g is the acceleration due to gravitation and h is the hydraulic head defined as:

$$h = z + \Psi \qquad 15$$

where z is the pressure head and Ψ is the elevation head. Water typically flows from regions of high hydraulic head to low hydraulic head. Although Darcy's law is useful in describing the steady state flow at constant hydraulic head gradient and conductivity, flow in typical disposal scenarios occurs in 3-D and is influenced by the properties of the waste deposit such as porosity, bed structure, bed packing and extent of homogeneity (Petersen, 1998).

According to Horton and Hawkins (1965), transport of water mainly occurs by downward displacement of water previously held within the pore spaces. This transport mechanism is also called "piston displacement". By using tritium tracer applied to the surface of a homogeneous column, these authors demonstrated that liquid water transport primarily occurs by "piston displacement" mechanism. These findings have been confirmed by the findings of other researchers (Warrick et al., 1971; Stephens, 1994). Furthermore, changes in the moisture content due to seasonal drying and wetting cycles also cause waste deposits to be characterised by transient flow and changing moisture content (Perkins et al., 1995; Petrie & Broadhurst, 2005).

As discussed previously, fluid flow in typical disposal scenarios occurs in 3-D. In most cases the vertical path of the fluid flow is characterised by preferential flow. Preferential flow is a term used to describe a situation in which a particular region of the waste deposit is more conductive than the surrounding material (Newman, 1999). Preferential flow can generally be divided into three types. The first type of preferential flow is called finger flow. This type of preferential flow occurs due to an unstable wetting front of a waste deposit that exhibit some degree of random distribution of pores (Luxmoore, 1991). When the wetting front approaches the coarse grained layer, water concentrates at certain locations forming coarse grained layers of finger like tongues (Fetter, 1993). Alternatively, finger flow can also occur when an infiltrating front moves through a soil underlain by an impermeable layer. When this happens, the air within the more permeable soil may be temporarily trapped between the wetting front and the less permeable strata. As the wetting front moves downwards, the trapped air gets compressed.

This impedes the downward movement of the wetting front (Latifi et al., 1994). As more water flows, both the pore pressure of the wetting front and the pressure of the compressed air increases. This process continues until bubbles of trapped air start moving upwards through the water filled pore spaces. When this happens, the infiltrating water proceeds downwards in finger-like pathways (Latifi et al., 1994).

The second type of preferential flow is called funnel flow (Kung, 1990b). This flow mechanism is mainly caused by formation of capillary breaks and impendence of downward flow of infiltrating water by the low hydraulic conductivity of the dense material. As a consequence, water flow along the slope of the interface of coarse grained layer and only travels vertically through the fine grained material at the end of the coarse grained layer interface (Kung, 1990b; Newman, 1999).

The third type of preferential flow is called macropore flow. This flow mechanism refers to the rapid movement of infiltrating water through structured soils. Macropore flow can further be divided into two categories namely short circuiting or bypass flow and macropore/micropore flow. Short circuiting or bypass flow refers to rapid movement of free water through large and continuous macropores that were initially filled with air. This flow mechanism can be significant where macropores are vertical and continuous over a significant depth (Stephens, 1994). The second type of macropore flow is called macropore/micropore flow. This flow mechanism refers to diffusion and adsorption of water from the macropore into the surrounding porous matrix (Horton & Hawkins, 1965). In this context, a macropore is defined as having a minimum radius equivalent to 0.15 cm. On the other hand, pores whose radii are less than this minimum are considered part of the porous matrix (micropores). This flow mechanism is dominant for soils containing shrinkage cracks and burrow holes (Newman, 1999). Flow of water into the micropore or porous matrix can happen when piston displacement of the antecedent water occurs (Horton & Hawkins, 1965).

Fluid flow in waste deposits is also characterised by fluid hold-up and transverse flow. Fluid hold up occurs if the pores are not connected (Petersen, 1998). This results in the formation of stagnant zones. Transverse flow is the flow of bulk liquid in the horizontal directions (Freeze & Cherry, 1979). Although, downward flow of bulk liquid is the main flow mechanism in waste deposits, transverse flow may become important particularly in tailing deposits that intersect the water table and underground water movement (Merkel & Planer-Friedrich, 2008). As the liquid flows through the pore spaces of the waste deposits, the dissolved weathering products (that include salts and other solutes) are transported along with the bulk liquid phase (Petersen, 1998; Afewu, 2009). In addition, infiltration dissolves the weathering products away from the mineral surfaces thereby exposing the fresh mineral surfaces to

further oxidation (Perkins et al., 1995). The bulk flow of fluid in a porous bed of solid particles under both partially and fully saturated disposal scenarios is shown in Figure 5.

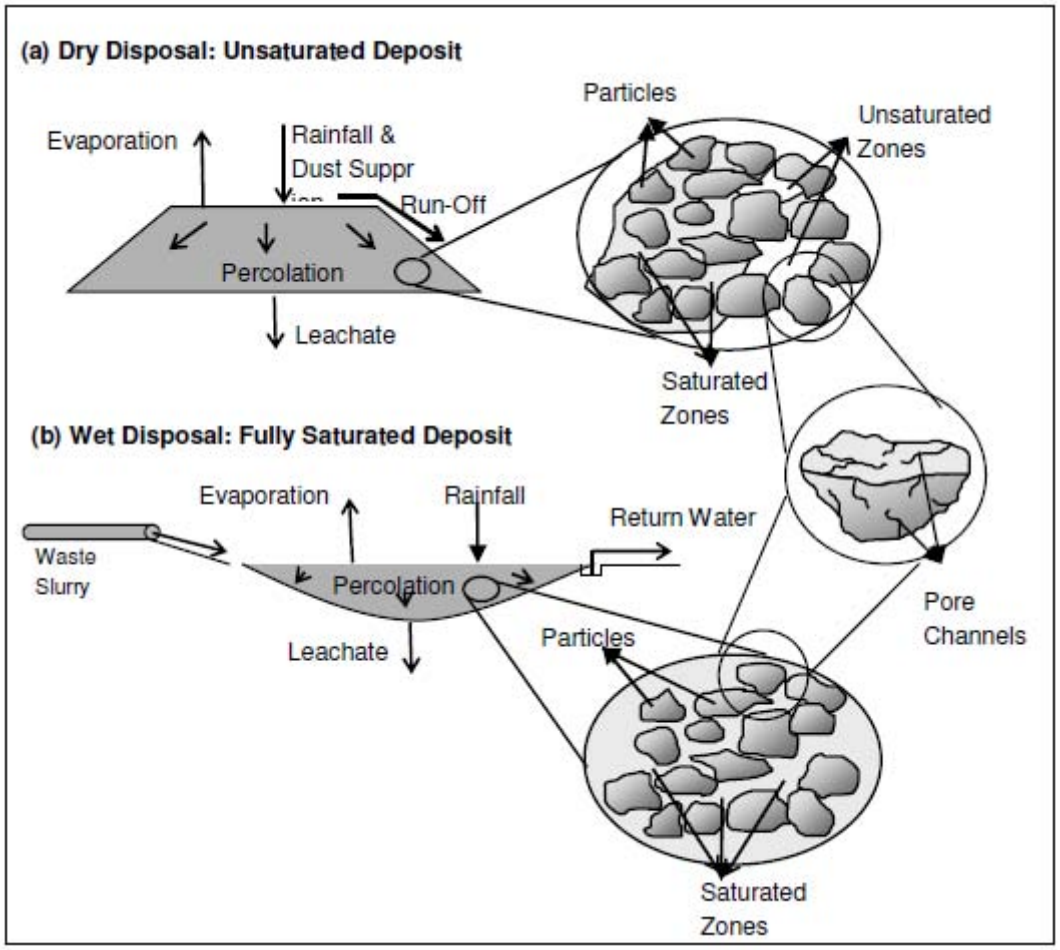

Figure 5: Bulk fluid flow through porous solid waste under (a) saturated and (b) undersaturated disposal scenarios (Petersen et al., 2000; Hansen, 2004)

2.2.2 Transport of soluble species

Solute transport involves the transport of the species dissolved in the bulk liquid. The transport of soluble species in waste deposits can take place with or within the bulk liquid phase and occurs at both the bulk deposit and particle level (Petersen, 1998).

Transport of soluble species at the bulk level

Transport of solute contaminants within the aqueous phase is governed by two main transport mechanisms namely advection and hydrodynamic dispersion (Hansen et al., 2008; Afewu, 2009).

- **Advection**

Advection is the process by which dissolved species are transported by the movement of the bulk liquid within the waste deposit (Freeze & Cherry, 1979).

The dissolved species are usually transported in the direction of the bulk liquid flow. Transport of solutes by advection is driven by hydraulic gradient and is affected by solution and waste deposit properties such as density and permeability (Afewu, 2009).

- **Hydrodynamic dispersion**

Hydrodynamic dispersion is the mixing process that occurs during bulk liquid flow when two liquids of different compositions come in contact with each other (Schwartz & Zhang, 2003). This process causes the solute front to spread to a much wider region than in pure advection transport. The spreading results in the dilution of the solute (Freeze & Cherry, 1979). Hydrodynamic dispersion is caused by two main mechanisms namely, molecular diffusion and mechanical dispersion. Molecular diffusion is the transport mechanism by which random movements of the molecules within the liquid results in the transportation of dissolved solutes from the region of higher concentration to that of lower concentration (Afewu, 2009). Molecular diffusion reduces the solute concentration by spreading the solutes uniformly throughout the bulk liquid. This process is driven by the concentration gradient and is independent of the bulk fluid flow. Molecular diffusion is the main solute transport mechanism at low fluid velocities and in stagnant zones or “dead pore” ends. However, at high velocity bulk fluid flow, the effects of diffusion are negligible. As such, the transport of solutes is dominated by advection (Afewu, 2009). Mechanical dispersion on the other hand is a process by which dissolved solutes are transported due to microscopic mechanical processes that take place when a fluid flows through the pores of a waste deposit (Petersen, 1998). As the fluid flows through the pore spaces, the solutes spread normal to the flow path as well as along the flow path. In most cases, the magnitude of dispersion is much stronger in the direction of flow than normal to the flow path (Freeze & Cherry, 1979; Zheng & Bennett, 2002).

The spreading of the fluid in the direction of the fluid flow is called longitudinal dispersion (LD) while the spreading in the direction normal to the fluid flow is called transverse dispersion (TD) (Petersen, 1998; Afewu, 2009). It is generally agreed that mechanical dispersion is governed by three main mechanisms (Petersen, 1998; Hansen, 2004; Afewu, 2009). These mechanisms are discussed below.

(a) Dispersion due to fluid velocity differences between individual pores of the waste deposit: Pore surface roughness creates a resistance that causes molecules near the surfaces of the pores to move at a much lower velocity than those far away from the pore surfaces. Hence, the velocity is maximum at the centre of the pores and minimum at the pore surfaces.

(b) Dispersion due to velocity differences along the flow path: This is caused by differences in pore shapes, surface area and sizes.

(c) Mixing effects due to fluctuations of the fluid flow paths: This is caused by tortuosity, branching and merging of pore channels.

The fluid velocities are higher in large pores than in small pores. The velocity is zero in stagnant zones or “dead pore” ends. These mechanisms are illustrated in Figure 6.

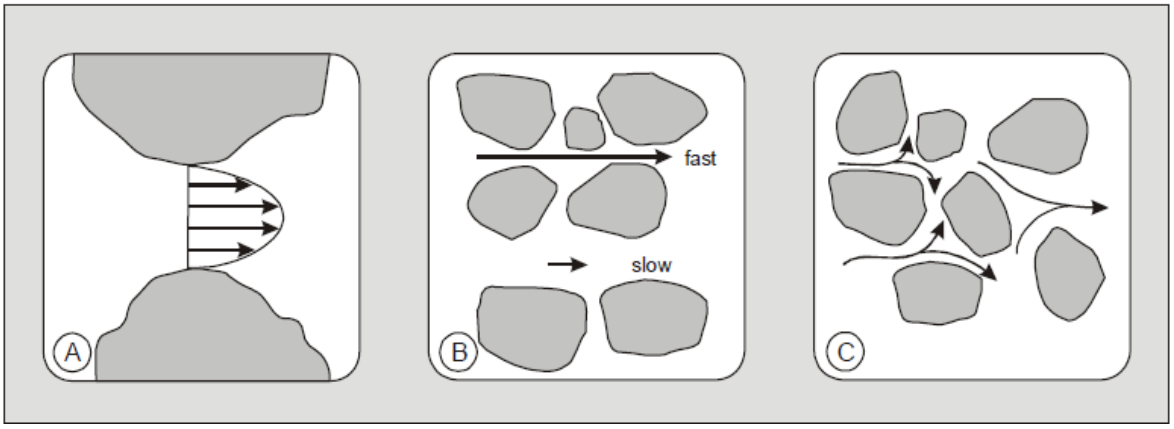

Figure 6: Mechanical dispersion due to: (a) velocity profiles in pores ;(b) distribution of flow velocities; (c) branching and merging of pores (Hansen, 2004)

Unlike diffusion, mechanical dispersion depends on the bulk fluid flow. This transport mechanism is dominant when the liquid velocity is high.

Transport of soluble species at particle level

At the particle level, the transport of solutes is mainly driven by molecular diffusion (Mayer et al., 2002). Mineral particles in the saturated media are surrounded by two layers, namely the stagnant liquid film and the leached layer (Perkins et al., 1995; Mayer et al., 2002). According to Perkins et al. (1995), intraparticle diffusion begins with the diffusion of oxidants from the bulk liquid to the mineral surface across the stagnant water film and the leached layer. Thereafter, the oxidants are adsorbed to the mineral surfaces. At the mineral surface, the oxidant (oxygen or bacteria) oxidises the ferrous to ferric iron that in turn becomes the main oxidant for the sulphide bearing mineral (Hansen, 2004). The reaction products from the reactive sites are transported by diffusion to the surface of the solid. This is followed by desorption of products from the mineral surface. Finally, the reaction products diffuse through the leached layer and the stagnant water film to the bulk solution (Mayer et al., 2002). The rate of diffusion of the reactant products is highly dependent on the availability and thickness of the leached layer, with the slowest of these processes becoming the rate controlling step in the generation of ARD (Perkins et al., 1995; Nicholson et al., 2003). In the generation of ARD, the oxidation of sulphide minerals is diffusion controlled if the consumption of oxygen in the pore spaces of the waste deposit is higher than its diffusion to the reaction site (Davis & Ritchie, 1986; Nicholson et al., 2003). On the other hand, the oxidation of sulphide minerals become surface controlled if the supply of oxygen to the

oxidation sites is higher than its consumption. The main diffusion processes at particle level are illustrated diagrammatically in Figure 7.

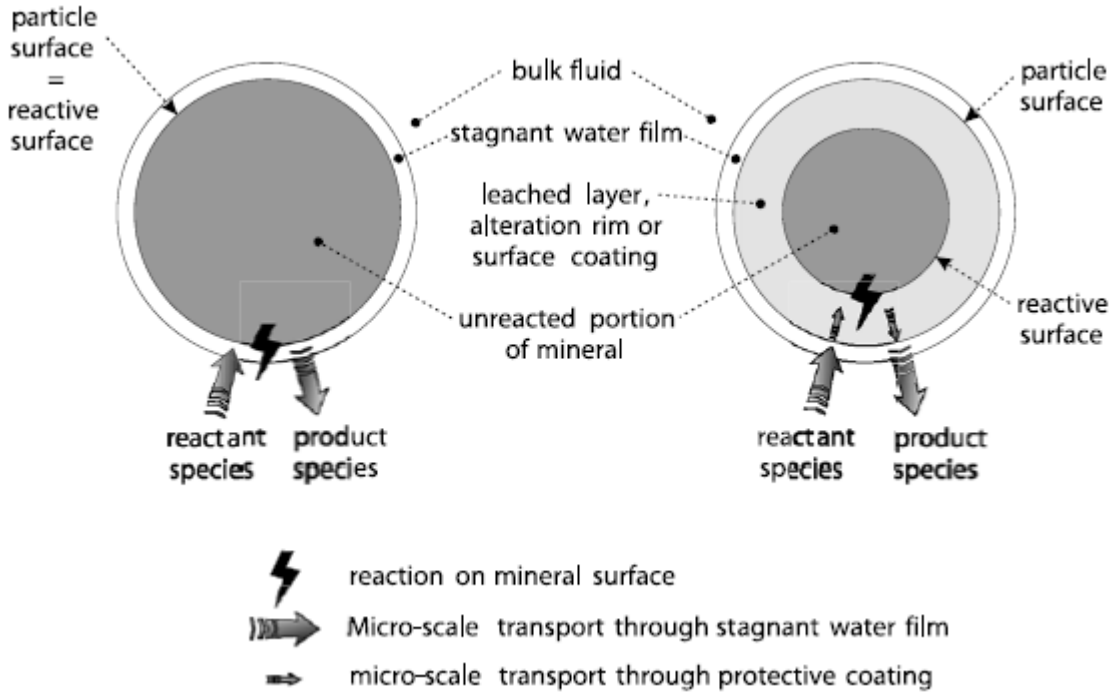

Figure 7: Intraparticle diffusion on the mineral particle surface (Mayer et al., 2002)

2.2.3 Microbial transport and attachment

As mentioned in section 2.1.1, microorganisms play a major role in the generation of ARD by catalysing iron and sulphur oxidising reactions. The presence of microorganisms on mineral surfaces depends to a large extent on their transportation and attachment. Microorganisms are usually present as free cells in the liquid phase or as strongly or weakly attached cells on mineral surfaces. Microorganisms present in the mobile region of the liquid phase are known as planktonic PLS (pregnant leach solution) cells while those in the immobile region are called interstitial cells (Chiume et al., 2012). The transport of microorganisms in waste deposits is closely related to the transport of the bulk liquid that is mainly driven by hydraulic pressure gradient, porosity and permeability distribution (Ginn et al., 2002). Microbial transport occurs within the liquid and the biofilm phases and is governed by a complex network of physical, biological and electrostatic and chemical processes (Ginn et al., 2002).

The distribution of microorganism in the different regions of the waste deposits is illustrated in Figure 8.

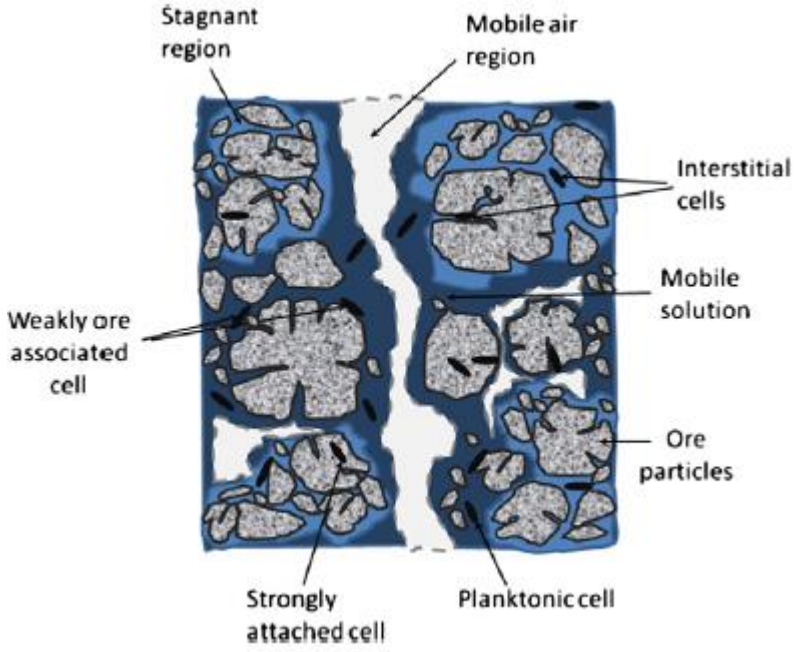

Figure 8: Distribution of microorganisms within the liquid phase and mineral surfaces (Chiume et al., 2012)

- **Physical processes**

Microbial transport in the liquid phase is mainly governed by physical processes such as advection, hydrodynamic dispersion, molecular diffusion, straining and physical filtration (Ginn et al., 2002). Advection involves the transportation of the microorganisms as particulates or as dissolved species with the bulk liquid. Hydrodynamic dispersion involves the spreading of microorganisms in the water path while molecular diffusion involves movement of microorganisms due to concentration gradients.

Generally, microorganisms migrate from regions of high cell concentration to those of lower cell concentration (Ginn et al., 2002). Advection and hydrodynamic dispersion are the main transport mechanisms for microorganisms in the mobile liquid phase while diffusion is the main transport mechanism for microorganisms in the immobile liquid phase (Jamal et al., 1994). Straining and filtration involves the removal of microorganisms from the liquid phase by physical forces. This can occur through either trapping of large microorganisms on pore openings (straining) or through collision of microorganisms with the surface (physical filtration).

Straining is particularly common for larger microorganism (Jamal et al., 1994; Ginn et al., 2002). Other processes governing the transport of microorganisms in the liquid phase include size exclusion, adsorption/desorption and sedimentation.

Size exclusion occurs when transported microorganisms move at a velocity faster than that of the pore water. Exclusion has been reported to increase the velocity of microorganism by as much as 70% greater than the average pore water velocity (Ginn et al., 2002). Adsorption/desorption involves the attachment and detachment of microorganisms to surfaces while sedimentation involves the settling of the particles that are too large to float on the moving water (Jamal et al., 1994; Ginn et al., 2002). These processes can either accelerate or retard the transportation of microorganisms.

- **Biological processes**

Unlike transport of microorganisms in the liquid phase that is mainly driven by physical processes, transport of microorganisms within the biofilm phase is mainly influenced by biological processes. These include microbial growth, decay, active adhesion/detachment and motility (Jamal et al., 1994; Ginn et al., 2002). The growth, decay and motility of microorganisms depend on the environmental conditions, such as temperature and availability of oxygen and nutrients. Microbial growth and decay results in microbial concentration changes that in turn affect their transport (Jamal et al., 1994). Active advection/detachment is a biologically driven process in which microorganisms either attach to, or detach from, a surface in response to nutrients. Motility, on the other hand, involves the migration of microorganisms towards the source of nutrients. This transport mechanism is commonly referred to as chemotaxis. Chemotaxis is common in areas with scarce nutrients (Ginn et al., 2002). The extent of chemotaxis by microbes depends on the nutrients to which they are attracted.

- **Microbial attachment and detachment**

Transport of microorganisms is also affected by microbial attachment to, and detachment from, solid surfaces. The attachment of microbes is initiated by their transport to the vicinity of mineral surfaces, mainly by advection, hydrodynamic dispersion, molecular diffusion and chemotaxis (van Loosdrecht et al., 1990). Initial attachment occurs by either reversible or irreversible adhesion. Adhesion of microbes to mineral surfaces is governed by electrostatic and hydrophobic forces between the microbes and mineral surfaces (Ginn et al., 2002; Africa et al., 2010). Reversible adhesion results in weak attachment and limited growth of microbes. In most cases, growth will only occur to obtain equilibrium between the attached and the non-attached microbes. The non-attached microbes may either be in the flowing liquid or in the stagnant liquid. Irreversible adhesion, on the other hand, result in the formation of extracellular polymeric substances (EPS) which envelope the microbes.

This results in strong attachment between the microbes and the minerals surfaces. Strongly attached microbes grow and form biofilms within the EPS (van Loosdrecht et al., 1990).

Studies by Africa et al. (2010) and Chiume et al. (2012) have shown that attachment of microbes to mineral surfaces occurs preferentially. Generally, microorganisms strongly associated with the waste are strongly attached (irreversible) while those that are loosely associated with the waste are weakly attached (reversible). For instance, *Acidithiobacillus ferrooxidans* are preferentially attached to sulphide minerals than gangue minerals (Jamal et al., 1994; Chiume et al., 2012). In addition, attachment of microbes mainly occurs on irregular mineral sites (Africa et al., 2010). Following the attachment of microbes to mineral surfaces, colonisation occurs with microbes growing within the EPS layer (Ghauri et al., 2007). Generally, weakly attached microorganisms are more likely to be detached by shear stress due to fluid flow than strongly attached microbes (Chiume et al., 2012).

2.2.4 Oxygen transport

As mentioned previously, oxygen transport in waste deposits is an important physical process because of its role in the oxidation of sulphide minerals and the survival of iron and sulphur oxidising microorganisms that catalyse ARD reactions. Oxygen transport can occur in the gas or in the liquid phase.

Oxygen transport in the gas phase

The transportation of oxygen in the gas phase occurs mainly by diffusion and advection. Oxygen transport by diffusion occurs due to the oxidation of sulphide minerals that creates a concentration gradient causing oxygen to diffuse from the bulk gas phase (atmosphere) into the oxygen depleted pore spaces of the waste deposit. Diffusion is a dominant oxygen transport mechanism in mill tailings due to their highly reactive surfaces that lead to high oxygen concentration gradients (Lefebvre et al., 2001a; Wels et al., 2003). Oxygen transport by advection, on the other hand, occurs due to bulk movement of the flowing air. Advection is a more efficient oxygen transport mechanism than diffusion. The transport of oxygen by advection in the gaseous phase is generally divided into two categories, namely advection by thermal gradient and advection due to barometric pumping. Thermal gradient advection transport of oxygen is driven by the convective current of air arising from the increase in temperature due to the oxidation of sulphide minerals within the waste deposit. The convective current can also be caused by the wind pressure gradient between the atmosphere and the interior pores of the waste deposits (Wels et al., 2003). The hot air with reduced density rises and exits through the surface of the waste deposit thereby allowing the flow of air into the pores of the waste deposit.

The amount of air transported by thermal advection is highly dependent on the coarseness of the particles (air permeability) and the geometry of the waste deposit.

Generally, the advection transport of air is high in coarse waste rock and less in fine mill tailings (Lefebvre et al., 2001a). Advection flow of air is also influenced by the height and the width of the waste deposit. The transport of air by advection increases as the height to width ratio of the waste deposit increases (Wels et al., 2003). Air transport by thermal gradient is also influenced by the mode of waste placement. As an example, waste piles with inclined slopes are more likely to form highly permeable channels that result in an increased transport of air due to thermal gradient (Wels et al., 2003). On the other hand, advection by barometric pumping occurs due to the compression of the air within the waste deposit as a result of changes in gas pressure and composition. The compression of air within the waste deposit creates a vacuum that causes air to flow from the atmosphere. Generally, oxygen transport by barometric pumping increases with an increase in the barometric pressure. The circumstances under which oxygen is transferred by barometric pumping are not yet fully understood (Wels et al., 2003). Unlike advection transport by thermal gradient, advection by barometric pumping is highly influenced by variation of ambient air pressure, air permeability, heterogeneity within the waste deposit and porosity (Wels et al., 2003).

Oxygen transport in the liquid phase

Within the waste deposit, oxygen is transported from the air in the pore spaces into the aqueous phase. The transfer of oxygen from the gas phase into the liquid phase also called the oxygen gas-liquid mass transfer is mainly driven by temperature, gas and liquid composition and gas-liquid interfacial area (Petersen, 2010a). Generally, the mass-liquid mass transfer is expressed mathematically using Newton's law of cooling as:

$$r_{O_2}ads = k_L a\,(C^* - C_b) \qquad 16$$

where $k_L a$ is the lumped mass transfer coefficient (incorporating specific gas–liquid surface area a, hydrodynamics and effective film thickness), C* is the equilibrium concentration of oxygen at the gas-liquid interface and C_b is the bulk concentration of oxygen in the solution.
Besides the gas-liquid mass transfer rate, the amount of dissolved oxygen depends on its solubility and consumption rate at the oxidation sites. The solubility of oxygen in the aqueous phase mainly depends on temperature, oxygen partial pressure in the gas phase and the inorganic electrolyte solute. Generally, the solubility of oxygen in the aqueous phase decreases with an increase in temperature due to water vapour effect (Galaction et al., 2004; Petersen, 2010a). In the aqueous phase, dissolved oxygen is transported by both advection and diffusion to oxidation sites.

Advection involves the transfer of oxygen due to the bulk movement of the flowing liquid. The transport of oxygen by advection is controlled by all the factors influencing the bulk movement of the liquid within the waste deposit. Unlike advection, oxygen transport by diffusion is independent of the bulk liquid flow. The consumption of oxygen at the mineral surfaces creates an oxygen gradient between the bulk liquid and the mineral surface. This causes oxygen to flow from the bulk liquid to the mineral surface by diffusion. By comparison, the transport of oxygen is more efficient in the gas phase than the liquid phase (Lefebvre et al., 2001a).

2.2.5 Heat transport

The oxidation of sulphide minerals such as pyrite is a strongly exothermic reaction that generates large amounts of heat. Lefebvre et al. (2001a) report that about 1409kJ of heat is produced for every mole of pyrite oxidised. Temperatures in waste deposits have been reported to be as high as 70°C (Gelinas et al., 1994).

The generated heat plays a critical role in the overall generation of ARD due to its effect on the transport of oxygen and the kinetics of microbially catalysed sulphide oxidation processes (Wels et al., 2003). The heat generated by the oxidation of sulphide minerals raises the temperature, thereby creating ideal conditions for the activities of the sulphur and iron oxidising microorganisms. Ideal conditions for microbial activities are in the range of 25 to 45ºC although some mesophiles are reported to thrive at temperatures of between 60 and 80ºC degrees (Lefebvre et al., 2001a).

Mechanisms of heat transfer in waste deposits

The heat generated by the oxidation of sulphide minerals within the waste deposits is transported by conduction, advection and diffusion (Wels et al., 2003). These heat transport mechanisms are discussed below;

- **Heat transport by conduction and diffusion**

Head transport by conduction through the material of the waste deposit occurs as high energy atoms in physical contact with each other vibrate and transfer energy (heat) to the neighbouring atoms. Conduction heat transport is driven by the temperature gradient through the waste material and is independent of mass transport (Herasymuik, 1996). Heat travels from regions of higher temperature to regions of lower temperature. The amount of heat flux is directly proportional to the magnitude of the temperature gradient. Conduction heat transport is controlled by a number of factors that include the geometry of the waste deposit, rate of heat generation, material conductivity, climatic conditions and physical

characteristics of the waste, for example particle size and distribution (Lefebvre et al., 2001a).

- **Heat transport by advection**

Heat transport by advection occurs by movement of molecules with high energy (heat) from one place to another by the bulk movement of the fluids (liquid or gas). Heat transport by advection also occurs by latent heat transfer (Lefebvre et al., 2001a). This occurs through the release or consumption of heat as the water changes from one phase to another. As a result, heat is transferred through the movement of the water vapour (Herasymuik, 1996). The amount of heat transferred through advection depends on the bulk flow of the air or liquid within the waste deposit (Lefebvre et al., 2001a). Thus, all the factors controlling the advection transport of air and water are responsible for the advection transport of heat.

- **Heat transport by diffusion**

Heat transport by diffusion is independent of the bulk movement of fluids (liquid and air) and occur by movement of high energy molecules (high heat) from regions of high heat to those of low heat. Like heat transport by conduction, heat transport by diffusion is driven by the temperature gradient across the diffusion path (gas or liquid). Due to the high temperature arising from the exothermic oxidation reactions, a temperature gradient is created between the hot air (or water) within the waste deposit and the cold air (or water) outside the waste deposit. This causes heat to be transported across the diffusion path from the region of high temperature to the region of low temperature (Lefebvre et al., 2001a). The amount of heat transferred by diffusion depends on the temperature gradient (Wels et al., 2003). Generally, diffusion heat transport is influenced by permeability, rate of heat generation, climate conditions and the internal structure and anisotropy of the waste deposit (Lefebvre et al., 2001a). As an example, the rate of heat transfer by diffusion is likely to increase during winter months due to an increase in the temperature gradient between the hot air inside the pores of the waste deposit and cold atmospheric air outside the deposit (Herasymuik, 1996; Wels et al., 2003). This results in an increased flow of hot air from the internal pores of the waste deposit to the outside. In contrast, the rate of heat transport is likely to reduce during summer months due to reduced temperature gradient.

2.3 The PHREEQC modelling code for simulating acid rock drainage

Numerous codes have been developed for modelling processes governing the generation of ARD in mine waste (Davis & Ritchie, 1986; Perkins et al., 1995; Crawford, 1999; Mayer et al., 2002; Maest et al., 2005). Some of these codes have been briefly described in the introduction. As earlier discussed in section 1.1.3 of Chapter 1, PHREEQC code is a widely used geochemical code with a wide range of capabilities.

PHREEQC code has capabilities to simulate many of the chemical and physical processes governing the generation of ARD described in sections 2.1 and 2.2. More specifically, the code has capabilities for simulating equilibrium controlled reactions (such as precipitation/dissolution, adsorption/desorption, speciation and solution saturation) and kinetically controlled reactions (such as oxidation of sulphide minerals and dissolution of carbonate and aluminosilicate minerals). Furthermore, the code has capabilities to simulate one-dimensional mass transport in the saturated media by pure advection as well as advection with dispersion and diffusion of dissolved species to stagnant zones. The model also accounts for heat transport in the saturated zone by diffusion (Parkhurst & Appelo, 1999). The capabilities, as well as the limitations of the PHREEQC code, in so far as they are of relevance to this study, are described and discussed in sections 2.3.1 to 2.3.4 below.

2.3.1 Aqueous model

The aqueous model is used for the simulation of interaction of species within the aqueous phase. The processes simulated include aqueous speciation, saturation indices calculation, complexation, redox processes and activity calculation. These processes are described in more detail in the sub-sections below.

Aqueous speciation and saturation indices calculation

Aqueous speciation is the most common type of geochemical modelling activity because of the link between the activities of aqueous species and their reactivity (Merkel & Planer-Friedrich, 2008). Aqueous speciation and saturation indices calculations is used to determine the distribution of species, their activities, redox state and degree of saturation within the aqueous phase. All species dissolved in the aqueous phase exist as free ions or complexes.

The total concentration of dissolved species is made up of both the free and complexed species (Herbert, 1996). The activities of dissolved species is related to their equilibrium constant of formation by the law of mass action equation as shown in Equations 17 and 18.

$$aM^{m+}_{(aq)} + bL^{l-}_{(aq)} = M_a\,L^{q}_{b(aq)} \quad 17$$

$$K_f = \frac{[M_a L_b^q]}{[M^{m+}]^q[L^{1-}]^b} \quad 18$$

where K_f is the equilibrium constant of formation and gives information about the stability of the complex. A high value of K_f indicates a high stability and high tendency for the formation of the complex. The other terms are the activities of the products and reactants as indicated. Generally, complexes are made up of positively charged and negatively charged ions. The positively charged ion is usually a metal or hydrogen ion while the negatively charged ion is usually a ligand (Herbert, 1996). Ligands exist as free ions or negatively charged complexes (e.g. SO_4^{2-}). All dissolved species are assumed to be in thermodynamic equilibrium among themselves except for redox elements where partial disequilibrium is allowed in initial solution calculations (Parkhurst & Appelo, 1999). Generally, equilibrium in a multicomponent system consisting of water, coexisting species, minerals and gases is described by a set of nonlinear Equations 19 to 22 with the variables in the equations described in Table 9.

$$M_w = n_w\left\{55.5 + \sum_j \frac{v_{wj}}{K_{j\gamma j}}\left[a_w^{v_{wj}}.\prod^{i}(\gamma_i m_i)^{v_{ij}}.\prod^{k} a_k^{v_{kj}}.\prod^{m} f_m^{v_{mj}}\right]\right\} \quad 19$$

$$M_i = n_w\left\{m_i + \sum_j \frac{v_{ij}}{K_{j\gamma j}}\left[a_w^{v_{wj}}.\prod^{i}(\gamma_i m_i)^{v_{ij}}.\prod^{k} a_k^{v_{kj}}.\prod^{m} f_m^{v_{mj}}\right]\right\} \quad 20$$

$$M_k = n_k + n_w\sum_j \frac{v_{kj}}{K_{j\gamma j}}\left[a_w^{v_{wj}}.\prod^{i}(\gamma_i m_i)^{v_{ij}}.\prod^{k} a_k^{v_{kj}}.\prod^{m} f_m^{v_{mj}}\right] \quad 21$$

$$M_m = n_w\sum_j \frac{v_{mj}}{K_{j\gamma j}}\left[a_w^{v_{wj}}.\prod^{i}(\gamma_i m_i)^{v_{ij}}.\prod^{k} a_k^{v_{kj}}.\prod^{m} f_m^{v_{mj}}\right] \quad 22$$

Table 9: Variables in the governing equations

Bulk composition, moles		Solvent mass,molalities,mole number	
M_w	Water component	n_w	Solvent mass,kg
M_i	Species component	m_i	Molarities of basic species
M_k	Mineral component	m_j	Molarities of secondary species
M_m	Gas component	n_k	Mole number of minerals
Activities and fugacities		Activity coefficient	
a_w	Water activity	γ_i	Basis species
a_i	Activities of basic species	γ_j	Secondary species
a_j	Activities of secondary species		
a_k	Mineral activities		
f_m	Gas fugacities		
Reaction coefficients		Equilibrium constants	
v_{wj}, v_{ij}, v_{kj}	Secondary species	K_j	Secondary species
v_{wl}, v_{il}, v_{kl}	Minerals	K_l	Minerals
v_{wn}, v_{in}, v_{kn}	Gases	K_n	Gases

In the equations above, a component is defined as a mathematical tool used to describe composition while a basis components refers to the minimum set of thermodynamic components used to describe composition. Typically, a basis is comprised of a solvent (e.g. water), gaseous species, aqueous species and a mineral in equilibrium with the system of interest. The basis species are the fundamental species that describe all the species that are found in the system while the secondary species are the species that are derived from the fundamental species. The main unknowns in the above equations are the mass of water n_w, the concentration m_i of the basis species and the mole number n_k of the mineral. These equations are solved using the Newton-Raphson method (Bethke, 2008). The equilibrium between the aqueous and the solid and gas phases are further described in section 2.3.2.

Redox processes

Reduction-oxidation reactions (Redox) involve the transfer of electrons or oxygen from one species to another (Merkel & Planer-Friedrich, 2008). Generally redox reactions are written as:

$$\{\text{Oxidised species}\} + n\,.\{e^-\} = \{\text{reduced species}\} \qquad 23$$

where n is the number of electrons e. In the PHREEQC code, redox reactions are assumed to be instantaneous and the redox couples are assumed to be in equilibrium with each other. This assumption may not always be valid as some redox reactions are slow and equilibrium is rarely attained. However, in most cases, redox reactions are microbially catalysed and therefore assumed to be fast (Herbert, 1996; Parkhurst & Appelo, 1999; Merkel & Planer-Friedrich, 2008). Generally, the redox potential is calculated from the Nernst equation as:

$$E_h = E^0 + \frac{R.T}{n.F} \ln \frac{\{ox\}}{\{red\}} \qquad 24$$

where, E^0 is the standard redox potential of a system, R is the ideal gas constant (8.3144 J $K^{-1}mol^{-1}$), T is the absolute temperature (K), n is the number of transferred electrons (e^-), F is the Faraday constant (96484 C/mol = J V^{-1} mol^{-1}), {ox} is the activity of the oxidized species while {red} is the activity of the reduced species. In the PHREEQC code, the redox potential is expressed as electron activity (pe). Usually, the electron activity is calculated from the ratio of the activities of the specified redox couple; however, if no redox couple is specified, the electron activity is calculated using the default redox couple (O (-2)/O (0)) (Parkhurst & Appelo, 1999). The electron activity (pe) is calculated as:

$$pe = -\log\{e^-\} = \frac{F}{2.303 \times T \times R} \times EH \qquad 25$$

And at 25ºC, pe is expressed as:

$\mathrm{pe} \approx 16.9\mathrm{EH}$, where EH is in V

The calculated pe is used for the distribution of all the redox sensitive elements. The value of pe indicates the oxidation state of the solution. Low pe means the solution is reducing while a high pe means the solution is oxidising (Merkel & Planer-Friedrich, 2008).

Activity

The concentration (molarity) and activity of species i dissolved in the aqueous phase a_i are related to each other as shown in Equation 26:

$$\mathrm{a_i} = \gamma_\mathrm{i} \mathrm{m_i} \qquad 26$$

where γ_i and $\mathrm{m_i}$ are the activity coefficient and molar concentration of species i respectively. In an ideal dilute solution, the value of the activity coefficient would be equal to 1. In this case, the activity of the dissolved species i would be equal to its concentration. However, most of the solutions encountered in everyday life are not dilute, thus the activity coefficient must be estimated (Parkhurst & Appelo, 1999). As the ionic strength increases due to the interaction amongst the solutes, the activity coefficient deviates from ideality. The activity coefficient and ionic strength of dilute water is approximately 1M and <0.1M respectively. Different models are used to predict the activity coefficient for non-dilute solutions (Herbert, 1996; Merkel & Planer-Friedrich, 2008). In the PHREEQC code, the activity coefficients of all the charged species are calculated using the Davies equation. For a dissolved species i, the activity coefficient is calculated as shown in Equation 27:

$$\log\gamma_\mathrm{i} = -\mathrm{A}\mathrm{Z}_\mathrm{i}^2 \left(\frac{\sqrt{\mu}}{1+\sqrt{\mu}} - 0.3\mu \right), \qquad 27$$

where A is a temperature dependent constant,Z_i is the ionic charge of the dissolved species i and μ is the ionic strength of the solution calculated using Equation 28 below;

$$\mu = \frac{1}{2} \sum_{\mathrm{i}}^{\mathrm{N_{aq}}} \mathrm{z_i^2} \frac{\mathrm{n_i}}{\mathrm{W_{aq}}} \qquad 28$$

where $\mathrm{N_{aq}}$ is the number of aqueous species, $\mathrm{Z_i}$ is the ionic charge of the dissolved species i,$\mathrm{W_{aq}}$ is the mass of solvent water in an aqueous solution and n_i is the number of moles in solution. For uncharged species, PHREEQC uses the Setchenow equation (WATEQ Debye-Huckel equation without first term) shown in Equation 29.

$$\mathrm{In}\gamma_i = b_i\,\mu \qquad 29$$

Where b_i is assumed to be 0.1 for all uncharged species (Parkhurst & Appelo, 1999).

Limitations of the aqueous model

In the first place, the aqueous model is applicable only up to an ionic strength of about 0.7 mol dm^{-3} (Parkhurst & Appelo, 1999; Merkel & Planer-Friedrich, 2008).

With the exception of sodium chloride dominated waters, the model breaks down at ionic strength higher than 0.7 mol dm^{-3}. The applicability of the aqueous model can be extended by using approaches that account for the interaction of aqueous solutions at high ionic strength. Fortunately, the ionic strength of most of the solutions encountered in acid rock drainage environments is much lower than 0.7 mol dm^{-3} (Parkhurst & Appelo, 1999). Secondly, the internal consistence of the thermodynamic database to the code has not been verified. PHREEQC database (equilibrium constants and enthalpies of formation) draws data from various databases including phreeqc.dat, minteq.dat and wateq4f.dat. These databases are consistent with other programs for example phreeqc.dat and wateq4f.dat are consistent with the aqueous model of WATEQ4F (Ball & Nordstrom, 1991) and the compilation of Nordstrom et al. (1990), while minteq.dat is consistent with the aqueous model of MINTEQA2 (Allison et al., 1990). The aqueous models used to derive these databases have not been verified and their consistence with the original experimental data is uncertain (Perkins et al., 1995; Parkhurst & Appelo, 1999).

2.3.2 Chemical equilibrium model

In the PHREEQC code, the equilibrium between the aqueous and the solid and gas phases is described using the chemical equilibrium model. The chemical equilibrium model is used to simulate reversible heterogeneous reactions between solid or gas phase assemblages and the aqueous phase (Parkhurst & Appelo, 1999). The main equilibrium controlled reactions that occur in mine waste are adsorption/sorption and the precipitation/dissolution reactions. However, only precipitation and dissolution reaction are discussed here due to their relevance to this study.

Equilibrium with the solid phase

Minerals either dissolve or precipitate in order to attain equilibrium with the aqueous phase. These precipitation and dissolution reactions occur at a much slower rate than complexation reactions (Herbert, 1996). The dissolution of the mineral ML into components M and L is represented by the mass action law as shown in Equation 30.

$$M_aL_{b(s)} \leftrightarrow aM^{m+}_{(aq)} + bL^{1-}_{(aq)} \quad 30$$

$$K_{dis} = \frac{[M^{m+}]^a[L^{1-}]^b}{[M_aL_b]} \quad 31$$

Where K_{dis} is the equilibrium dissolution constant and the brackets represents the activities of the products and mineral ML respectively. Equation 31 can further be simplified as:

$$K_{sp} = K_{dis}[M_aL_b] \quad 32$$

If the solid mineral is assumed to be in its standard form (pure), its activity can be assumed to be equal to 1 (i.e. $[M_aL_b] = 1$). Thus, the equilibrium dissolution constant and the equilibrium solubility constant becomes the same.

$K_{dis} = K_{sp}$

A higher value of solubility constant indicates higher solubility while a lower value indicates low solubility. The saturation index of each mineral is therefore defined as:

$$SI = \log\frac{IAP}{K_{sp}} \quad 33$$

where IAP is the ionic activity product and K_{sp} is the equilibrium solubility constant (product of ion activities).The saturation index indicates if the solution is undersaturated, oversaturated or at equilibrium with respect to a particular solid. A saturation index of less than zero (SI < 0) means that the system is undersaturated while the saturation index of greater than zero (SI > 0) means that the system is oversaturated. Lastly, the system is at equilibrium if the saturation index is equal to zero (SI=0). The saturation indices generally show the degree of saturation of a system.

Equilibrium with the gas phase

The amount of a gas that dissolves in the aqueous phase at a known pressure and temperature is calculated using the Linear Henry's law coefficient (Merkel & Planer-Friedrich, 2008). The partial pressure of each gas component is assumed to be equal to its activity (assumes ideal gas behaviour). The Henry's law coefficient is used to relate the partial pressure of a gas to its activity in the aqueous phase as:

$$a_i = K_{Hi} \times pi \quad 34$$

where

a_i = fugacity (activity) of the gas (mol dm^{-3}).

K_{Hi} = Henry constant of the gas i.
pi = partial pressure of the gas i (kPa).

In general, the partial pressure of a gas is related to the activity of the aqueous phase in accordance with Equation 35.

$$P_g = \frac{1}{K_g}\prod_{m}^{M_{aq}} a_m^{C_{m,g}} \qquad 35$$

Where P_g is the partial pressure of gas component g, M_{aq} is the total number of aqueous master species, K_g is the Henry's law constant for the gas component g, C_{mg} is the stoichiometric coefficient of the aqueous master species of gas component g in the dissolution reaction while a_m is the activity of the aqueous master species. The value of $C_{m,g}$ may either be negative or positive. As an example, if an ideal gas law assumption is used, the partial pressure of atmospheric carbon dioxide can be related to the activity of aqueous carbon dioxide at equilibrium using Henry's law as:

$$P_{CO_{2(g)}} = 10^{1.468} a_{CO_{2(aq)}} \qquad 36$$

where P_{CO_2} (atm) is the partial pressure calculated using activities in the aqueous phase and $10^{1.468}$ (atm) is the Henry's law constant for carbon dioxide.

Limitations of the chemical equilibrium model

The main limitations of the chemical equilibrium model relates to the selection of appropriate secondary minerals and their respective solubility constants. Since the approach of secondary mineral selection is such that only secondary minerals with positive saturation indices are considered, minerals that precipitate and re-dissolve before attaining equilibrium may not be accounted for. The other limitation relates to the selection of the solubility constant to be included in the model. Due to the large number of solubility constants reported in literature, the selection of the suitable constant highly depends on the user. Other limitations involve the cases where the model predicts precipitation of secondary minerals that are not likely to form due to unfavourable experimental conditions. In such cases, the onus is on the user to decide the secondary minerals that should be allowed to precipitate. Model application is thus subject to the knowledge and judgement of the operator.

2.3.3 Kinetic model

The kinetic model is used to simulate chemical reactions that do not attain equilibrium within the experimental or model time frames.

These reactions include the dissolution of minerals and other solid reactants. Simple cases of kinetically controlled homogeneous reactions can also be simulated (Parkhurst & Appelo, 1999). In the PHREEQC code, all kinetic reactions are represented by appropriate rate laws and rate constants. Different rate laws and rate constants have been published for various sets of reactions under specific conditions (Hodson et al., 1998; Palandri & Kharaka, 2004; Andre, 2009; White, 2011).

However, since rate laws differ from one condition to another, the PHREEQC code has included an embedded basic interpreter in its program that allows the formulation of user defined rate expressions for the kinetic reactions in the input file. These rates are integrated over the time interval specified by the user while the changes in the concentration of the solution and reaction rates are accounted for (Parkhurst & Appelo, 1999).

Mathematical description

Generally, the change in the concentration of an aqueous species i as a result of a kinetically controlled reaction is expressed as:

$$\frac{\mathrm{dm_i}}{\mathrm{dt}} = \mathrm{C_{i,min}}\ \ \mathrm{R_{min}} \qquad 37$$

where $C_{i,min}$ is the stoichiometric coefficient of species i in the kinetic reaction and R_{min} is the overall reaction rate for the mineral (mol m^{-2} s^{-1}). The differential equations that describe the kinetic reactions in PHREEQC are solved by the Runge-Kutta (RK) algorithm which integrates the rates over time. By defining the error tolerance in the input file, the Runge-Kutta automatically increases or decreases the time interval to maintain the error within a given tolerance. In PHREEQC code, the dissolution expression of mineral or solid reactants is written as:

$$\mathrm{R_{min}} = \mathrm{r_{min}} \times \left(\frac{\mathrm{A_0}}{\mathrm{V}}\right) \times \left(\frac{\mathrm{m}}{\mathrm{m_0}}\right)^{\mathrm{n}} \times (1 - \mathrm{SR"mineral"}) \qquad 38$$

where $\mathrm{r_{min}}$ is the specific reaction rate for the mineral (mol $dm^{-2}s^{-1}$), (A_0/V) is the initial mineral surface area (m^2) per solution volume (dm^3), $\mathrm{m_0}$ is the initial moles of solids, while m is the moles of solids at any given time.

At the beginning of the simulation, m and $\mathrm{m_0}$ will be equal but m reduces as the reaction progresses. The factor $(m/m_0)^n$ accounts for the selective dissolution and ageing of the solid. The exponent n is assumed to be 2/3 for uniformly dissolving spheres and cubes (Parkhurst & Appelo, 1999; Mayer et al., 2002).

As an example, given the specific rate of pyrite oxidation by dissolved oxygen as $10^{-8.19}m_{O_2}^{0.5}m_{H^+}^{-0.11}$ (Williamson & Rimistidt, 1994), where $10^{-8.19}$ is the temperature dependent rate constant (mol $m^{-2}s^{-1}$), $m_{O_2}^{0.5}$ is the rate dependence on the molarity of oxygen and $m_{H^+}^{-0.11}$ is the rate dependence on the activity of the hydrogen ion. The overall rate of pyrite is written as:

$$R_{pyrite} = 10^{-8.19}m_{O_2}^{0.5}m_{H^+}^{-0.11} \times \left(\frac{A_0}{V}\right) \times \left(\frac{m}{m_0}\right)^n \times (1 - SR"mineral") \quad 39$$

This approach is repeated for all the minerals included in the kinetic model. The overall rate expression is multiplied by the term (*1-SR"mineral")* where "SR" is the saturation ratio. This term accounts for the effects of the solution composition (i.e. distance from equilibrium) on the reaction rate. The inclusion of this term causes the rate of the forward reaction to reduce as the saturation ratio becomes more positive. However, for kinetically controlled reactions, the solution is far from equilibrium thus the term (1-SR"mineral") is approximately 1. The rate laws and constants are obtained from the general literature. The literature rate laws and constants are derived from detailed laboratory experiments carried out on pure minerals under different conditions (Williamson & Rimistidt, 1994; Palandri & Kharaka, 2004).

Mineral dissolution

The dissolution of a mineral as represented by Equations 38 and 39 requires a definition of its initial amount and surface area. The initial amount of a dissolving mineral is entered into the model as a molar amount. This parameter is represented as the term (m_0) in Equations 38 and 39 respectively. The initial amount of each solid reactant is manually calculated using the equation below (Parkhurst & Appelo, 1999; Williamson & Eary, 2006; Talman et al., 2013).

$$m_0 = \frac{(1 - \phi)\rho W_i}{100 M_i \phi_w} \quad 40$$

where W_i, M_i, ρ, ϕ and ϕ_w represent the mineral weight percentage, molar mass (g $mole^{-1}$), rock density (g dm^{-3}), total porosity and water filled porosity respectively. As an example, if the ore contains 0.2 weight percent pyrite (py) with 0.4 and 0.09 bed porosity and moisture content respectively, then the pyrite content to be entered in PHREEQC would be:

$$m_{0(py)} = \frac{(1 - 0.4) \times 2700 \times 0.2}{(100 \times 120 \times 0.09)} = 0.3 \ (\text{mol dm}^{-3}) \quad 41$$

where 2700 g dm^{-3} is the bulk density, 120 g $mole^{-1}$ is the molar mass of pyrite and 0.2 is the weight percent pyrite in ore. The initial contents of all the minerals are calculated using this formula.

The second parameter that needs to be specified for description of mineral dissolution is the initial mineral surface area represented by the term (A_0/V) in Equations 38 and 39. The initial mineral surface area also called the wetted surface area or reactive surface area gives an estimate of the mineral surface area in contact with the liquid phase. Because of the first order dependence of mineral dissolution rate on surface area, this parameter has a significant influence on the mineral dissolution rate. The initial surface area of each mineral (solid reactant) is calculated using Equation 42 below.

$$\text{Surface area } (\mathrm{m^2 dm^{-3}}) = \mathrm{A_{sp} M_i m_i X_i} \qquad 42$$

where $\mathrm{A_{sp}}$ is the specific surface area ($m^2\ g^{-1}$), $\mathrm{M_i}$ is the molar mass of the mineral (mol g^{-1}), $\mathrm{m_i}$ is the amount of solid reactants (mol dm^{-3}) and X_i is the mineral volumetric fraction in the grain. The methods used for estimation of mineral specific surface area used in the calculation of initial mineral surface areas in Equation 42 are discussed further below.

Estimation of mineral specific surface areas

The specific surface area ($\mathrm{A_{sp}}$) of a particle is defined as the surface area per unit mass or volume of particles and is usually expressed as area per unit mass $m^2\ g^{-1}$ (Brantley & Mellott, 2000). The specific surface area is usually determined by the BET (Brunauer-Emmett-Teller) method (Brunauer et al., 1938). The BET method is based on adsorption of gas on a mineral surface. The amount of gas adsorbed at a specific pressure is used to determine the surface area (Brunauer et al., 1938; Hodson et al., 1998; Brantley & Mellott, 2000). The specific surface area determined by the BET method (BET surface area) comprises both the external and the internal contributors. The internal component of the surface area is made up of all connected pores that are accessible to the aqueous phase, whilst the external surface area is made up of the external surface of the mineral (Brantley & Mellott, 2000). In the absence of BET surface area, particles can be assumed to be spherically shaped and the specific surface area can be estimated by the geometric method as described by Equation 43 (Brantley & Mellott, 2000).

$$\mathrm{A_{geo}}(\mathrm{m^2\ g^{-1}}) = a'\rho^{-1}\mathrm{r}^{(d-3)} \qquad 43$$

where a' is the geometric parameter (6 for a cube, 3 for a sphere), r is the radius of the particle, ρ is the density of the solid. For Euclidean solids, d=2 and the exponent for r is -1.

For smooth spheres, Equation 43 thus becomes:

$$\mathrm{A_{geo}}(\mathrm{m^2\ g^{-1}}) = \frac{6}{\mathrm{d_e}\rho} \qquad 44$$

Where d_e is the effective spherical diameter (m), ρ is the rock density of the rock (g m^{-3}) and the number 6 is a geometric parameter. Although, the geometric method gives a good estimate of the specific surface area, its accuracy is highly questionable. Unlike the BET surface area, the geometric surface area assumes hypothetical smooth spherical particles and does not account for the internally connected pores and surface roughness (Hornberger & Brady, 2009). Thus, specific surface area determined by geometric method is always less than the BET surface area due to the non-inclusion of internal pores and surface roughness in the geometric surface area estimation. The surface roughness can be accounted for by multiplying the geometric specific surface area by a surface roughness factor. Generally, the BET surface area can be related to the geometric surface area as:

$$\mathrm{A_{bet}}\,(\mathrm{m^2 g^{-1}}) = \gamma \mathrm{A_{geo}} \qquad 45$$

Where γ is the surface roughness and A_{bet} and A_{geo} are the BET and geometric surface areas respectively. The surface roughness factors (γ) for fresh created silicate surfaces are reported to be in the range of 2.5 to 15 (or slightly higher) whilst those for naturally weathered surfaces is in the range of 100 to 1000, depending on the cleavage characteristics, grain shape and extend of weathering (Anbeek, 1992; White & Brantley, 2003). The surface roughness factor is influenced by the cleavage characteristics of the minerals, for instance, minerals with poor cleavage will break into grains with high surface roughness while those with better cleavages tends to form much finer grains (Hodson et al., 1997a).Thus, the shapes of the minerals and their respective surface roughness factors will largely be influenced by their cleavage characteristics. Generally, the surface roughness factor increases with time due to increased surface pitting, etching and formation of internal surface structures like micropores during weathering (Anbeek, 1992; White & Brantley, 2003).

For particles with different ranges of size classes, the specific surface area is either calculated from an average particle size of all the size classes or as the sum of the surface areas in the different size classes. For a pure mineral grain, the specific surface area will be equal to the calculated BET or geometric surface area of the grain. However, in most cases grains contain multiple minerals. A number of approaches are used to estimate the specific surface area of each mineral in the grain. The common approach is to assume that the specific surface area of each mineral in the grain is equivalent to its volumetric fraction in the grain (Stromberg & Banwart, 1994; Linklater et al., 2005; Hansen et al., 2008; Gudbrandsson et al., 2011; Pham et al., 2011).Thus, for a multi-mineral grain with geometric specific surface area A_{geo}, the specific surface area of mineral i in the grain is calculated as shown in Equation 46:

$$\text{Specific surface area } (\mathrm{m^2 g^{-1}}) = \mathrm{A_{geo}\ X_i\ \gamma} \quad 46$$

where $\mathrm{X_i}$ is the mineral volumetric fraction in the grain and γ is the surface roughness factor that accounts for grain surface roughness. Alternatively, if the specific surface area is determined by the BET method, the specific surface area of a mineral i in the multi-mineral grain is calculated as shown in Equation 47.

$$\text{Specific surface area } (\mathrm{m^2 g^{-1}}) = \mathrm{A_{bet}\ X_i} \quad 47$$

where $\mathrm{A_{bet}}$ is the BET surface area of the grain and X_i is as defined in Equation 46. Since the BET surface area estimation accounts for internal pores and grain surface roughness, Equation 47 is not multiplied by the surface roughness factor.

Limitations and key assumptions

The limitations of the kinetic model consist of both the inherent limitations of the code and those arising from the accuracy of key input parameters such as mineral surface area. In the first place, the kinetic model adopted in PHREEQC code is limited to surface controlled reactions and does not account for diffusion controlled reactions. Due to this limitation, the model will give misleading results when the leaching mechanism shifts from surface controlled to diffusion controlled. Secondly, PHREEQC does not account for differences in mineral liberation and distribution within the grain. This limitation can result in an overestimation of the mineral dissolution rates as some of the minerals within the grain may not have access to the leaching reagent due to liberation limitations and differences in distribution (Perkins et al., 1995; Cordoba et al., 2008b). For instance, minerals inside the grain and those not connected to the pores are not likely to have access to the leaching reagent while those at grain surface are likely to easily dissolve.

In relation to model input parameters, the calculation of geometric specific surface area from an average diameter is a potential source of uncertainty. The uncertainty is further exacerbated if the range of particle sizes is large (Koptsika et al., 2003). Whereas the geometric method assumes flat particle distribution between the maximum (d_{max}) and minimum (d_{min}) particle sizes, studies have shown that most of the weathering occur in the smaller size fractions (Stromberg & Banwart, 1999). By using the average grain size, the influence of grains in smaller size classes on mineral dissolution rates is underestimated. This results in the underestimation of the mineral dissolution rates (Stromberg & Banwart, 1999; Koptsika et al., 2003). Furthermore, the estimation of specific surface area of a mineral in a multi-mineral grain is problematic.

The assumption that the surface area of each mineral in a multi-mineral grain is equivalent to its volumetric fraction may not always be accurate due to differences in the mineral distribution, morphology, grain sizes and liberation (Linklater et al., 2005). For instance, a mineral with a much higher surface roughness are likely to have higher surface area even though its volumetric fractions are low. Because of the uncertainty surrounding the estimation of the specific surface areas of the minerals, the initial mineral surface area (A_0/V) is usually treated as a fitting parameter obtained by model calibration.

2.3.4 Transport model

PHREEQC code has capabilities to simulate a number of mass transport processes that occur in waste deposits. The code can simulate advective transport, diffusion transport, a combination of advection and dispersion transport as well as advection and dispersion transport with diffusion to stagnant zones. These processes can be combined with equilibrium and kinetically controlled reactions to simulate the feedback mechanisms between the chemical reactions and mass transport processes in a waste deposit scenario. The mass transport capabilities of PHREEQC code are described further in the following sub-sections.

Fluid transport

PHREEQC code assumes that transport of fluid and solutes only occurs in the saturated zone and are simulated using the mixing cell modelling approach (Parkhurst & Appelo, 1999). The flow channel is divided into a number of cells or boxes, each containing a mass of particles in contact with the volume of solution. During each time step, the solution in each cell is transferred to the next higher or lower numbered cell depending on the flow direction.

For advection transport, the time step is the time associated with each advective step while for diffusion, it is defined as the time associated with each diffusion period (Parkhurst & Appelo, 1999). In the 1-D model approach, bulk mass transport of liquid and aqueous species is considered to occur by advection, dispersion and diffusion to stagnant zones (Parkhurst & Appelo, 1999). At the start of the simulation, both the inflow or feed solution and the initial solution in contact with the solids need to be defined. The amount of solution contained in each cell is called “pore volume”. With every advection flow, a shift moves water from one cell to the next higher or lower-numbered cell.

The movement of fluid and solutes from one cell to the next as simulated by PHREEQC code is illustrated in Figure 9.

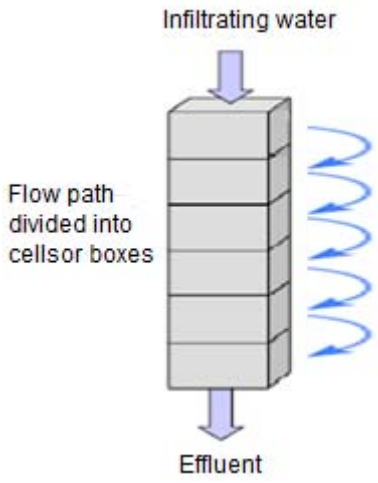

Figure 9: Conceptual model of waste rock dump (Nicholson et al., 2003)

The transport of solute through a one-dimensional saturated media is represented by the advection-reaction-dispersion equation as:

$$\frac{\partial C}{\partial t} = -v\frac{\partial C}{\partial x} + D_L\frac{\partial^2 C}{\partial x^2} - \frac{\partial q}{\partial t} \qquad 48$$

The term $-v\frac{\partial C}{\partial x}$ represents advective transport, $D_L\frac{\partial^2 C}{\partial x^2}$ represents dispersive transport, and $\frac{\partial_q}{\partial_t}$ is the change in concentration in the solid phase due to reactions. The term *C* is concentration in water (mol dm^{-3}), t is time (s), v is pore water flow velocity (m s^{-1}), *x* is distance (m), D_L is the hydrodynamic dispersion coefficient (m^2 s^{-1}), *q* is the concentration in the solid phase (mol dm^{-3}) and D_L is defined as:

$$D_L = D_e + \alpha_L v \qquad 49$$

where D_e *is* the effective diffusion coefficient, α_L is the dispersivity (m). The terms of the advection-reaction-dispersion equation are illustrated diagrammatically in Figure 10 in the next page.

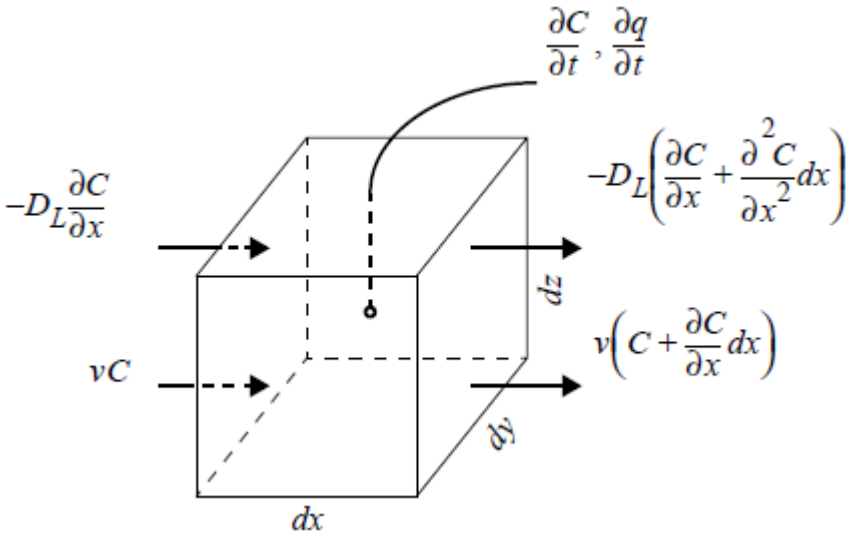

Figure 10: Terms in the advection-reaction-dispersion equation (Parkhurst & Appelo, 1999)

The explicit finite difference scheme is used to solve the transport part of the advection-reaction-dispersion equation while the chemical interaction term is calculated separately for each time step (Merkel & Planer-Friedrich, 2008). The time step is defined as the time taken to move one pore volume from one cell to the next during a transport simulation. All the transport and chemical reaction processes are calculated for each time step. The sequence starts with calculation of advective transport followed by kinetic and equilibrium reaction calculation. Thereafter, the dispersive transport is calculated which is again followed by the kinetic and equilibrium reactions. Thus, the kinetic and equilibrium reactions are calculated after both the advection step and the dispersion step (Parkhurst & Appelo, 1999). The key input parameters required to simulate transport processes are; advective time step, number of shifts, longitudinal dispersivity, cell number and size.

The derivations of these parameters are explained below.

- Time step

  The advective time step $(\Delta t)_A$ (for advective transport) is calculated from the irrigation rate and the resident moisture content as:

$$(\Delta t)_A = \frac{PV}{Q} \qquad 50$$

  where PV is the pore volume or resident moisture content (m^3) and Q is the irrigation rate defined as the flow rate of water into the column waste deposit ($m^3\,s^{-1}$). In the transport model, the time step indicates the time taken to transfer liquid from one cell to the next.

If transport and kinetic reactions are combined, the time step also indicates the integration steps of the mineral dissolution rates.

- Number of shifts

  The number of shifts is calculated from the time step and the simulation time as:

$$\text{Shifts} = \frac{t}{(\Delta t)_A} \qquad 51$$

  where t is the total simulation time (s). The number of shifts indicates the number of times the solution is transferred from one cell to another. This parameter depends on the simulation time and the advective time step. Both the time step and the number of shifts need to be adapted to the grid size (number of cells).

- Longitudinal dispersivity

  In the PHREEQC code, longitudinal dispersivity is essentially the mixing of contents of adjacent cells (Parkhurst & Appelo, 1999). This parameter is usually obtained experimentally by fitting measured breakthrough curves with the analytical solution of the advection-dispersion equation (Parkhurst & Appelo, 1999). However, in the absence of sufficient experimental information, the value of the longitudinal dispersivity is estimated empirically using the method proposed by Newman (1990) shown in Equation 52.

$$\text{Longitudinal dispersivity} = 0.0175L^{1.46} \qquad 52$$

  where L is the distance of travel or flow path (m). In the PHREEQC model, longitudinal dispersivity is essentially the mixing of the contents of the adjacent cells. The value of the longitudinal dispersivity gives an indication of the degree of mixing.

- Number and size of cells

  The number of cells in a flow path is a user-defined parameter based on the stability of the numerical solution. Ideally, the numerical solution should be the same despite the number of cells chosen. However, if there are variations, the grid size can be adjusted until numerical stability is obtained. The size of each cell in the flow path is calculated from the height of the flow path (column) and the number of cells as:

$$\text{Cell length} = \text{column height}/\text{number of cells} \qquad 53$$

  where the height is in metres.

Fluid and solute transport in real disposal scenarios is often not an “ideal” plug-flow, while part of the water in the flow path is mobile, some remains immobile or stagnant (Petersen &

Petrie, 2000; Broadhurst et al., 2007). Transport mechanisms between these two parts occur through diffusion. These processes can be simulated in PHREEQC in a simplified manner.

This is achieved by formulating mixing process terms between the mobile and the immobile waters (Merkel & Planer-Friedrich, 2008). In this approach, each mobile cell is associated to one or more immobile cells. The exchange of constituents between the mobile and immobile cells occurs by diffusion. Diffusion into stagnant zones adjacent to the 1-D flow path is simulated through the "dual porosity" model. The diffusion between the mobile and stagnant zones can be described as:

$$\frac{\partial \mathrm{M_{im}}}{\partial \mathrm{t}} = \theta_{\mathrm{im}} \times \mathrm{R_{im}} \frac{\partial \mathrm{C_{im}}}{\partial \mathrm{t}} = \alpha(\mathrm{C_m} - \mathrm{C_{im}}) \qquad 54$$

where "m" and "im" represents mobile and immobile zones respectively. $\mathrm{M_{im}}$ represents the moles of a species in the immobile zone and $\mathrm{R_{im}}$ represents the retardation factor of the immobile zone. C_m and C_{im} represent the concentrations (mol dm^{-3}) in the mobile and immobile zone, respectively, α is the exchange factor (1/s). The transport model can be coupled with the kinetic and equilibrium reactions to simulate the interaction between the infiltrating water and solids in a flow-through scenario.

Transport of heat

The transport of heat or change in temperature within the saturated media is represented as:

$$(\theta\rho_{\mathrm{w}}\mathrm{k_w})\frac{\partial \mathrm{T}}{\partial \mathrm{t}} + (1-\theta)\rho_{\mathrm{s}}\mathrm{k_s}\frac{\partial \mathrm{T}}{\partial \mathrm{t}} = -(\theta\rho_{\mathrm{w}}\mathrm{k_w})\mathrm{v}\frac{\partial \mathrm{T}}{\partial \mathrm{x}} + \frac{\partial^2 \mathrm{T}}{\partial \mathrm{x}^2} \qquad 55$$

where T is the temperature in (°C), θ is the porosity, ρ is the density kg m^{-3}, $\mathrm{k_w}$ and $\mathrm{k_s}$ are the specific heat capacity (kJ°$C^{-1}$$kg^{-1}$) of the water and solid respectively, accounting for the heat dispersion by advective flow and the heat conductivity of the system (kJ°$C^{-1}$$m^{-1}$$s^{-1}$) (Parkhurst & Appelo, 1999). The temperature T is assumed to be uniform over the volume of the water and solid. Dividing Equation 55 by $\theta\rho_{\mathrm{w}}\mathrm{k_w}$ yields:

$$\mathrm{R_T}\frac{\partial \mathrm{T}}{\partial \mathrm{T}} = -\mathrm{v}\frac{\partial \mathrm{T}}{\partial \mathrm{x}} + \mathrm{K_L}\frac{\partial^2 \mathrm{T}}{\partial \mathrm{x}^2} \qquad 56$$

where $\mathrm{R_T} = 1 + \frac{(1-\theta)\rho_{\mathrm{s}}\mathrm{K_s}}{\theta\rho_{\mathrm{w}}\mathrm{K_w}}$ is the temperature retardation factor and $\mathrm{K_L} = \frac{\mathrm{K}}{\theta\rho_{\mathrm{w}}\mathrm{K_w}}$ is the thermal dispersion coefficient representing both pure diffusion and dispersive advection respectively (Parkhurst & Appelo, 1999).

Limitations and major assumptions

The transport model adopted in PHREEQC only applies to the saturated media and is limited to 1-D. In addition, PHREEQC transport model does not consider transverse fluid flow, preferential flow paths or changing moisture contents.

Although the flow of fluid and solutes in waste deposits is dominated by the one-dimensional downward flow, transverse flow can occur and may become important in some cases for example, in tailings deposits that intersect the water table (Merkel & Planer-Friedrich, 2008). In such cases, ignoring the effects of liquid dilution due to transverse flow may result in an overestimation of the solute concentrations.

However, these processes can be simulated by adopting a 2-D or 3-D modelling approach that account for the effects of transverse and transient flow. The effects of preferential flow and changing moisture can also affect the accuracy of the model output if they are significant as is often the case in unsaturated waste rock deposits that are subjected to seasonal wetting and drying cycles. However, the quantification of these processes is problematic. Furthermore, the complexity surrounding their inclusion and sourcing of the relevant input parameters does not warrant their incorporation into the model (Perkins et al., 1995; Parkhurst & Appelo, 1999; Mayer et al., 2002; Afewu, 2009). In the light of the above, a 1-D (or 2-D at most) is generally considered to be sufficient for early stage project decision making.

Furthermore, the PHREEQC code does not account for the transport of oxygen in the unsaturated media but rather assumes that oxygen is dissolved and uniformly distributed within the liquid phase. For fully saturated waste deposits, the oxygen supply to cells can be assumed to be non-uniform. In such cases, the top cell can be assumed to have high availability of oxygen as compared to the lower cells. This can be modelled in PHREEQC by defining much lower oxygen partial pressure for the lower cells as compared to top cell. However, in the present study, oxygen supply to all the cells is assumed to be unlimited while the mass transfer of oxygen within the liquid phase is assumed to be instantaneous. Likewise, the transport of heat is also assumed to occur only in the saturated media by diffusion. While these assumptions may be sufficient for aerated columns and engineered heap leaching where oxygen supply is not the limiting factor, they may result in an overestimation of mineral dissolution rates in large and unsaturated waste deposits where oxygen transport is a limiting factor. Such cases require more rigorous modelling approaches that account for heat and gas transport in the unsaturated media. However, the inclusion of these processes increases the model complexity and the computational efforts required. This may only be warranted for site specific case studies where model input

parameters are readily available. For a generic and early stage decision making, a more simplified approach, in which gas transport only occurs in the saturated fraction of the waste deposit, is generally acceptable, or even preferable (Nicholson et al., 2003).

Another limitation of the PHREEQC transport model is that the code does not account for microbial transport and attachment. Once again inclusion of these processes would increase model complexity and data input requirements and is unlikely to be warranted in the case of early stage project decision making.

2.4 Summary

The literature review has shown that generation of ARD is a complex process involving a combination of chemical reactions and physical processes. The generation of acid from mine waste depends on the relative rates of acid producing and acid neutralising reactions. Acid is mainly produced by the oxidation of sulphide minerals such as pyrite, pyrrhotite and chalcopyrite. Oxygen is the main oxidant at weakly acidic to circumneutral pH while ferric ion is the main oxidant at acidic pH (pH<3.5). Acid is also produced by the secondary precipitation of hydroxysulphate and/or oxyhydroxides, with the hydroxysulphates being favoured by high sulphate concentrations (>1000-5000ppm) and acidic to weakly-acidic conditions, and the oxyhydroxides occurring at lower sulphate concentrations (<1000-2500 ppm) and/or higher pH values. The main iron bearing hydroxysulphates are jarosite and schwertmannite whilst aluminium forms mainly jurbanite and, to a lesser extent, alunite and basaluminite. However, when exposed to fresh circumneutral to neutral waters (pH >5) over time, iron and aluminium hydroxysulphate transform to their respective iron and aluminium oxyhydroxides, namely ferrihydrite and gibbsite respectively. These transformation reactions result in the generation of acid in the long term.

The acid generated by the oxidation of sulphide minerals and precipitation of hydroxysulphates and oxyhydroxides is mainly neutralised by the dissolution of carbonates such as calcite and dolomite. However, at low pH conditions, aluminosilicate and iron and aluminium bearing oxyhydroxides also become important acid neutralisers. The rates and extents of acid producing and acid neutralising reactions are mainly governed by key waste specific characteristics and physical transport processes. The main waste specific characteristics influencing ARD generating reactions are mineralogy, particle size, permeability, solid-liquid ratio and waste material heat conductivity while the main physical transport processes are bulk liquid and solute transport, air transport, heat transport and microbial attachment and transport. Fluid transport is responsible for the transport of oxidation products from mineral surfaces while gas and heat transport are responsible for the supply of oxygen to oxidation sites.

PHREEQC is a relatively simple and open-access geochemical-mass transport model which has capabilities to simulate many of the chemical and physical processes governing the generation of ARD. Firstly, PHREEQC has capabilities to simulate kinetically controlled oxidation of sulphide minerals and dissolution of carbonate and aluminosilicate minerals. These are simulated as surface controlled reactions and defined using literature rate laws and constants. The precipitation/dissolution of hydroxysulphates and oxyhydroxides is simulated as equilibrium controlled reactions using literature solubility constants.

PHREEQC also simulates transport of solutes in 1-D by advection-dispersion and diffusion to stagnant zones under saturated condition while the transport of heat is transported by diffusion only within the saturated media. On the other hand, equilibrium conditions are assumed between the dissolved and the atmospheric oxygen (and other gases). The extent of oxygen dissolution is specified by the partial pressure.

Despite its flexibility, PHREEQC has several limitations. In the first place, the aqueous model used for estimation of activity coefficients is limited to low ionic strength. At high ionic strength (> 0.7 mol dm-3), the aqueous model breaks down. However, this limitation is not likely to affect the present study since the ionic strength of most ARD and heap leach solutions is low. In the second place, PHREEQC simulates kinetically controlled reactions as surface controlled and does not account for diffusion controlled reactions. Chemical reactions can becomes diffusion controlled due to oxygen limitations particularly in the lower levels of saturated deposits or deposit with covers. Precipitation of secondary minerals can also cause the reactions mechanism to shift from surface controlled to diffusion controlled due to the isolation of the mineral surface from the leaching reagents. However, this limitation did not affect this study as the column leach tests used in the study were well aerated. In the third place, PHREEQC code does not distinguish between differences in particle sizes and mineral liberation. Instead, all minerals are assumed to be fully liberated and contained in particle sizes of equal size. Hence the model is likely to underestimate mineral reaction rates in the case of finer particles, and overestimate mineral reaction rates in the case of coarser particles. The assumption that there is no mineral occlusion or passivation of mineral surfaces is also likely to overestimate mineral reaction rates.

Furthermore the transport model in PHREEQC code only applies to the saturated media and is limited to 1-D transport of fluids and solutes. Although the 1-D transport approach is sufficient for the present study where the fluid flow was dominated by the downward flow, the approach may not be sufficient for scenarios where the effects of transverse flow are significant. In such cases, the model will overestimate the concentration profiles since the effects of dilution due to transverse flow are not taken into consideration. Likewise, the

limitations of heat and gas transport to the saturated media limits the ability of the code to accurately simulate scenarios where heat and gas transport in the unsaturated media are the main governing mechanisms (e.g. aerated heaps and waste rock piles). In such cases, assuming that gas and heat transport only occurs in the saturated media is likely to underestimate the concentration profiles as the transport of oxygen and oxidation rates of sulphide minerals are much faster in the unsaturated than saturated media.

The other limitations of PHREEQC are related to uncertainties surrounding the estimation of key input parameters such as mineral surface areas, selection of appropriate secondary minerals and solubility constants. The limitations with respect to key input parameters are partly addressed through model calibration with respect to mineral surface areas and precipitating secondary minerals. Nevertheless, reliable input data is essential in terms of model accuracy and reliability. The key model input parameters and their derivation are summarised in Table 10 below.

Table 10: Description and derivation of key model input parameters

Parameter description	Derivation
Kinetic model	
Amount of solid reactants	Calculated from mineral content, molar mass, total and water filled porosity
Mineral surface area	Calculated from specific surface area,molar mass and amount of solid reactant
Rate laws and constants	Obtained from literature
Chemical equilibrium model	
Precipitating phase or dissolving gas	Specified by user
Target saturation indices	Specified by user (usually zero)
Transport model	
Cell length	Cell length=(column height)/(number of cells)
Flow velocity	(Cell length) / (time step)
Time step	$(\Delta t)_A$=PV/Q, where PV and Q are pore volume and irrigation rate respectively
Shifts	Shifts=t/$(\Delta t)_A$, where t is the total simulation time.
Longitudinal dispersivity	Estimated from equation $\propto_x$=0.0175L^1.46, where L is the height of column.

Chapter 3 develops a generic model based on the capabilities of PHREEQC geochemical code. The modelling methodology is demonstrated on a low grade copper sulphide ore in a column-leach scenario.

3 METHODOLOGY

The literature review in Chapter 2 has highlighted the main chemical and physical mechanisms governing the generation of ARD from mine waste. The review also provided an in-depth understanding of the modelling methodology, capabilities, main input parameters, key assumptions and limitations of the PHREEQC geochemical code. This chapter uses the information gathered from the literature review to develop a PHREEQC based model. The model is applied on an existing low-grade copper sulphide case study data set with a view of addressing the research key questions (4) and (5) that seek to analyse the effects of key variables on the accuracy and reliability of the model for simulating ARD profiles in a flow-through scenario and to assess the conditions under which the PHREEQC code can be used for ARD prediction. Although the case study conditions were designed to determine the extraction of copper during heap bioleaching of low grade copper sulphide ore, there are many similarities between heap bioleaching of sulphide bearing ores and ARD generation from sulphide mine waste. Both processes involve the dissolution of minerals, bacterial oxidation of sulphide minerals, diffusion of dissolved species through the porous matrix, dynamics of transport of microbes and dissolved species within the stagnant solution in the pores and dynamics of solution flow through the bed. The case study can thus be viewed as an advanced stage of biologically mediated ARD generation in which the effluent is highly acidic and the diffusion of oxygen is not rate limiting.

The study was carried out in five stages, namely data collection, model development, model calibration, model validation and model sensitivity analysis. Data collection involved the collection of the model input data and the extension of the input database, while model development entailed the identification and description of the main controlling processes and derivation of key input parameters. In the model calibration stage, predicted concentration profiles were fitted to experimental results through further adjustment of certain model input parameters, specifically minerals surface areas and precipitating secondary minerals. Once calibrated, the model was validated using an independent dataset in order to assess its predictive capability. Finally, model sensitivity analysis was carried out to assess the sensitivity of the model output to changes in key model input parameters.

The summary of the general research approach is illustrated in Figure 11 below.

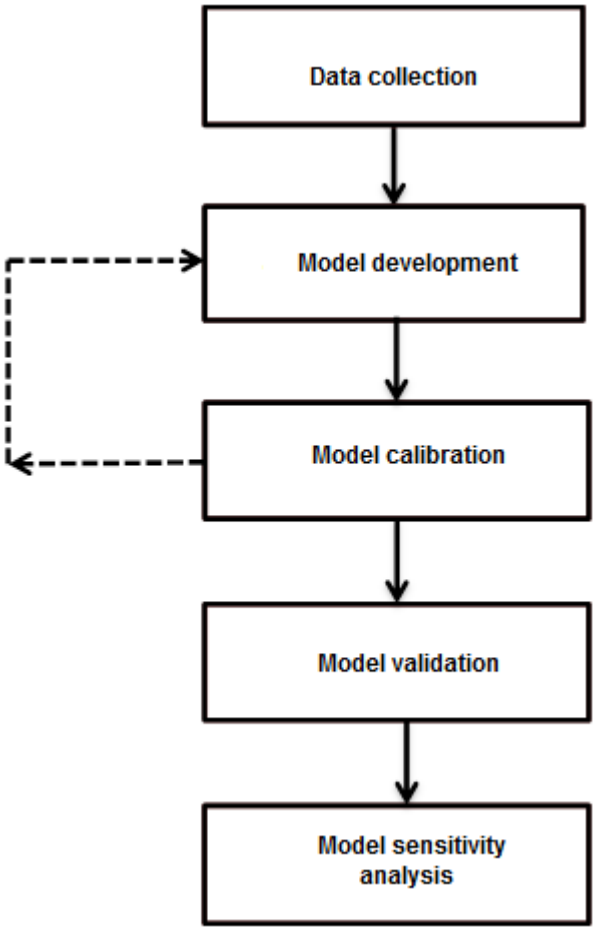

Figure 11: Methodological approach (stages) for the study

These methodological stages are discussed in sections 3.1 to 3.5.

3.1 Data Collection

The datasets used in the study were obtained from a column bioleaching experimental program carried out on low grade copper sulphide ore over the period 2004 to 2006 through the Australian Minerals Industry Research Association AMIRA project P768A (Watling, 2006).

3.1.1 Ore characteristics

The characteristics of the bulk sample with respect to particle size and mineralogy is described below. The bulk mineralogy is summarised in Table 11.

Table 11: Ore mineralogical composition as determined by QEMSCAN (Watling, 2006)

Mineral	Chemical formula	Amount (wt. %)
Chalcopyrite	$CuFeS_2$	1.3
Pyrite	FeS_2	0.2
Quartz	SiO_2	17.9
*Albite	$(Na, Ca)Al(Al, Si)Si_2O_8$	8.7
*K-feldspar	$KAlSi_3O_8$	39.6
Biotite	$K(Mg, Fe)_3AlSi_3O_{10}(OH)_2$	21.4
Chlorite	$(Mg, Fe, Al)_6AlSi_3O_{10}(OH)_8$	3.3
Kaolinite	$Al_4Si_4O_{10}(OH)_8$	1.9
Fe-oxides	Fe_3O_4	0.3
Rutile	TiO_2	0.2
Apatite	$Ca_5(PO_4)(Cl, F, OH)$	0.9
Calcite	$CaCO_3$	1.4
Other silicates		1.2
others		1.7
Total		100

*Plagioclase was assumed to be present as albite while orthoclase was present as K-feldspar

Calcite was the only carbonate mineral identified while chalcopyrite and pyrite were the main sulphide minerals in the ore. The rest of the ore was comprised mainly of aluminosilicate minerals, quartz, as well as traces of magnetite, rutile and apatite. Chalcopyrite and pyrite were the primary acid producing minerals. Potential acid neutralising minerals included calcite, biotite, albite and, to a lesser extent, K-feldspar with the reactivity decreasing in the order calcite>biotite>albite>K-feldspar (see Table 3 in Chapter 2). Table 12 below shows the distribution of key elements among the minerals.

Table 12: Element association in the bulk minerals

Mineral	Amount of element contained (wt. %)						
	Cu	Mg	Al	Fe	S	K	Ca
Chalcopyrite	100			5.01	80.95		
Pyrite				1.18	19.05		
Albite			19.69				50.24
K-feldspar			52.96			79.43	
Biotite		85.36	13.67	77.74		20.57	
Chlorite		14.64	8.20	13.32			
Kaolinite			5.48				
Magnetite				2.75			
Apatite							23.26
Calcite							26.51
Total	100	100	100	100	100	100	100

As shown in Table 12, most of the elements were contained in multiple minerals except for copper that was only contained in chalcopyrite. Sulphur was contained in pyrite and more significantly chalcopyrite (80.95 wt. %). In addition, pyrite and chalcopyrite also contained iron though in small amounts as compared to that contained in biotite and chlorite. Biotite and chlorite were the major sources of magnesium and iron and minor sources of aluminium. Due to its abundance in the ore sample, K-feldspar was the major source of both potassium and aluminium. Albite was the major source of calcium, followed by calcite and apatite. However, due to the slow dissolution rates of albite and apatite as compared to calcite, much of the dissolved calcium is likely to be generated from calcite dissolution. The ore varied over a wide range of particle sizes with the smallest size fraction being less than 1.18 mm and the largest particle size fraction having an average particle size of about 13.2 mm. The particle size distribution is presented in Table 13 and Figure 12.

Table 13: Particle distribution in size classes

Particle size (mm)	+13.2	-13.2+9.5	-9.5+6.5	-6.5+3.35	-3.35+1.18	-1.18
Wt.%	38.6	21.5	10.7	10.5	6.9	11.9

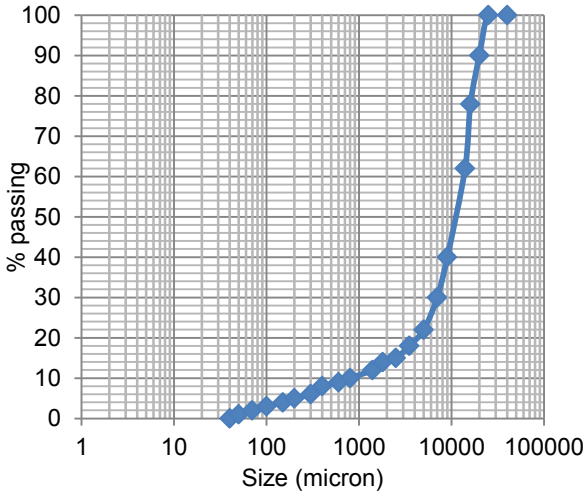

Figure 12: Particle size distribution of the bulk sample

The particle size distribution curve (Figure 12) shows that most of the particles (approximately 90%) were larger than 1mm, with 60% of the particles being larger than 10 mm. The distribution of minerals in different size classes is shown in Table 14 below.

Table 14: Mineral distribution (wt. %) in size classes

Size classes (mm)	+13.2	-13.2+9.5	-9.5+6.5	-6.5+3.35	-3.35+1.18	-1.18
Chalcopyrite	29.33	19.76	9.12	10.64	7.60	23.56
Pyrite	21.67	12.22	6.11	6.11	7.78	46.11
Quartz	32.92	19.89	9.92	10.42	7.74	19.11
Plagioclase	45.80	21.98	10.70	9.09	5.75	6.67
Orthoclase	38.77	22.26	11.08	11.11	7.12	9.67
Biotite	40.93	22.20	10.98	10.42	6.36	9.11
Chlorite	40.06	19.88	10.40	10.09	6.42	13.15
Kaolinite	42.86	19.58	10.58	10.05	6.35	10.58
Magnetite	36.49	20.38	15.17	9.95	6.64	11.37
Rutile	38.5	21.5	10.5	10.5	7	12
Apatite	39.24	21.3	10.76	9.42	6.95	12.33
Calcite	29.17	15.28	9.03	9.72	6.94	29.86
Other silicates	34.06	22.71	10.54	10.54	6.73	15.41
Other	38.60	21.64	9.36	10.53	5.85	14.04

Table 14 shows that most of the minerals were contained in the +1.18 to +13.2 mm size fractions. By comparison pyrite and chalcopyrite had the highest abundance (46 and 24% respectively) in the smaller size fractions (-1.18 mm) as compared to silicate minerals. Of the silicate minerals, quartz and kaolinite had the highest abundance in the small size fraction (19 and 10.6 wt. % respectively). The rest of the silicate minerals had less than 10 wt. % abundance in the small size fraction.

3.1.2 Column leach tests

The column leach tests were carried out in small and large leach columns. Small columns were run for 79 days while large columns were run for 273 days. Prior to loading into the columns, the ore was agglomerated with sulphuric acid in order to create an environment suitable for the survival of microorganisms. An equivalent of 20 kg/tonne acid was added during ore agglomeration. The ore in the column had a porosity of approximately 40 % and a moisture content of 9 % by volume. The columns were inoculated with a consortium of bacteria (mesophiles, moderates and thermophiles) to assist in the extraction of copper. The feed pH was fixed at 1.5 while the temperature was maintained at 40°C to optimise conditions for bioleaching. The columns were operated with a heated water jacket and drip feed irrigation system, while the solution management was done in a closed cycle mode i.e. effluent was recycled back as feed into the column. The feed pH was fixed at 1.5 while the temperature was maintained at 40°C to optimise conditions for bioleaching. Two separate datasets were derived from the case study.

The dataset from the small leach column was used for model calibration while the dataset from the large leach column was used for model validation. A comparison of the key leaching conditions for the two columns used in the study is summarised in Table 15.

Table 15: Parameters of the column leaching experiments

Variable	Small column experiment (model calibration)	Large column experiment (model validation)
Irrigation rate	1.02 mL/min	1.7 mL/min
Height of column	0.36 (m)	1.28 (m)
Weight of ore in column	4.18 (kg)	36.42 (kg)
Duration	79 (days)	273 (days)

*Total and water filled porosity were 0.4 and 0.09 respectively, temperature was at 40ºC and inlet solution pH was at 1.5. The height does not include beads.

The effluents from both columns were periodically collected from the bottom and analysed for pH, copper, magnesium, iron, aluminium, sodium, potassium and sulphate concentrations. In addition to the above, the leachate from the large column was also analysed for calcium and silicon concentrations. The experimental set up and the results of the small and large column experiments are attached in Appendices A and B respectively.

3.2 Model development

The model was developed by first carrying out a detailed literature review in order to identify the main mechanisms likely to control the leachate quality in mine waste. The key chemical reactions included oxidation of sulphide minerals and dissolution of carbonate and aluminosilicate minerals, precipitation and dissolution of secondary minerals while the physical transport processes included the transport of solutes, gases and heat within the waste deposit. The model was implemented using the public domain code PHREEQC (Parkhurst & Appelo, 1999). Due to the limitations of the PHREEQC code, simplifying assumptions were made to represent some of the physical transport processes. Transport was assumed to occur only in 1-D, while oxygen and carbon dioxide were assumed to be dissolved in the aqueous phase. Furthermore, heat was assumed to be distributed uniformly and the catalytic effect of microorganisms on iron and sulphur oxidation was accounted for by assuming a highly oxidising environment in the column. These processes were combined and formulated into a modelling framework using the Basic language program imbedded in the input file of the PHREEQC code. All inputs parameters were entered in the input file using specific keyword data blocks. The default-PHREEQC.dat database file was extended to include all the relevant thermodynamic database and rate laws.

Since the column was irrigated in recycle mode, the inlet fluid composition for each irrigation period and their corresponding shifts were predefined in the input file of the model. Transport was combined with kinetic and equilibrium reactions to simulate the feedback mechanisms between transport and chemical reactions. The model outputs were viewed under the output file while the specified element concentrations and pH were printed to the grid file.

The printed results were then exported to an Excel spread sheet and manipulated into different forms. The main processes included in the model and their key input parameters are summarised in Table 16 below.

Table 16: Summary of key model input parameters and outputs

Process description	Model input parameters	Model output
Slow kinetic processes	Amount of solid reactants	Solution description Distribution of species Saturation indices Precipitating secondary minerals Amounts of remaining kinetic reactants
	Reaction rate laws and constants	
	Mineral surface area	
Fast equilibrium processes	Precipitating secondary minerals	
	Dissolved gases	
	Target saturation indices	
1-D mass transport of fluid	Number of cells	
	Cell length	
	Flow velocity	
	Time step	
	Shifts	
	Dispersivity	

Further description of the main processes incorporated in the model and the derivation of the key input parameters are described in sub-sections 3.2.1 to 3.2.3.

3.2.1 Kinetic reactions and rate expressions

The oxidation of sulphide minerals and the dissolution of carbonate and aluminosilicate minerals were included in the model and were defined as kinetically controlled using the general expression shown in Equation 38 of section 2.3.3 (Chapter 2).

$$R_{min} = r_{min} \times \left(\frac{A_0}{V}\right) \times \left(\frac{m}{m_0}\right)^n \times (1 - SR"mineral")$$

where r_{min} is the specific reaction rate for the mineral (mol dm^{-2} s^{-1}), (A_0/V) is the initial mineral surface area (m^2 dm^{-3}), m_0 is the initial moles of solids while m is the moles of solids at any given time. At the beginning of the simulation, m and m_0 will be equal but m reduces as the reaction progresses. The factor $(m/m_0)^n$ accounts for the selective dissolution and ageing of the solid. The exponent n is assumed to be 2/3 for uniformly dissolving spheres

and cubes. On the basis of the literature review and mineralogical composition of the ore, the key minerals and reaction mechanisms likely to be dominant under the column leach conditions were identified and included in the model.

The minerals included were chalcopyrite, pyrite, K-feldspar, albite, biotite and calcite. Reaction stoichiometries used to define their reaction mechanisms are shown in Table 17.

Table 17: Stoichiometry of the main reactions included in the model

Reaction number	process
1.	Pyrite oxidation by ferric iron
	$FeS_2 + 14Fe^{3+} + 8H_2O \rightarrow 15Fe^{2+} + 2SO_4^{2-} + 16H^+$
2.	Chalcopyrite dissolution
	$CuFeS_2 + 16Fe^{3+} + 8H_2O \rightarrow Cu^{2+} + 17Fe^{2+} + 2SO_4^{2-} + 16H^+$
3.	Biotite dissolution
	$KMg_{1.5}Fe_{1.5}Al_3O_{10}(OH)_2 + 10H^+ \rightarrow K^+ + Al^{3+} + 1.5Mg^{2+} + 1.5Fe^{2+} + 3H_4SiO_4$
4.	Albite dissolution
	$NaAlSi_3O_8 + 4H_2O + 4H^+ \rightarrow Na^+ + Al^{3+} + 3H_4SiO_4$
5.	K-feldspar dissolution
	$KAlSi_3O_8 + 4H_2O + 4H^+ \rightarrow K^+ + Al^{3+} + 3H_4SiO_4$
6.	Kinetic calcite dissolution mechanisms
	$CaCO_3 + CO_2 + H_2O \rightarrow Ca^{2+} + 2HCO^-_3$
7.	Oxidation of ferrous iron to ferric iron by dissolved oxygen*
	$Fe^{2+} + 1/4\ O_2 + H^+ \leftrightarrow Fe^{3+} + 1/2H_2O$

*The rate of ferrous iron oxidation to ferric iron is increased by microbial activity

Ferric iron was assumed to be the main oxidising agent for pyrite and chalcopyrite due to low pH under which the columns were operated and the resulting high ferric iron concentration. As discussed in Chapter 2, ferric iron is a more rapid oxidant of sulphide minerals than oxygen. All dissolved sulphur species were assumed to be present as sulphate while the ferrous iron generated from the oxidation of pyrite and chalcopyrite was assumed to be instantaneously oxidized to ferric iron due to the presence of microbes. The dissolution rates of carbonate and aluminosilicate minerals were assumed to be pH dependent. Chemical reaction kinetics (surface controlled) and congruent dissolution of minerals were assumed. The standard literature rate laws and constants used to define the mineral dissolution reactions (described in Table 17) are shown in Table 18 below. The rate laws and constants listed in Table 18 were formulated into rate expressions in the form of Equation 38, using the

Basic language program imbedded in PHREEQC code. The parameters that needed to be derived were initial amount of reactants (m_0) and initial mineral surface areas (A_0/V).

Table 18: Rate laws and constants included in the model

Reaction number	[1]Rate law	[2]Rate constant at 25ºC			[3]Ref
		K1	K2	K3	
1.	$r_{py} = k[Fe^{3+}]^{0.93}[Fe^{2+}]^{-0.4}$	$10^{-5.72}$			⟨a⟩
2.	$r_{cpy} = k[Fe^{3+}]^{0.43}$	$10^{-6.75}$			⟨b⟩
3.	$r_{bt} = k_1[H^+]^{0.525} + k_2$	$10^{-9.84}$	$10^{-12.55}$		⟨c⟩
4.	$r_{ab} = k_1[H^+]^{0.457} + k_2 + k_3[OH^-]^{0.57}$	$10^{-9.16}$	$10^{-11.56}$	$10^{-14.6}$	⟨c⟩
5.	$r_{kf} = k_1[H^+]^{0.5} + k_2[OH^-]^{0.82}$	$10^{-10.06}$	$10^{-12.41}$	$10^{-21.21}$	⟨c⟩
6.	$r_{cc} = k_1[H^+] + k_2[CO_2] + k_3[H_2O]$	$10^{-5.49}$	$10^{-11.3}$	$10^{-5.08}$	⟨d⟩

[1]r_1 is the dissolution rate of mineral i (mol $dm^{-3}s^{-1}$), [ ] denotes a concentration in units of moles per dm^3 for all the reactions listed above with the exception of calcite where it denotes activity for the ions or molecules, [2]The terms k_1,k_2 and k_3 are the temperature-dependent rate constants (k) (mol $m^{-2}s^{-1}$) in the acidic, neutral and base media respectively. All rate constants are in moles per cubic meters per second (mol $m^{-3}s^{-1}$). [3]The reference ⟨a⟩ represents Williamson & Rimstidt 1994, ⟨b⟩ represents Rimstidt et al., 1994, ⟨c⟩ represents Palandri and Kharaka 2004 and ⟨d⟩ represents Plummer et al., 1978.

Amount of initial mineral reactants (m_0)

The amounts of solid reactants represented as m_0 in the overall general rate expression shown in Equation 38 of section 2.3.3 (Chapter 2).

$$m_0 = \frac{(1-\phi)\rho W_i}{100 M_i \phi_w}$$

where W_i, M_i, ρ, ϕ and ϕ_w represent the mineral weight percentage, molar mass (g $mole^{-1}$), rock density (g dm^{-3}), total porosity and water filled porosity, respectively. The calculated amounts of initial solid reactants based on the ore mineralogy shown in Table 11 are shown in Table 19 below.

Table 19: Initial amounts of solid reactants and their respective surface areas

Mineral	Amount (mole dm^{-3})
Chalcopyrite	1.27
Pyrite	0.3
Biotite	7.57
K-feldspar	25.54
Albite	4.73
Calcite	2.51

*The rock density of 2700 g dm^{-3} and the total and water filled porosity of 0.4 and 0.09 respectively were used in the calculations.

Mineral surface areas

All surface controlled kinetic reactions required an estimation of the initial mineral surface area represented by the term A_0/V in the general rate expression in Equation 38.

The initial mineral surface area is generally calculated from BET specific surface area. However, in the absence of BET specific surface area, the geometric specific surface area of a 1kg sample of the ore was calculated as the sum of the surface areas of particles in all the size classes.

$$\mathrm{A_{geo}} = \sum_{\mathrm{i}} \mathrm{A_{i,t}} \qquad 57$$

where $\mathrm{A_{i,t}}$ is the total geometric specific surface area in size class i. The calculated geometric specific surface area $(\mathrm{A_{geo}})$ is the sum of the surface areas in all the size classes per mass of sample. The surface area of a 1 kg sample was calculated as 0.7 m^2 which is equivalent to 0.0007m^2g^{-1} (see Appendix C 2 for details). Finally, the initial surface area (A_0/V) of each mineral was calculated from the calculated geometric specific surface area, using Equation 42 in section 2.3.3 (Chapter 2) as:

$$\text{Surface area } (\mathrm{m^2 dm^{-3}}) = \mathrm{A_{geo} M_i m_i X_i \gamma}$$

where $\mathrm{A_{geo}}$ is the geometric specific surface area ($m^2.g^{-1}$), Mi is the mineral molar mass ($g.mol^{-1}$),m_i is the amount of mineral ($mol.dm^{-3}$), Xi is the volumetric fraction and γ is the surface roughness factor. The surface roughness factor γ accounted for the grain surface roughness and internal pores not accounted for by the geometric specific surface area calculation. In the calculation, the surface area of each mineral in the multi-mineral grain was assumed to be proportional to its volumetric fraction in the grain. The mineral volume fractions were calculated from their respective weight percentages (see Appendix C1 for details). The calculated initial mineral surface areas (A_0/V) and the parameters used for their calculations as defined in Equation 42 are shown in Table 20.

Table 20: Calculated initial mineral surface areas or mineral surface areas to volume ratios (A_0/V)

Mineral	Molar masses (g mol^{-1})	Mineral volumetric fractions	surface area (m^2 dm^{-3})
Chalcopyrite	184	0.0088	0.02
Pyrite	120	0.0011	0.0004
Biotite	584	0.2	9.10
K-feldspar	278	0.43	32.41
Albite	329	0.092	1.50
Calcite	100	0.015	0.038

The geometric calculated specific surface area of 0.0007 m^2g^{-1} was used in all the calculations while initial amount of minerals were obtained from Table 18. A literature obtained surface roughness factor of 15 was used in all the calculations (White & Peterson, 1990).

3.2.2 Equilibrium controlled reactions and solubility constants

All dissolved species were assumed to be in equilibrium with each other. The oxidation of ferrous iron and sulphur generated from the dissolution of sulphide minerals was assumed to be instantaneous due to the presence of iron and sulphur oxidising bacteria. As a consequence, iron and sulphur existed mainly existed as ferric iron and sulphate, respectively. The catalytic effect of iron and sulphur oxidising bacteria was incorporated into the model by running the model under a highly oxidising environment consistent with bacterially catalysed sulphide oxidation processes. The interaction between the aqueous and other phases was described using equilibrium relationships. As stated earlier, precipitate formation and dissolution reactions were also included in the model and were defined as equilibrium controlled reactions, using solubility constant values obtained from the literature. These secondary minerals were not initially present but were allowed to precipitate. Only secondary minerals that showed positive saturation indices and those that were known to form in the acidic column leach conditions were considered in the simulations. These minerals were assumed to be in equilibrium with the aqueous phase. The list of secondary minerals considered together with their respective equilibrium solubility constants are shown in Table 21.

Table 21: Secondary minerals included in the model and the solubility constants defined

Mineral	Log k at 25ºC	Source
K-jarosite	-9.21	PHREEQC database
Schwertmannite	-18.0	(Bigham et al., 1996)
Ferrihydrite	4.891	PHREEQC.dat database
Gypsum	-4.58	PHREEQC.dat database
Jurbanite	-3.23	WATEQ4F.dat database
Basaluminite	22.7	WATEQ4F.dat database
Alunite	-1.4	PHREEQC.dat database
Gibbsite	8.11	PHREEQC.dat database
Kaolinite	7.435	PHREEQC.dat database

By specifying the target saturation indices to zero, these minerals were allowed either to precipitate or to dissolve in order to maintain equilibrium with the aqueous phase. In this way, their effects on the pH and metal concentrations were studied. Oversaturation was imposed on specific secondary minerals that were not considered likely to form under experimental conditions and time frames under consideration. These include minerals such as hematite and magnetite. In this way, these minerals were prevented from precipitating

and therefore had no effect on the model results. Interaction between the aqueous and gas phase was incorporated in the model by assuming equilibrium between dissolved and atmospheric oxygen and carbon dioxide.

The amounts of these gases were entered in the model as the logarithm of their partial pressures. The default PHREEQC thermodynamic database was extended to include all the defined equilibrium controlled reactions.

3.2.3 Transport processes and parameters

As discussed in Chapter 2, PHREEQC code uses the mixing cell model to simulate 1-D mass transport by advection and dispersion and diffusion to stagnant zones. In this modelling approach, transport was assumed to be dominated by advective-dispersive flow, and diffusion of constituents to stagnant zones was assumed to be insignificant at the high flow-through rates used in the case study. Since no discernible differences were observed in the model results when simulations were carried out at different cell sizes, a 3 cell model was chosen for both small and large column due to its simplicity. The flow paths in both small and large columns were divided into three equal cells or boxes, containing equal amounts of solid reactants and liquid volumes.

Chemical reactions were assumed to take place in each cell with different phases precipitating and dissolving. The transport parameters entered into the model were derived from the column sizes and leach conditions. These were entered into the model using the TRANSPORT keyword data block. The set of key transport parameters entered into the model and their derivations are shown in Table 22.

Table 22: List of key model input transport parameters

Parameter	Derivation	Small column	Large column
Number of cells	Determined by user (can vary)	3	3
Cell length	(Column height)/(number of cells)	0.16	0.5
Time step	PV/Q	5541	24200
Flow velocity per cell (m s^{-1})	$\Delta x/(\Delta t)_A$	0.0000289	0.0000207
Total simulation time	Determined by user (can vary)	79 days	273 days
Shifts	$t/(\Delta t)_A$	1232	975
Dispersivity	Longitudinal dispersivity =0.0175L^1.46	0.004	0.025

Where PV is pore volume (m^3), Q is irrigation rate ($m^3 s^{-1}$), t is the total simulation time (s), $(\Delta t)_A$ is the advective time step (s), L is the flow path or column height (m) and Δx is the cell length (m).

3.3 Model calibration

Model calibration is the process of adjusting values of specific model input parameters within an acceptable range in an attempt to match the model output to observed or measured data. Model calibration was performed manually by the trial and error parameter adjustment procedure using the small column leach test dataset described in section 3.1.2. The goodness of model fit was based on visual judgement from graphs.

The mineral surface areas and precipitating secondary minerals were treated as fitting parameters due to their high degree of uncertainty and influence on the model output. Model calibration through surface area adjustment and inclusion of appropriate secondary precipitates are described in sub-sections 3.3.1 and 3.3.2 respectively.

3.3.1 Calibration of mineral surface areas

Model calibration with respect to initial mineral surface areas was carried out in three steps. In the first step, the initial mineral surface areas calculated from the geometric specific surface area were used as input into the model in order to assess the preliminary fit of the model to the experimental data. In the second step of model calibration, the surface areas of all the minerals were multiplied by a coefficient of 100 in order to account for the specific surface areas of the minerals that were lower than the values reported in the literature. In the third and last step, the surface areas of selected minerals (chalcopyrite, biotite and K-feldspar) were individually adjusted to improve the model fit to the measured pH and selected elements. Based on the pH and release rates of key elements, the surface areas of these minerals (chalcopyrite, biotite, K-feldspar) were adjusted until a reasonable agreement between the model prediction and experimental data was attained. During model calibration, chalcopyrite was assumed to be the only source of dissolved copper while biotite was assumed to be the main sources of dissolved magnesium. After correcting for the contribution of biotite towards the dissolved aluminium flux, the rest of aluminium was assumed to be generated from K-feldspar dissolution. Effluent pH (at early stage) was used as a guide for calcite dissolution. The variables that were used as tracers for mineral dissolution rates during model calibration are summarised in Table 23 below.

Table 23: Dissolving minerals and their dissolution tracers

Dissolving mineral	Tracer
Chalcopyrite	Cu
Biotite	Mg
K-feldspar	Al
Calcite	pH

Meanwhile, sulphate, iron and potassium were not used as tracers due to their extensive precipitation.

3.3.2 Selection of secondary mineral

The second stage of model calibration involved the selection of appropriate secondary minerals to be included in the model. As discussed in Chapter 2, the precipitation of secondary minerals is critical due to their effect on the pH and pore water composition.

However, some of the secondary minerals that the model predicts may not necessarily form in the course of the experiment due to slow precipitation rates and unfavourable experimental conditions (see section 2.1.4). Therefore the user needs to select precipitates that are allowed to form under the given experimental conditions. Table 21 in section 3.2.2 indicates formation of a number of possible secondary precipitates by Fe (III) and Al (III) ions. Irons bearing secondary minerals of potential relevance are K-jarosite, schwertmannite and possibly ferrihydrite. Aluminium bearing secondary minerals of potential relevance include jurbanite, alunite, basaluminite, gibbsite and kaolinite. Model calibration was carried out to determine which, if any, of these iron and aluminium precipitates was likely to be of significance under the case study test conditions. This was done by evaluating the influence of each iron bearing secondary minerals on the model fit for dissolved iron concentration, and the influence of each aluminium bearing secondary minerals on the model fit for dissolved aluminium concentration. The effects of the inclusion of secondary minerals and model fits during model calibration are presented in sub-section 4.1.2 of Chapter 4.

3.4 Model validation

The main goal of model validation was to assess if the calibrated model captures all the essential processes that describe the system being simulated. The calibrated model was validated against the large Column leach test data. In this way the performance of the model against experimental data was demonstrated. With the exception of system parameters such as column height, longitudinal dispersivity, experimental duration and time step, the set of parameters used for model validation were exactly the same as those used in small columns. The sets of parameters used during model validation are attached in the disk accompanying the dissertation while the results of model validation are presented and discussed in section 4.2 of Chapter 4.

3.5 Model sensitivity analysis of influencing parameters

The model was subjected to an extensive single parameter sensitivity analysis study in order to gain insight into the sensitivity of key input parameters on the model output of interest. The parameters investigated were pyrite content, calcite content and liquid flow velocity. In

each scenario, the model was run for 273 days and the model outputs were compared to the base case scenario on the basis of effluent pH and element concentrations. The large column parameters were used as basecase for all the scenarios considered. The results of model sensitivity analysis are presented and discussed in section 4.3 of Chapter 4. The sensitivity of model output to mineral surface areas and secondary mineral precipitation were not considered during model sensitivity analysis as their effects were established during model calibration.

4 RESULTS AND DISCUSSION

This chapter presents and discusses the results of model calibration, validation and sensitivity analysis in relation to the case study in order to provide an insight into the capabilities of PHREEQC code for ARD generation. The chapter is divided into three main sections. Section 4.1 presents and discusses the results of the model calibration study while section 4.2 presents and discusses the results of the model validation study and lastly sections 4.3 presents and discusses the results of the model sensitivity study of the key influencing parameters.

4.1 Model calibration results

As stated in Chapter 3, model calibration was carried out by adjustment of mineral surface areas and selection of appropriate secondary minerals. The results for model calibration by initial surface area adjustment and secondary mineral selection are discussed in sub-sections 4.1.1 and 4.1.2 respectively.

4.1.1 Mineral surface areas and model fits

As already mentioned, model calibration was first accomplished by stepwise adjustment of initial mineral surface areas in three steps until a reasonable was observed between the simulated and experimental data. The initial values for minerals surface areas (A_0/V) used in the first step of model calibration were calculated from the geometric specific surface area of an average particle using Equation 44 (Chapter 2, section 2.3.3). A comparison of the geometric specific surface area calculated in the present study to the values reported in literature is shown in Table 24 below.

Table 24: Comparison of the calculated grain specific surface area to literature values

Range of particle size (mm)	[1]Average particle size (mm)	Surface area (m^2/g)	[2]Method	Source
-1.18+13.2	4.05	[3]0.0007	geo	Present study
0.1– 4.7	1.19	1±0.4	BET	Stromberg & Banwart,(1994), Linklater et al.(2005)
0.12	0.12	[4]0.019	geo	Williamson & Eary (2006)
0.115	0.115	0.236	BET	Brantley & Mellott (2000)

[1]The average particle size was calculated by assuming a flat particle distribution between the maximum and minimum particle size. [2]Method used to obtain the specific surface area (BET for BET surface area and geo for geometric surface area). [3]Equating to a BET surface area of 0.002-0.01 for fresh mineral surfaces and up to 0.07-0.7 for weathered minerals. [4]Equating to a BET surface area of between 0.05 and 0.29 for fresh material and up to 0.19-1.9 for weathered minerals.

The results in Table 24 indicate that the calculated specific surface area is significantly smaller than the values reported in the literature. This discrepancy can be attributed to the wide range of particle size classes in the present study as compared to those reported in literature. The geometric method used for surface area calculation assumed flat particle size distribution in each size class i.e. every particle from d_{min} to d_{max} has an equal population density (Tester et al., 1994). This assumption resulted in a much lower specific surface area as the average particle sizes in most of the size classes were larger than those reported in the literature (see Table 13). By using the geometric specific surface area of an average grain, the specific surface area of individual minerals were calculated in accordance with Equation 42 (Chapter 2, section 2.3.3) and compared to literature values (Table 25)

Table 25: Comparison of calculated and literature mineral volumetric fractions and specific surface areas

Mineral	Stromberg and Banwart (1994), Linklater et al., (2005)[1]		Present study[2]	
	Volumetric percentage	Specific surface area (m^2g^{-1})	Volumetric percentage	Specific surface area (m^2g^{-1})
Chalcopyrite	0.09	0.0009	0.88	0.000092
Pyrite	0.57	0.0057	0.11	0.000012
Biotite	8	0.08	19.6	0.0021
K-feldspar	24	0.24	43.4	0.0046
Albite	13	0.13	9.19	0.00096
Calcite	0.1	0.001	1.46	0.00015

[1]The specific surface area of an average grain used in the study was 1 m^2g^{-1}. [2]The specific surface areas of the average grain used in the present study is as shown in Table 24. The specific surface areas of the individual minerals shown above were calculated from their volumetric fractions by assuming that the specific surface area of each mineral in the multi-mineral grain is equivalent to its volumetric fraction. The geometric surface areas calculated in the present study were multiplied by a surface roughness factor of 15 in order to account for surface roughness and internal pores.

As seen in Table 25, the mineral specific surface areas obtained in the present study were approximately 2 orders of magnitude less than the literature values with silicates having much higher specific surface areas than sulphides and carbonates. Using the mineral specific surface areas in Table 25 as initial values, the mineral surface areas (A_0/V) were calculated for step 1 of model calibration. Since the values of the surface area depends on the specific surface areas (see Equation 42 in Chapter 2, section 2.3.3) , all the mineral surface areas were multiplied by a coefficient of 100 in step 2 of model calibration in order to account for the specific surface areas that were 2 orders of magnitude less than literature values. In the third and last step of model calibration, the model was fitted to the experimental data by trial and error. Based on the pH and concentration of selected

elements, best fits were obtained when the surface areas of chalcopyrite and biotite were multiplied by 3 and K-feldspar by 2.

The differences in the coefficients by which the minerals were multiplied in step 3 of model calibration arise from the variations in surface roughness, liberation and distribution of each individual mineral in the size classes. The surface areas of the rest of the minerals were not adjusted as the model fits were reasonable. The sets of surface areas obtained during different steps of model calibration are presented in Table 26.

Table 26: Steps in model calibration study indicating variables that were adjusted

Mineral	Step 1		Step 2		Step 3	
	[1]A_{sp} (m^2g^{-1})	[2](A_0/V) (m^2dm^{-3})	[3]Coefficient	(A_0/V)	[3]Coefficient	(A_0/V)
Chalcopyrite	0.000092	0.0215	100	2.15	3	6.45
Pyrite	0.000012	0.000425	100	0.0425	1	0.0425
Biotite	0.0021	9.10	100	910	3	2730
K-feldspar	0.0046	32.41	100	3241	2	6482
Albite	0.00096	1.50	100	150	1	150
Calcite	0.00015	0.0384	100	3.84	1	3.84

[1]A_{sp} is the mineral specific surface areas,[2](A_0/V) is the mineral surface area to volume ratio or simply mineral surface area calculated from specific surface area using Equation 42. [3] The coefficient by which the surface areas (A_0/V) obtained in steps 1 and 2 were multiplied to obtain the final surface areas in steps 2 and 3 respectively.

The model fits to experimental data obtained during different stages of model calibration with respect to mineral surface areas are shown in Figure 13. The model fit after the first step of model calibration as indicated by the dashed black line shows the preliminary fit of the model to the experimental data. Generally, all the elements concentrations and pH were underestimated. The results after the second step of calibration as shown by the dashed green line indicate an overall improvement in the model fit to the experimental data. Finally, the best fits were obtained after the third step of model calibration. During the third step of model calibration, copper was used as a tracer for chalcopyrite dissolution while magnesium and aluminium were used as tracers for biotite and K-feldspar dissolution respectively. The model fits obtained after the third step of calibration as shown by the dashed red lines are considered adequate for the purpose of this study. The model fits to experimental data were largely enhanced by the effect of recycled leach solution. It should, however, be noted that the feed solutions were predefined in the model for each irrigation step, and the model is thus not likely to significantly deviate from the expected trend. In this way, the accuracy of the model is judged by its ability to simulate the changes that occur to the feed solution as it passes through the column over a specified number of irrigation steps.

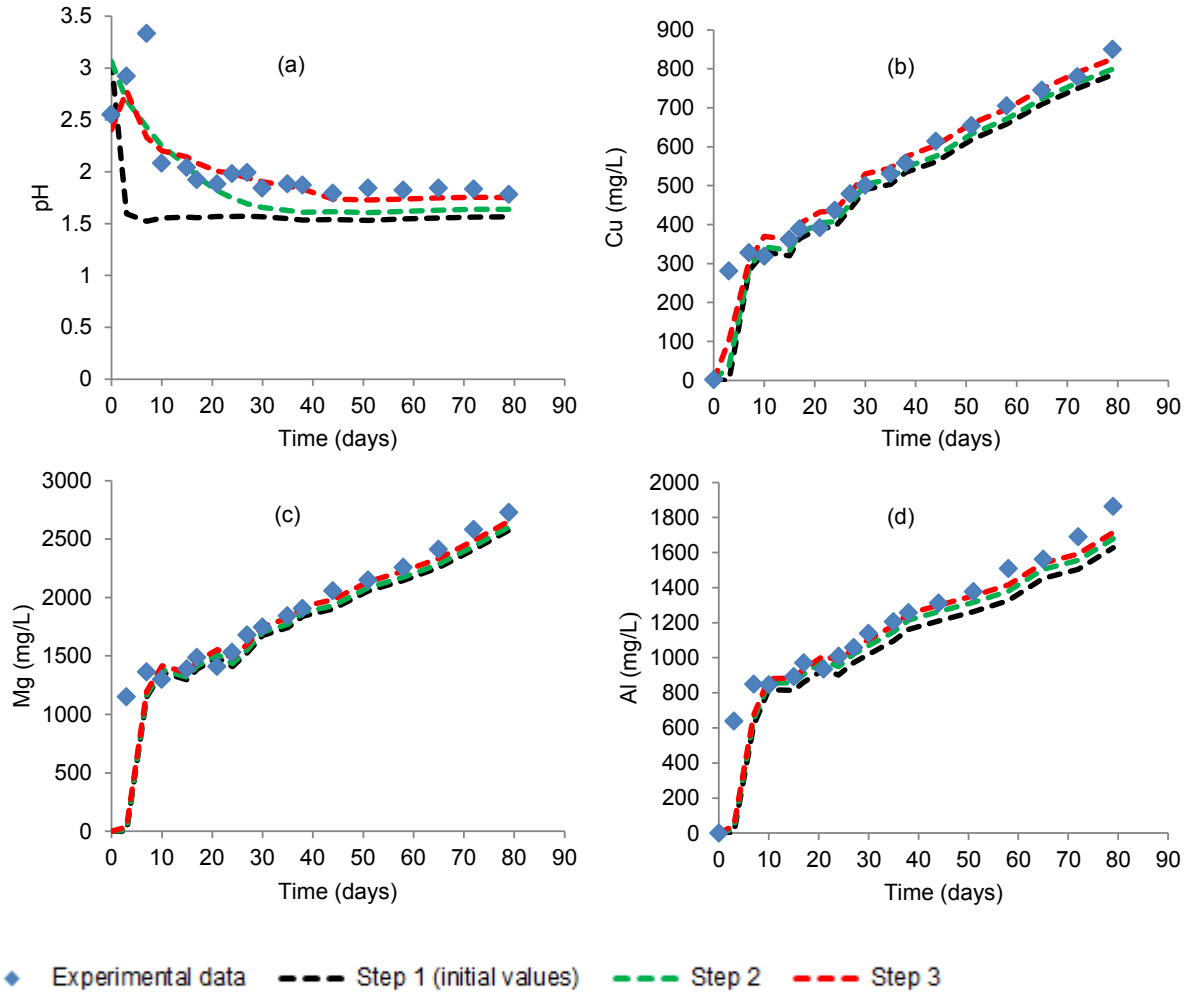

Figure 13: Model fits to experimental data during calibration with respect to initial mineral surface areas

The surface areas at which the model fitted the experimental data were significantly higher than the initial values (step 1 in Table 26). This can be attributed to a number of factors. In the first place, most of the mineral dissolution reactions are likely to occur in the fine size fractions (with large surface areas) where minerals are sufficiently liberated, whereas the initial surface areas were an average that included particles in large size classes that are not likely to react due to liberation limitations. In the second place, initial weathering of the ore may have occurred and this may have resulted in a much higher surface roughness factor than that used in the study. A surface roughness factor of 15 was used in the study while surface roughness of weathered mineral surfaces is reported to be in the range of 100 to 1000 (White & Peterson, 1990; Brantley & Mellott, 2000).

In order to assess the effect of secondary mineral precipitation on model fits of dissolved iron and aluminium concentration, further calibration was carried out with respect to secondary mineral precipitation. The results of these simulations are presented and discussed in section 4.1.2.

4.1.2 Effects of secondary minerals precipitation

The model was calibrated with respect to secondary mineral precipitation in order to identify the secondary minerals likely to form under column leach conditions and to assess their effects on the concentrations of specific elements i.e. iron and aluminium. A number of iron, aluminium and calcium bearing secondary minerals were introduced into the model. The surface areas obtained after the third step of model calibration (Table 26) were used in all the simulations presented in this sub-section.

Effect of secondary minerals on iron and potassium concentration

The iron bearing secondary minerals considered were K-jarosite, schwertmannite and ferrihydrite. These minerals were included in the model on the basis of literature information (see discussions in Chapter 2, section 2.1.4 and Chapter 3, section 3.2.2), and equilibrium conditions were assumed between each mineral and the aqueous phase. The results of the simulations are presented in Figure 14 below.

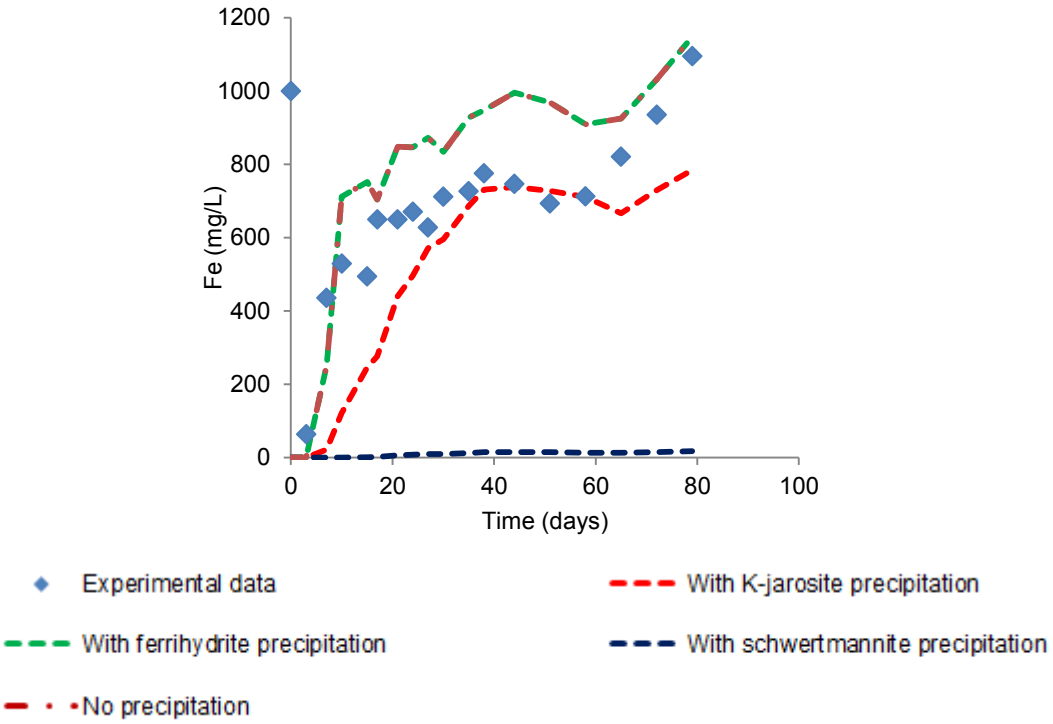

Figure 14: Comparison of Fe concentrations at different equilibrium conditions

As can be seen in Figure 14 above, the curve for simulated equilibrium conditions with ferrihydrite was exactly the same as when no secondary mineral precipitation was considered. Saturation indices results showed that the solution was consistently undersaturated with respect to ferrihydrite. Based on this observation, ferrihydrite was not considered in the subsequent simulations. On the other hand, the inclusion of K-jarosite and schwertmannite constrained the concentration of iron in solution as seen from the low concentration of dissolved iron in Figure 14.

Saturation indices calculations showed that the effluent solution was consistently saturated with respect to both K-jarosite and schwertmannite suggesting their precipitation. Based on the solubility constants used, the simulated iron concentration for equilibrium with K-jarosite was closer to experimental data than that for equilibrium with schwertmannite. As a result, K-jarosite was selected as the most likely iron bearing secondary mineral likely to control the concentration of dissolved iron in solution. The low concentration of iron obtained for equilibrium conditions with schwertmannite can be attributed to relatively high stability constant reported for schertmannite (see Table 21 in Chapter 3, section 3.2.1).

Effects of secondary minerals on aluminum concentration

A wide range of aluminium bearing secondary minerals were considered for their effect on dissolved aluminium concentration. The set of minerals considered were jurbanite, alunite, basaluminite, kaolinite and gibbsite. These minerals were considered due to their likelihood to precipitate at acidic to weakly acidic pH conditions. Equilibrium conditions were considered between each mineral and the aqueous phase. The results of the simulation are shown in Figure 15 below.

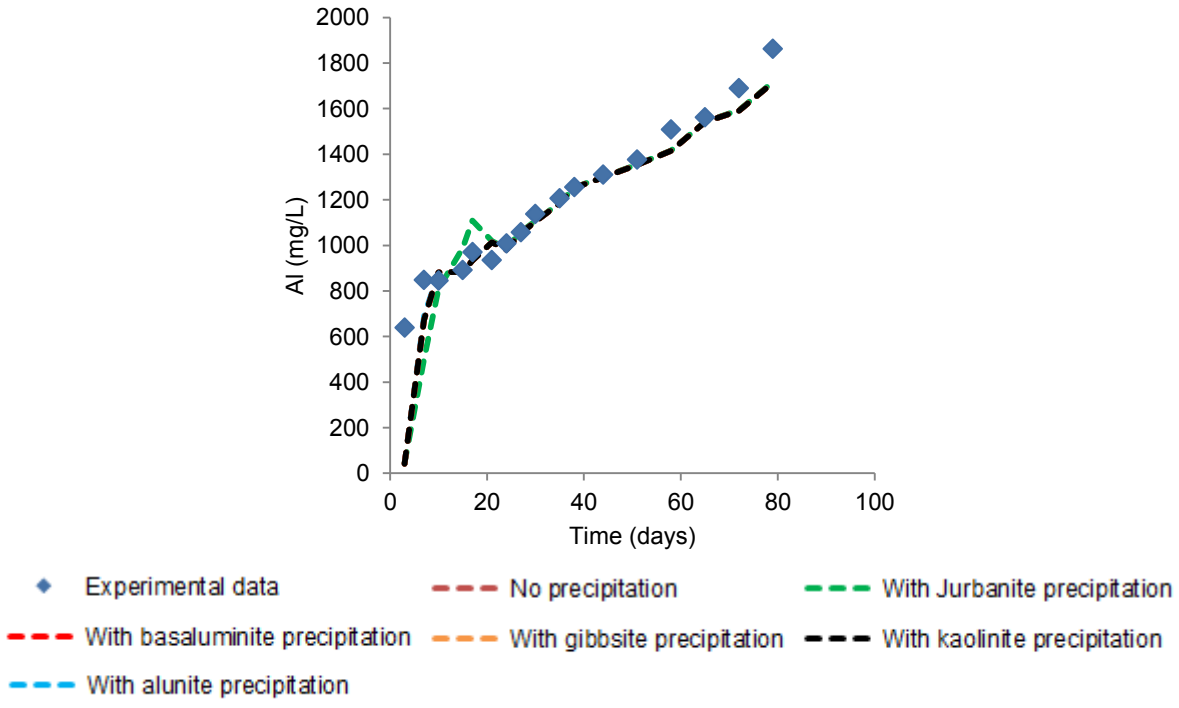

Figure 15: Comparison of Al concentrations at different equilibrium conditions

With the exception of jurbanite that was slightly saturated in the first 20 days, the rest of the minerals remained dissolved in solution as seen from the match of their trends to that without secondary mineral precipitation. Saturation indices calculation confirmed that the solution was undersaturated with respect to these minerals.

Generally, the effect of secondary mineral precipitation on aluminium concentration was insignificant, thus no aluminium bearing secondary mineral was considered in the rest of the simulations. The other secondary mineral included in the model was gypsum. Gypsum was included in the model due to the observed high sulphate and calcium concentration in the effluent. The effect of gypsum precipitation is further discussed under model validation in section 4.2.4.

4.2 Model validation results

Once the mineral surface areas and the secondary minerals likely to precipitate were established by model calibration, the model was validated against the leach test data from the large column. The results of the simulations of the large column and their comparison to experimental data are presented and discussed in section 4.2.1 to 4.2.8 below.

4.2.1 Copper concentration

A comparison of experimental and simulated copper concentration is shown in Figure 16 below.

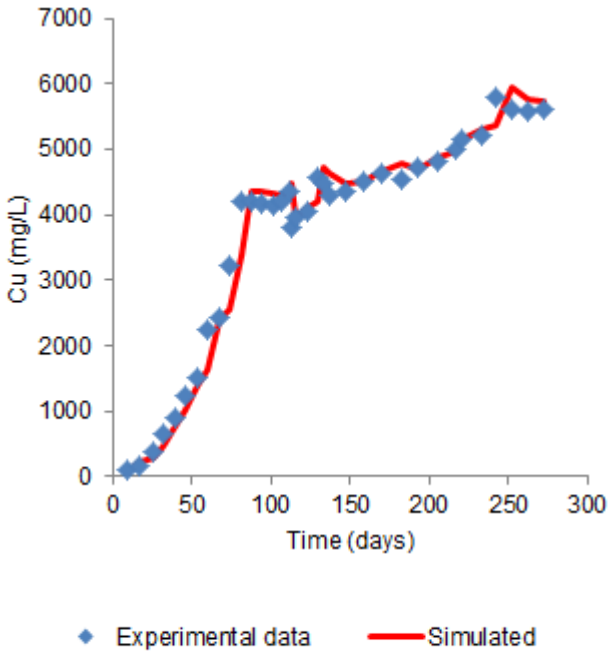

Figure 16: Comparison of experimental and simulated copper concentration

As seen from Figure 16 above, the concentration of copper increased linearly in the first 94 days of the experiment due to the rapid release of copper from fine chalcopyrite grains and possibly easily soluble traces of other copper sulphide minerals such as chalcocite. However, the release rate of copper reduced from day 94 to the end of the experiment as seen from the levelling off of copper concentration during that period of the experiment. The reduction in the copper release rate can be attributed to a number of possible factors.

In the first place, the copper release rate may have reduced due to the depletion of fine grains of chalcopyrite and other copper bearing minerals. Secondly, the increase in redox potential, iron and sulphate concentrations may have resulted in the precipitation and nucleation of K-jarosite on chalcopyrite mineral surfaces, resulting in surface passivation. Chalcopyrite leaching is often characterised by a rapid initial leaching rate that levels off with time mostly due to depletion of liberated minerals and passivation of secondary minerals on the chalcopyrite mineral surfaces (Cordoba et al., 2008b).

In contrast, the simulated dissolution rate of chalcopyrite was initially slow, but remained constant after a leach period of 100 days (see Figure 17).

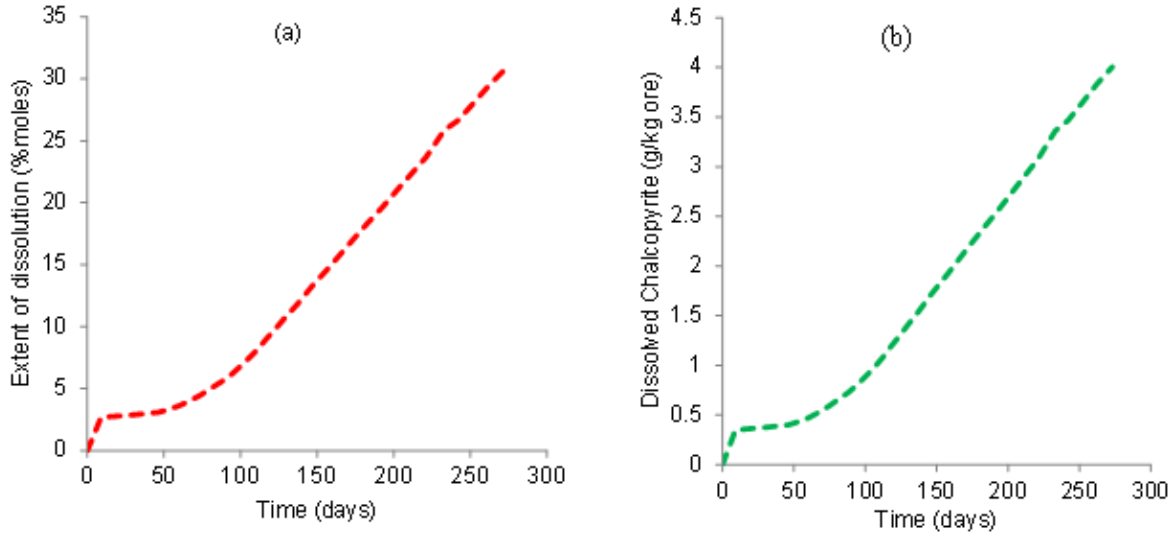

Figure 17: Simulated chalcopyrite dissolution as a function of time, showing (a) extent of dissolution and (b) amount dissolved

The discrepancy between the initial rapid increase in the measured copper concentration and the relatively slow simulated rate of chalcopyrite dissolution can probably be attributed to the variations in the dissolution rates of mineral grains due to differences in sizes (surface areas). This phenomenon was not well captured in the simulated dissolution of chalcopyrite since the model did not distinguish between fast dissolving fines and slow dissolving coarse grains. Furthermore, the rate law used to define the dissolution of chalcopyrite had a ferric iron dependence of 0.43 (see Table 18). Thus, the simulated dissolution rate was lower in the initial stages due to low ferric iron concentration arising from the precipitation of iron bearing secondary minerals and initial fast dissolution of calcite and other acid neutralising minerals respectively. According to the model prediction, about 30.8 % of chalcopyrite dissolved during the experimental period.

4.2.2 Magnesium concentration

As in the case of copper, the correlation between the experimental and simulated Mg concentrations was generally very good (Figure 18). Discrepancies in the initial stages of the column leach can most likely be attributed to the initial acidification of the ore during agglomeration, which resulted in rapid dissolution of fines and/or surface oxides, arising from weathering.

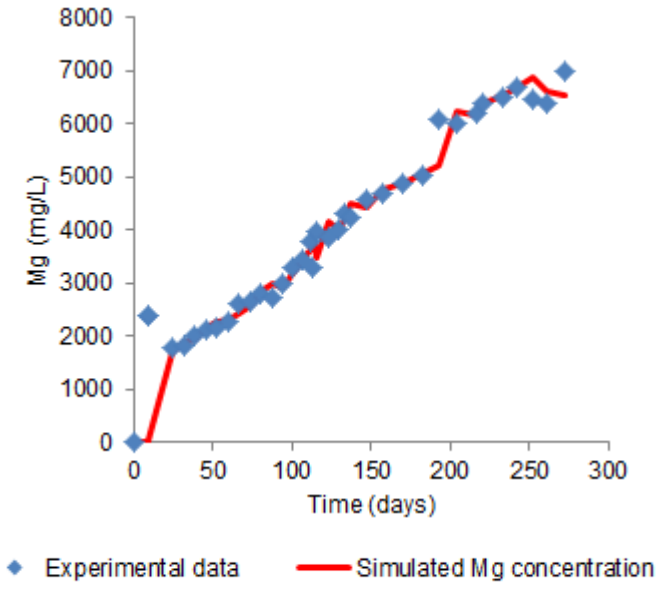

Figure 18: Comparison of experimental and simulated magnesium concentration

The concentration-time profile in Figure 18 indicated that the concentration of measured magnesium increased rapidly to over 2000 mg/L in the first 25 days of the experiment. Thereafter, the magnesium concentration profile remained constant, suggesting a relatively constant dissolution rate throughout the experiment-although results after 250 days indicates that the dissolution rate may have started to decline. In accordance with Table 12, biotite was the main magnesium bearing mineral. Despite the close correlation between the simulated and the experimental data, biotite dissolution rate (Figure 19) indicates a different initial leach profile to that obtained in practice.

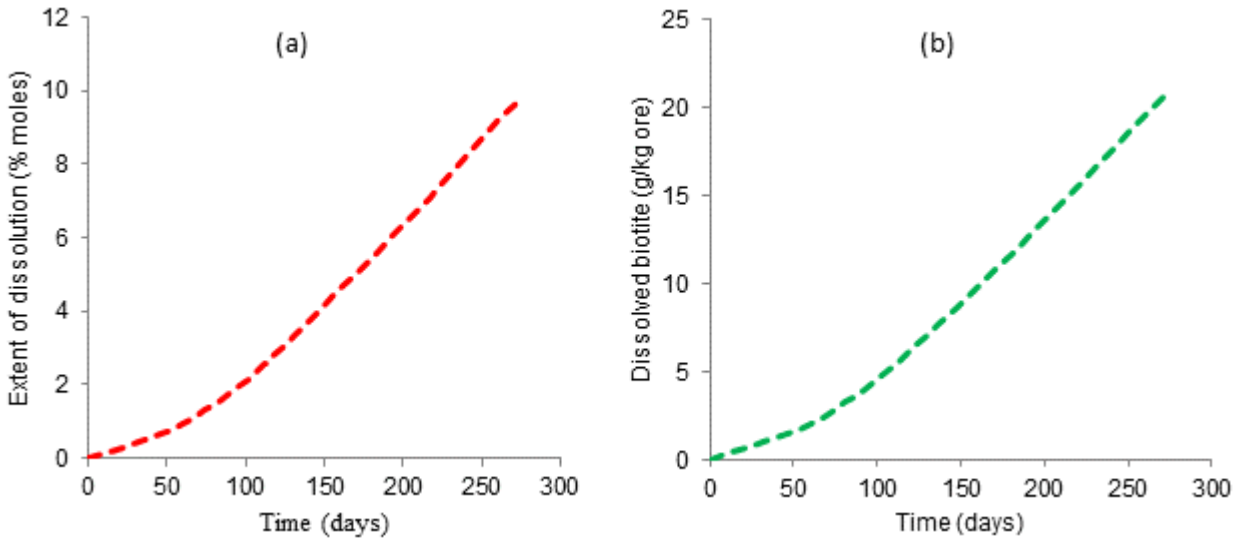

Figure 19: Simulated biotite dissolution as a function of time, showing (a) extent of dissolution and (b) amount dissolved

Whereas the measured magnesium concentration was characterised by a rapid rise at the start of the experiment, the simulated dissolution of biotite was slower in the initial stages, reaching a steady state after approximately 50 days. The rate law used to define the dissolution of biotite was pH dependent, thus the dissolution of biotite was slower in the initial stages due to high pH. Generally, the simulated dissolution rate of biotite remained constant from day 100 to the end of the experiment following the decrease in pH to about 2. Saturation indices calculations showed that the effluent was undersaturated with respect to magnesium bearing secondary minerals.

4.2.3 Aluminium concentration

Figure 20 in the next page compares simulated and measured aluminium concentration. As in the case of Mg, elevated Al concentrations in the initial stages of the leach experiment can probably be attributed to acid agglomeration of the ore. However, the overall level of agreement between simulated and experimental data was good.

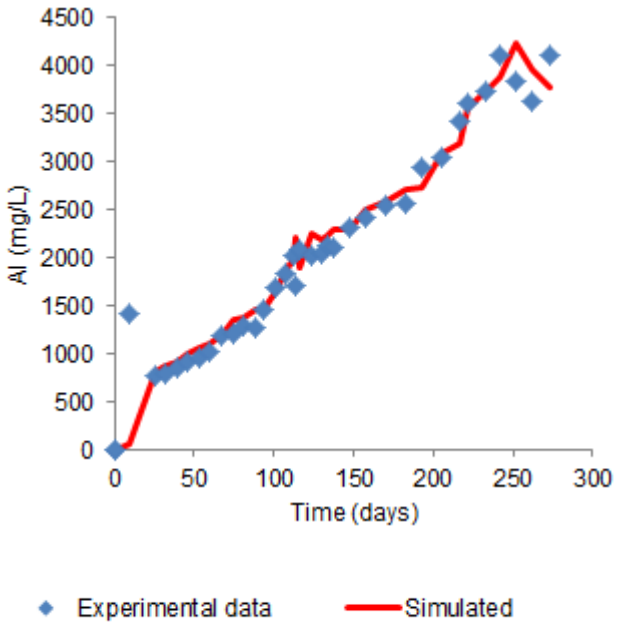

Figure 20: Comparison of experimental and simulated aluminium concentration

Generally, the Al concentration profile was relatively constant for most of the leach period, with some indication of a decrease towards the end. A similar decrease in metal concentration towards the end of the experiment was also observed for copper and magnesium. The exact cause of this decrease is unknown, but could be attributed to an experimental anomaly. Aluminium was generated by the dissolution of multiple aluminosilicate minerals present in the ore, the main ones being biotite, K-feldspar and albite (see Table 14). The contribution of these minerals towards aluminium fluxes are shown in Figure 21 below.

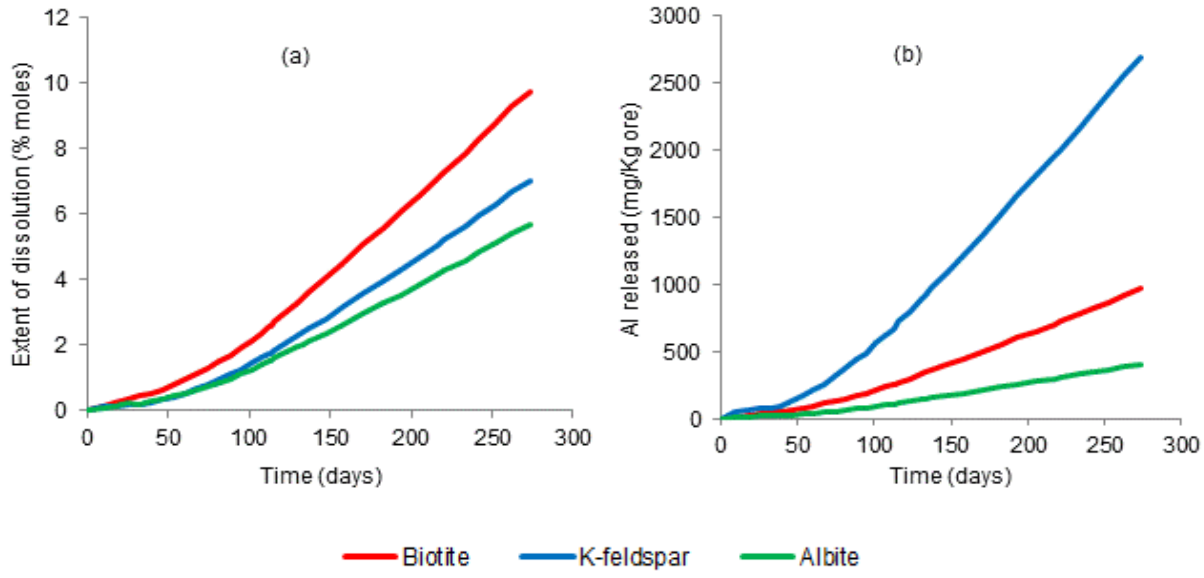

Figure 21: Simulated mineral dissolution rates and their release of aluminium as a function of time, showing (a) extent of dissolution and (b) amount of Al released

As in the case of biotite, the simulated dissolution rates were slow in the initial stages but remained steady after about 90 to 100 days. In accordance with the model prediction, the mineral with the highest percentage of dissolved amount was biotite followed by K-feldspar and last albite. However, despite having a small percentage of dissolved amount due to its high abundance in the ore, K-feldspar had the highest quantity dissolved compared to biotite and albite. In accordance with the model prediction, K-feldspar was the main source of soluble aluminium followed by biotite and lastly albite. The high release rate of aluminium from K-feldspar compared to biotite and albite can be attributed to its high surface area (see Table 20). The abundance and surface areas of the three minerals increased in the order albite<biotite<K-feldspar, whilst their dissolution rates increased in the order K-feldspar<biotite<albite.

4.2.4 Calcium concentration

Figure 22 compares the simulated and measured calcium concentrations, with and without the precipitation of gypsum. Whereas the simulation of calcium concentration without gypsum precipitation overestimated the measured calcium concentration in the first 150 days, the model reproduced the experimental dissolved calcium concentration when gypsum precipitation was taken into account until day 200, when some discrepancies occurred.

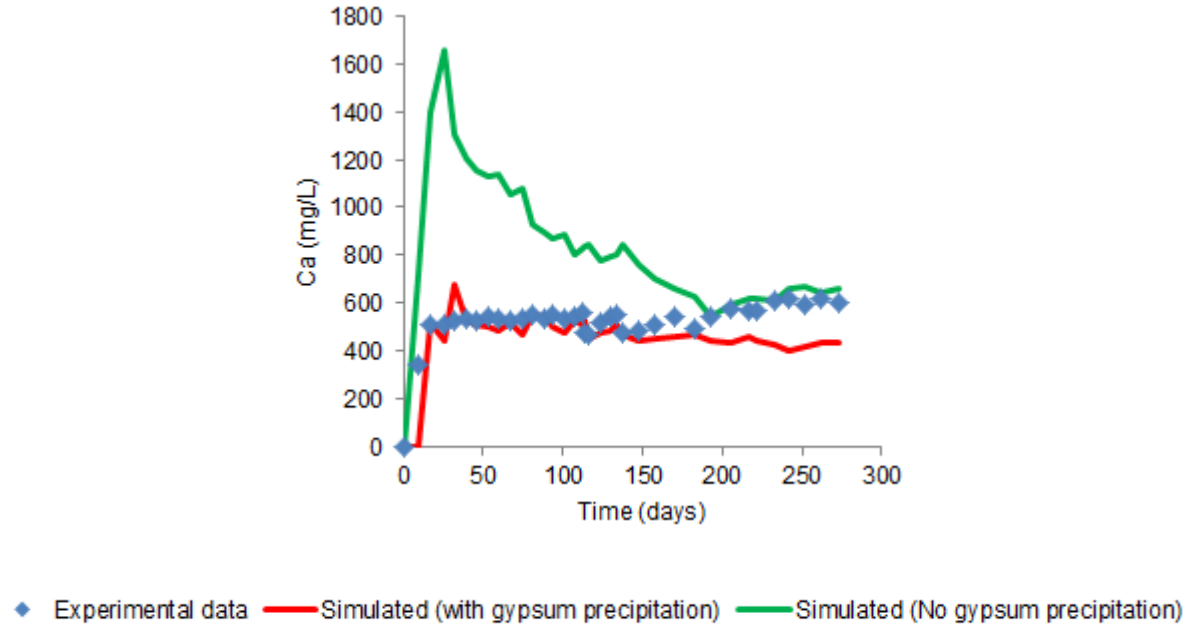

Figure 22: Comparison of experimental and simulated calcium concentration

The concentration-time profiles in Figure 22 show that, the concentration of measured calcium increased rapidly to 508 mg/L in the first 17 days of the experiment and remained virtually constant for the rest of the experiment.

A comparison of simulated Ca concentration profiles with and without gypsum precipitation indicates rapid dissolution of calcite, followed by precipitation of gypsum in accordance with the reaction in Equation 58.

$$Ca^{2+} + SO_4^{2-} + 2H_2O \rightarrow CaSO_4 : 2H_2O \qquad 58$$

The model confirmed that the aqueous solution was saturated with respect to gypsum throughout the simulation, indicating that the soluble calcium concentration was largely controlled by secondary gypsum precipitation. Although contained in calcite, albite and apatite (Table 12), dissolved calcium was mainly generated from the rapid dissolution of calcite due to its fast dissolution rate (see Table 3). The simulated dissolution rate of calcite and the corresponding amount of calcite dissolved per 1 kg ore are shown in Figure 23.

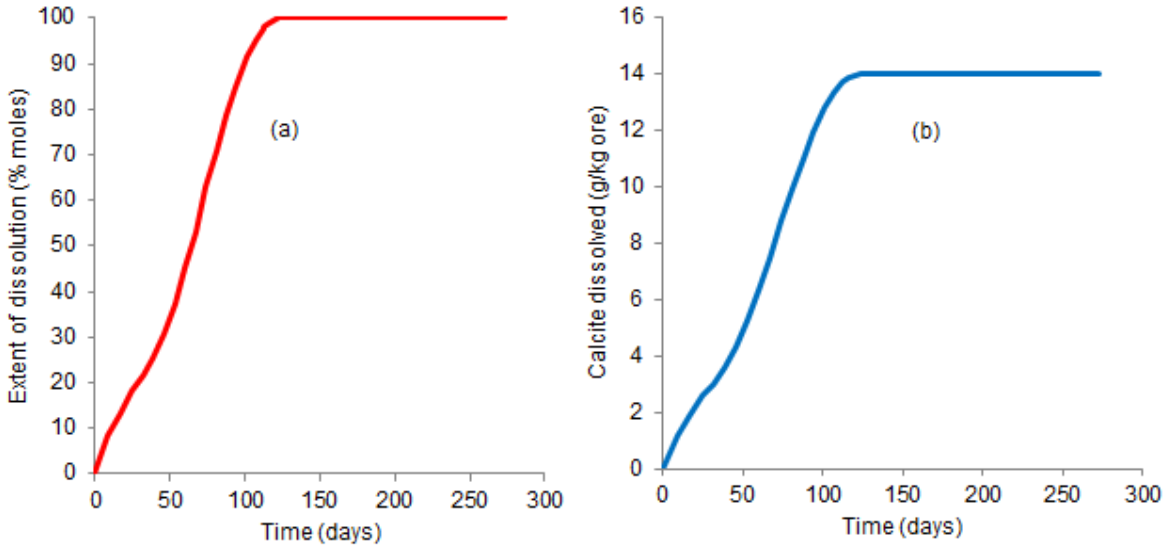

Figure 23: Comparison of simulated calcite dissolution rate and calcium dissolved per 1 kg ore.

The model predicted complete dissolution of calcite within the first 123 days of the experiment.

4.2.5 Iron concentrations

The simulated concentrations of dissolved iron, both with and without K-jarosite precipitation, are compared to experimental iron concentrations as shown in Figure 24. Despite the discrepancies in the early and late stages, the fit of the model to the experimental data was good when the precipitation of K-jarosite was taken into account. As observed for magnesium and aluminium, the discrepancy in the early stages was probably caused by acidification of the ore during agglomeration, whilst the cause for the discrepancy towards the end is not known but it can be attributed to an experimental anomaly.

A similar discrepancy was observed between simulated and experimental calcium concentration towards the end of the simulation period.

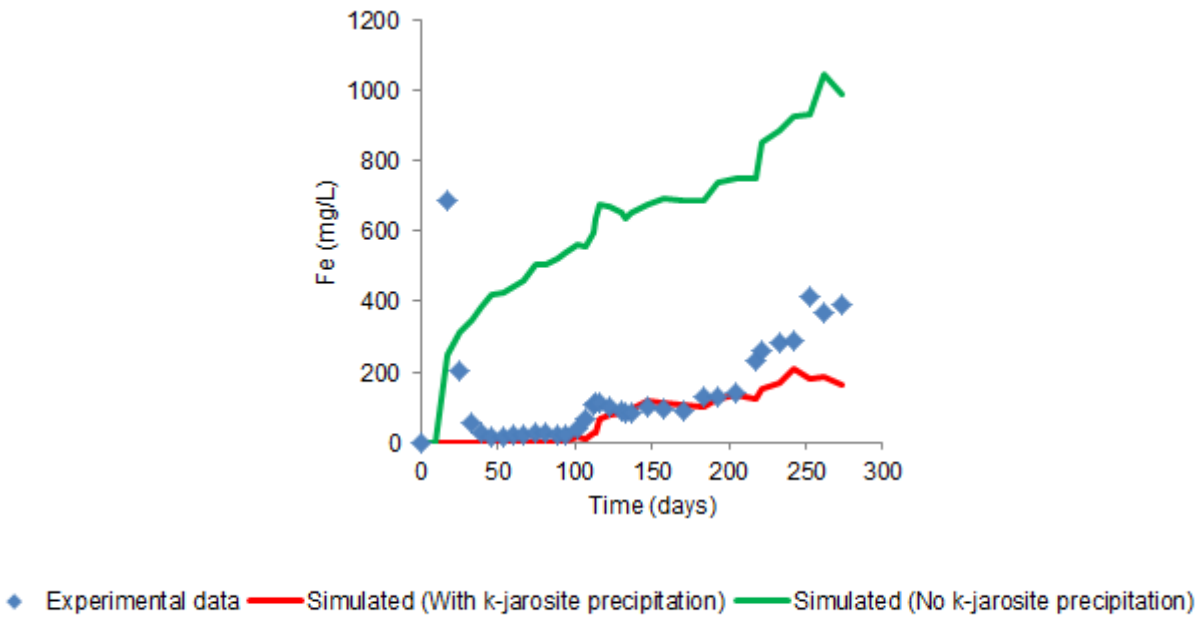

Figure 24: Comparison of experimental and simulated iron concentration

As seen in Figure 24 above, the measured concentration of dissolved iron was characterised by an abrupt increase to over 600 mg/L after the start of the experiment. After attaining the maximum value, the concentration decreased until it reached its lowest value of 15 mg/L on day 46. Thereafter, the concentration gradually increased throughout the experiment. The abrupt increase at the start of the experiment can be attributed to the rapid dissolution of fine grains and metal oxides on mineral surfaces. The decrease in iron concentration that followed can be attributed to the depletion of fine grains and the removal of dissolved iron through K-jarosite precipitation as seen in the comparison of the two simulations. The precipitation of K-jarosite was consistent with the saturation indices calculations, which showed that the effluent was saturated with respect to K-jarosite. The precipitation reaction of K-jarosite is represented by Equation 59 below.

$$3Fe^{3+} + K^{+} + 2SO_4^{2-} + 6H_2O \rightarrow KFe_3(SO_4)_2(OH)_6 + 6H^{+} \qquad 59$$

The amounts of precipitated K-jarosite during this period are shown in Figure 25 in the next page.

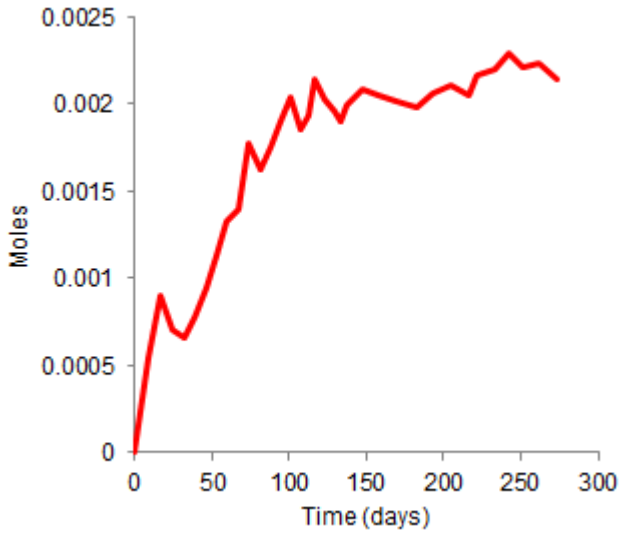

Figure 25: Simulated K-jarosite precipitation as a function of time

In accordance with model predictions, K-jarosite precipitation rate was highest in the first 100 days; thereafter the precipitation rate declined considerably. The reduction in the precipitation rate of K-jarosite with stabilisation of the pH (see sub-section 4.2.8), may have been caused by a buffering effect, with the dissolution of K-jarosite occurring at the same rate as its formation (see Equation 59).

4.2.6 Potassium concentration

A comparison of simulated and measured potassium concentrations is shown in Figure 26 below.

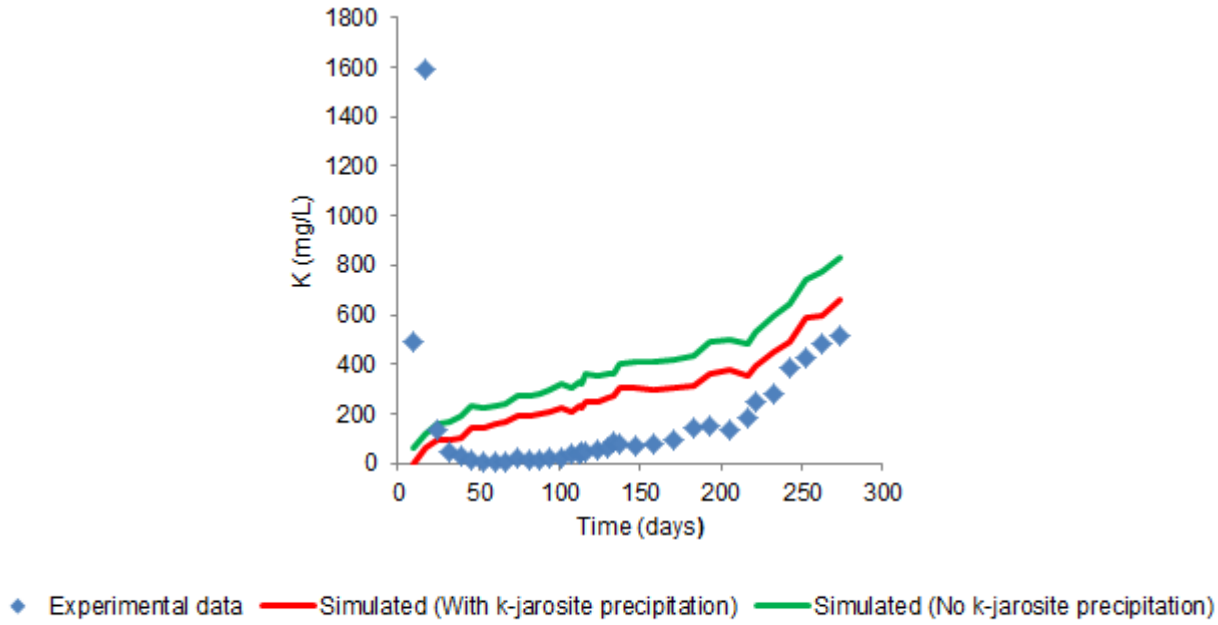

Figure 26: Comparison of measured and simulated potassium concentration

As seen in Figure 26 above, with the exception of the initial leach stages, the model overestimated the concentration of dissolved potassium throughout the experimental period. The simulated trends indicate that the precipitation of K-jarosite reduced, but did not control, the concentration of soluble potassium, which increased gradually over the leach period. In contrast, the concentration of measured potassium was characterised by a sharp increase in the initial stages of the experiment, which can probably be attributed to the solubilisation of fine particles or surface oxides. However, after attaining the maximum concentration of about 1600mg/L, it decreased sharply, remaining at low levels until over 100 days, before gradually increasing. The observed discrepancy may be attributed to either an overestimation of the extent of dissolution of K-bearing minerals or an underestimation of the extent of K precipitation through the use of a high solubility product in the simulations.

4.2.7 Sulphate concentration

Generally, the model reproduced the measured sulphate concentration as seen from the comparison of simulated and measured sulphate concentration (Figure 27).

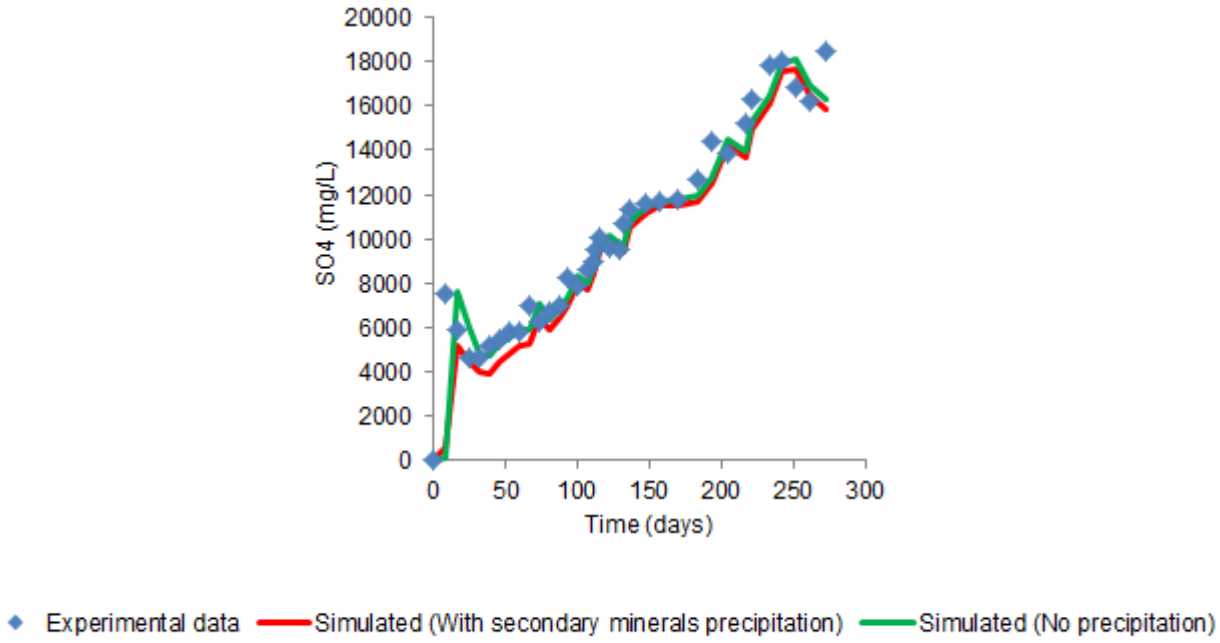

Figure 27: Comparison of measured and simulated sulphate concentration with and without precipitation of secondary minerals (gypsum and K-jarosite)

The concentration of sulphate rapidly increased to 4731 mg/L in the first 25 days of the experiment. Thereafter, it increased linearly and attained a maximum concentration of 18012 mg/L on day 242 of the experiment before suddenly reducing to 16192 mg/L on the last day of the experiment (see comments in section 4.2.3).

Although sulphate was generated from the oxidation of the sulphide minerals, chalcopyrite and to a lesser extent, pyrite, a significant amount of sulphur was also introduced into the column through the addition of sulphuric acid that was used to correct the pH of the recycled feed solution.

4.2.8 Effluent pH

The effluent pH was controlled by a series of processes that included primary mineral dissolution, precipitation of secondary minerals, as well as the addition of acid to the column in the recycled solution. A comparison of measured and simulated pH with and without K-jarosite precipitation is shown in Figure 28 below.

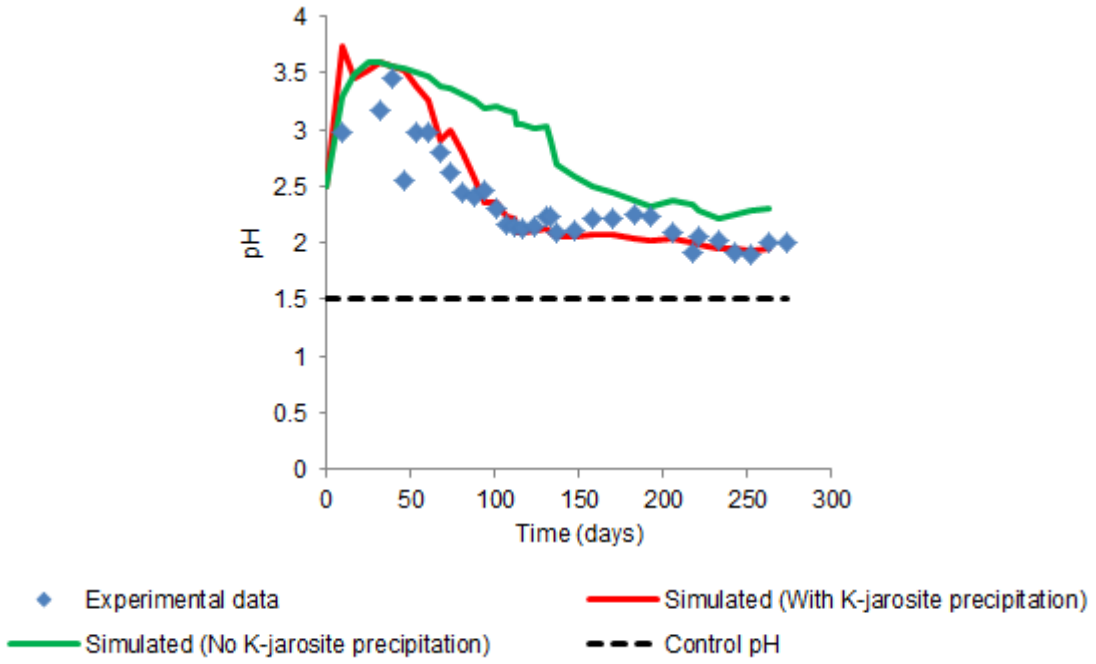

Figure 28: Comparison of experimental and simulated pH with and without K-jarosite precipitation

As shown in Figure 28 above, the pH profile was characterized by a rapid initial increase largely due to the rapid dissolution of calcite (see sub-section 4.2.4). This was followed by a decline in pH from day 39-137, as the calcite became depleted and the extent of acid formation, due to sulphide oxidation and the subsequent precipitation of K-jarosite, increased. A comparison between the simulation of pH with and without K-jarosite precipitation indicates that its formation had a significant effect on pH during this period. After 137 days, the pH stabilised at a value close to 2, before declining slightly after 200 days. The pH profile indicates that the pH of the effluent solution was buffered to a constant value of about 2 by the dissolution of non-carbonate minerals after the depletion of calcite (123 days). The effect of calcite and aluminosilicate mineral dissolution on the effluent pH was investigated by running simulations with each of the potential acid neutralising minerals.

In this way, the contribution of each mineral towards the overall acid neutralisation was investigated. The results of these simulations were compared to the measured pH as shown in Figure 29 below.

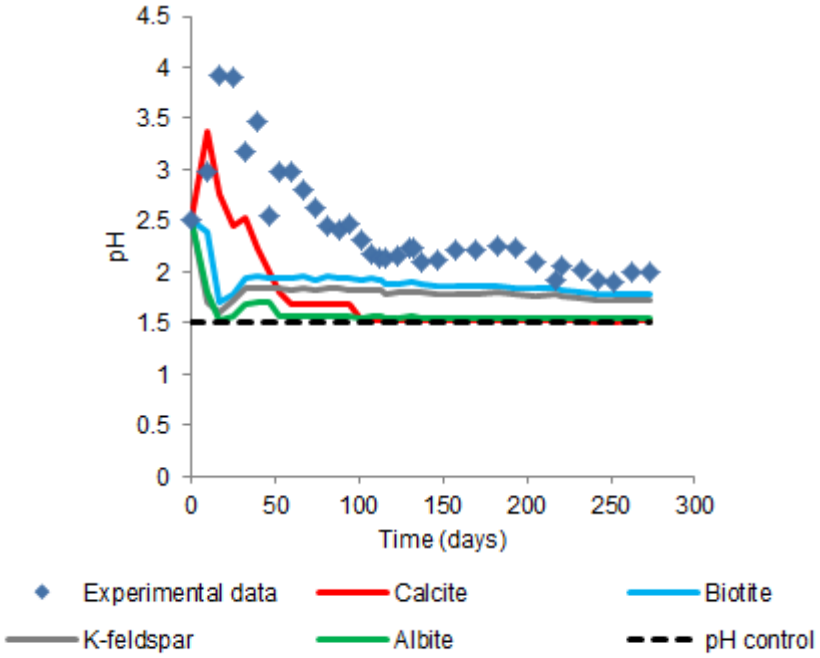

Figure 29: Acid neutralisation mineral dissolution processes

The simulated results in Figure 29 indicate that calcite was the dominant acid neutralisation mineral in the early stages of the experiment. However, after the depletion of calcite the pH was mostly buffered by the kinetic dissolution of biotite and K-feldspar (see reaction in Table 4, Chapter 2). Biotite and K-feldspar maintained the pH of the effluent close to 2 for the rest of the experimental period despite the column being fed with highly acidic solution (1.5 pH solution). Albite had negligible neutralising capacity. As seen in Figure 29, the contribution of albite towards acid neutralisation was almost insignificant due to its low calibrated surface area that resulted in slow dissolution rate.

4.3 Model sensitivity analysis of influencing parameters

The results of the model sensitivity study are presented and discussed in this section. The parameters investigated were pyrite content, calcite content and liquid flow rates.

4.3.1 Pyrite content

Pyrite is the most abundant sulphide mineral in mine waste and its concentration and availability in relation to acid neutralising minerals has a significant effect on the acid generating properties of mineral wastes. Typical pyrite content in mine wastes such as mill tailings range from less than 0.5 wt. % to about 5 wt. %, although pyrite content as high as 18 wt. % has been reported in very rare cases (Blowes et al., 2003a).

The pyrite content of 0.2 wt. % in the sample used for this case study is considered to be relatively low. The effect of pyrite content on simulated pH values was investigated by adjusting the pyrite content to range of values consistent with those reported for typical mine wastes, namely 2 and 5 wt. %. The results of these simulations were compared to the base case of 0.2 wt. % pyrite in Figure 30.

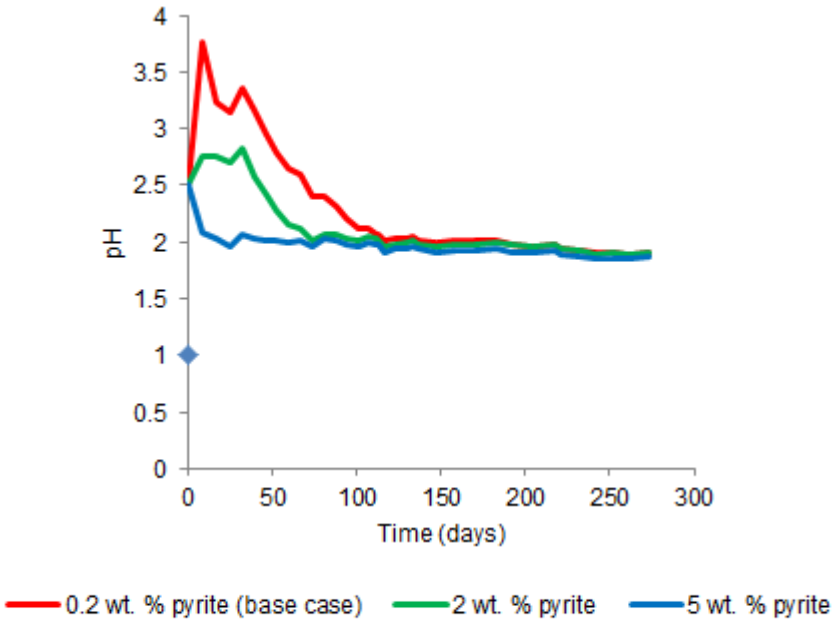

Figure 30: Simulated pH at different pyrite contents

As seen in Figure 30 above, there was a clear difference in pH profiles in the first 123 days of the simulation. However, the difference in pH profiles became insignificant as the amounts of pyrite were depleted in all the three scenarios. The pH profiles did not drop to below 1.5 (pH control) due to the increased reactivity of the pH dependent biotite and K-feldspar dissolution at lower pH. The dissolution of these minerals maintained the pH above 1.5. The model results show a general decrease in pH as the pyrite content is increased. This is consistent with the acid producing oxidative dissolution of pyrite represented by Equation 3 (Chapter 2, section 2.1.1) below.

$$FeS_{2(s)} + 14Fe^{3+}{}_{(aq)} + 8H_2O_{(l)} \rightarrow 15Fe^{2+}{}_{(aq)} + 2SO_4^{2-}{}_{(aq)} + 16H^{+}{}_{(aq)} \qquad 60$$

As shown in this equation, the oxidation of pyrite by ferric iron generates significant amount of acid and other oxidation products such as iron and sulphate. The release of sulphate and iron into solution results in the precipitation of ferric iron bearing secondary minerals such as K-jarosite, schwertmannite and ferric hydroxides. The precipitation of these minerals generates more acid.

4.3.2 Calcite content

Carbonates are the most effective acid neutralising minerals in mine waste particularly due to their fast dissolving rates (Perkins et al., 1995). Typical calcite contents in mine waste can range from less than 1 wt. % to as high as 10 wt. % (Jurjovec et al., 2002; Blowes et al., 2003a). The pH buffering effects of calcite was investigated by carrying out simulations with varying calcite input values. The range of calcite values selected is consistent with those reported in typical disposal scenarios. For the purpose of demonstrating the effect of calcite content on model output, average calcite content values of 4 and 8 wt. % were selected while the case study calcite content of 1.4 wt. % was used as the base case. The results of these simulations were compared on the basis of pH in Figure 31.

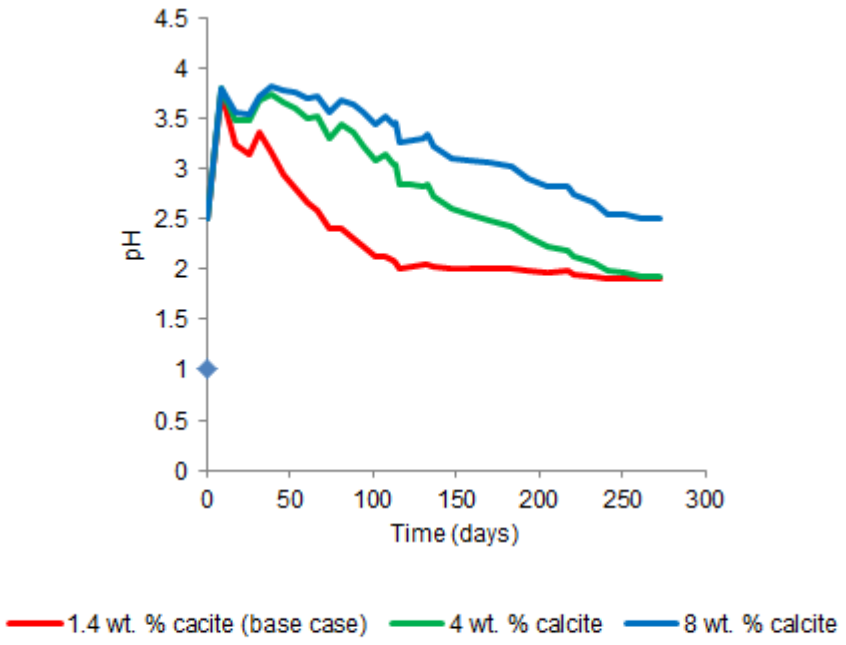

Figure 31: Effects of calcite content on effluent pH

As can be seen from Figure 31, the pH-time profiles were the same for all calcite concentrations. The pH profiles were characterised by an initial increase, followed by a decline as the calcite becomes depleted. Finally, the pH stabilised after all the calcite completely reacted. Generally, an increase in the concentration of calcite delayed the lag period before the decline of the pH. In addition, an increase in calcite concentration also decreased the rate at which the pH decreased whilst extending the period prior to pH stabilisation.

4.3.3 Sensitivity to fluid velocity

The transport of bulk liquid and solutes within waste deposits are important physical processes because of their effect on the loading and composition of the effluent solution. The sensitivity of liquid and solute transport to the model output was investigated by running simulations at different time steps. Assuming that the moisture content is constant, a decrease in the time step results in an increase in the liquid flow rate while an increase in the time step results in a decrease in the liquid flow rate. Thus, the case study time step was reduced (halved) and increased (doubled) in order to investigate the effects of high and low liquid velocity on calcite dissolution rate and pH profile. These were compared against the case study time step of 24200 s (equivalent to 2.28 x 10^{-5} m s^{-1} liquid velocity) that was used as the base case. The results of the simulations are shown in Figure 32.

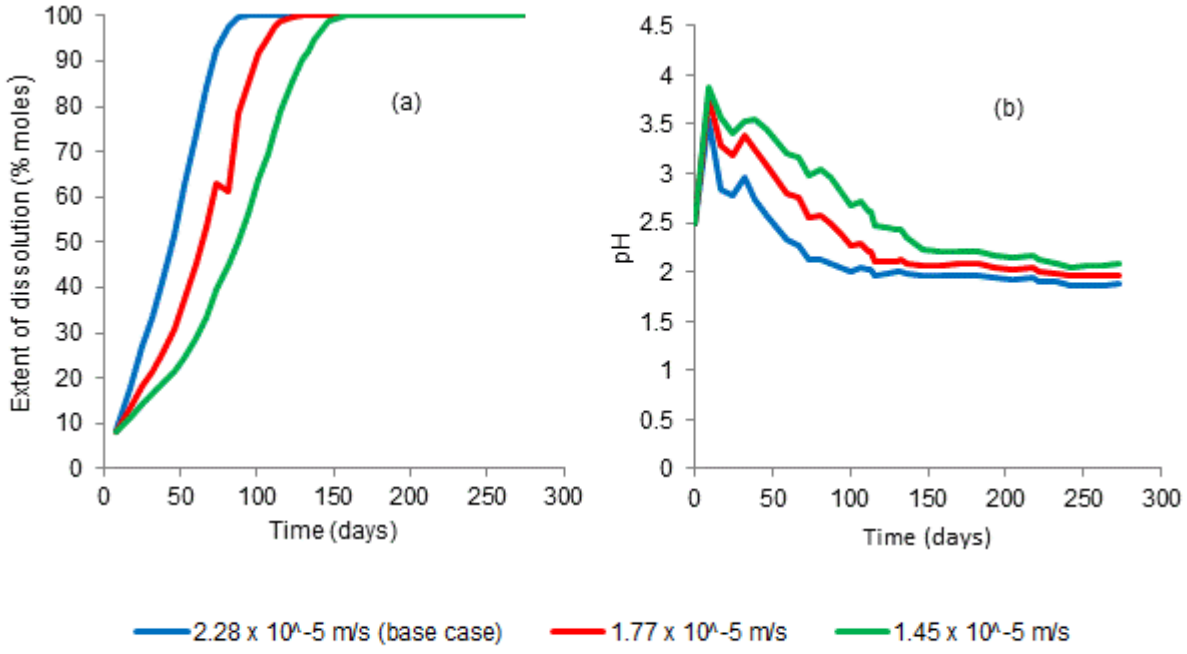

Figure 32: Calcite dissolution and pH at different fluid velocities

As can be seen from Figure 32, an increase in flow rate of low pH water (pH 1.5) resulted in an increase in the acid loading and hence a decrease in the solution pH and increase in the acid dissolution rate of calcite. Infiltration rates in typical disposal scenarios vary, depending on the seasonal rainfall patterns but are reported to be in the range of 100 to 500 mm/yr or approximately 3x10^{-9} to 1.5x10^{-8} m s^{-1} (Nicholson et al., 2003; Linklater et al., 2005). These values are much less than the flow rate used in the case study. At such low flow rates, transport is likely to be dominated by both transverse and advection-dispersion flow. As a result, the assumption that transported only occurs by advection-dispersion is likely to overestimate the concentration profiles of elements at the base of the waste deposit.

5 CONCLUSION AND RECOMMENDATIONS

Although laboratory-scale tests are useful in characterising the acid generating potential of sulphide bearing mine waste, their extrapolation to full-scale waste deposit scenarios requires the subsequent use of mathematical models which take into account the governing chemical reaction and physical transport mechanisms. However, current ARD prediction models are both complex and resource intensive in terms of data and time, and only warranted in the case of detailed site-specific predictive studies. This project explored the use of simple geochemical mass transport models suitable particularly for early stage project decision making. The two main objectives of the study were; (i) to review and assess the existing literature pertaining to the main processes governing the generation of ARD at mine waste (ii) to demonstrate the capabilities and limitations of PHREEQC geochemical code by developing an ARD predictive model and applying it on unsaturated flow-through column scenario. These objectives were achieved by answering the following research key questions;

(1) What are the key waste characteristics and mechanisms governing the generation and quality of ARD from solid mine wastes?
(2) To what extent can the mechanisms identified in (1) be incorporated into PHREEQC based model?
(3) What are the main input parameters required in a PHREEQC based model?
(4) What are the effects of key variables on the accuracy and reliability of the model for simulating ARD profiles in a flow-through column scenario?
(5) Under what conditions can the PHREEQC code be used for ARD prediction?

The above research key questions were addressed through literature review, model development and its application to a selected case study. More specifically, the literature review presented in Chapter 2 addressed the first three key questions of this study. Firstly, the main chemical and physical mechanisms governing the generation of ARD from mine waste were identified in sections 2.1 and 2.2 of the literature review. Based on the knowledge of the main governing mechanisms and the detailed literature review of the capabilities of PHREEQC geochemical code, the model was developed. The key processes incorporated into PHREEQC and their input parameters were identified from the literature. To address the last two key questions, the model was applied to a case study entailing the laboratory-scale column bioleaching of a low grade copper sulphide ore.

The outcomes of this study in the light of the key question mentioned above are communicated in sections 5.1 and 5.2. Section 5.3 makes recommendations for future work.

5.1 Summary of key research findings

Section 5.1.1 summarises the key findings in terms of the capabilities and limitations of the PHREEQC code in predicting ARD generation rates, extents and leachate quality. Sub-section 5.1.2 presents the key outcomes from the case study.

5.1.1 PHREEQC for predictive modelling of ARD

The review of the literature in Chapter 2 showed that the generation of ARD is governed by a complex network of chemical and physical reaction mechanisms and their influencing parameters. Of key relevance are the kinetically-controlled oxidation of sulphide minerals and dissolution of acid neutralising minerals, such as carbonates and aluminosilicates. Also of key importance are the equilibrium-controlled secondary precipitation reactions, including formation of iron and aluminium oxyhydroxides and hydroxysulphates, secondary aluminium silicates such as kaolinite, as well as gypsum. In a flow-through scenario, such as that which occurs in a waste deposit, the rates and extents to which these chemical reactions occur will be governed to a large extent by physical transport processes, with the main one being solute transport, gas and heat transport and microbial transport and attachment. These chemical and physical reaction mechanisms are, furthermore, influenced by a number of factors including ore characteristics and climatic conditions.

PHREEQC is able to simulate many of the relevant chemical and physical reaction mechanisms while taking into account the key influencing parameters. The model also makes a number of simplifying assumptions and generalisation. Model capabilities and limitations in terms of simulating kinetic, equilibrium and physical transport processes are discussed in more detail in the sub-sections below:

- Kinetically-controlled chemical reactions

Acid producing and consuming kinetically controlled reactions are simulated as surface-controlled reactions and defined by means of user-defined rate laws and constants. The PHREEQC code does not consider diffusion controlled reactions. This limitation can result in an overestimation of the mineral reactions rates when the dissolution mechanism shifts from a surface controlled to a diffusion controlled reaction due to passivation and oxygen limitation. The kinetic model also assumes that all minerals are fully liberated and in contact with the leaching reagent. This can result in an overestimation of mineral dissolution rates in cases where minerals are partially or completely occluded in other minerals, or when passivation of mineral surfaces by secondary precipitates occurs.

Key model inputs include the molar amount of each specific mineral, the mineral surface areas and the rate laws and constants. The initial molar amount is derived from the bulk

density, porosity and mineral content (weight percent). Mineral surface areas are normally estimated from the specific surface area of the solid, based on the average particle size.

- Equilibrium controlled reactions

PHREEQC code has capability to simulate precipitation/dissolution reactions. These reactions are assumed to be equilibrium controlled reactions and are simulated using literature solubility constants. The main input parameters required for the simulation of precipitation/dissolution reactions are the name of the precipitating secondary mineral and the target saturation indices. By specifying the target saturation indices to zero, the specified mineral is allowed to precipitate at saturation or to dissolve when the solution becomes under-saturated in order to attain equilibrium with the aqueous phase. The main limitation and key source of uncertainty relates to the selection of the precipitating secondary minerals and their corresponding solubility constants. Since a large number of solubility constants are reported in the literature, the effect of the precipitating mineral on the effluent quality depends largely on the solubility constant value used. Furthermore, the model may, in some cases, predict the precipitation of minerals that are unlikely to form in practice, due to their slow precipitation rates, particularly under ambient conditions. In such cases, the selection of the minerals to be included in the model depends on the modeller expertise and experience, thus making the process somewhat subjective. Equilibrium conditions between the gas phase and the aqueous phase can also be simulated by specifying the name of the gas and its partial pressure. The main limitation of this approach relates to oxygen mass transfer limitations that are not accounted for in the model. This may result in an overestimation of the oxidation rates of solid minerals and aqueous species, particularly in the lower levels of the saturated deposits or in deposits with covers. The main input parameters required for simulation of gas-liquid equilibria are gas types and their respective partial pressures.

- Physical transport processes

The PHREEQC code uses the mixing cell modelling approach to simulate 1-D transport processes by advection-dispersion and diffusion to stagnant zones in the saturated media. Transport processes are combined with equilibrium and kinetically controlled reactions to simulate the feedback mechanisms between the chemical reactions and mass transport processes in a flow-through scenario. The movement of solution is vertical for advection-dispersive transport and horizontal for diffusion transport. The dispersion of fluid during transport is accounted for by mixing the cell contents during each transport process. The model does not take into account the effects of transverse and transient flow.

The effects of preferential flow and changing moisture are also not included in the model. Although these effects can be fairly significant in unsaturated waste deposits, their quantification is complex and requires extensive input data. As such their inclusion in a first-order prediction model is unlikely to be warranted. In the PHREEQC code transport model, fluid velocity is represented as time step where a high time step represents a low fluid velocity whilst a low time step represents a high fluid velocity. The key parameters required for simulation of mass transport processes are time step, number of transport processes (shifts), dispersivity, diffusion coefficient (for diffusion transport), and the number and size of cells.

Due to the fact that it is limited to saturated scenarios, the PHREEQC code uses simplifying assumptions to represent heat transport and oxygen availability. Heat transport is assumed to occur by diffusion within the saturated media, while the reacting gases (mainly oxygen and carbon dioxide) are assumed to be uniformly dissolved in the aqueous phase. Mass transfer limitations during gas transport are not accounted for in the model. These assumptions may result in an overestimation of the rates and extents of gas-solid and gas-solute reactions, particularly in the case of unsaturated waste deposits. Furthermore, PHREEQC does not account for microbial transport and attachment mechanisms. However, through its user defined rate laws, the code allows for definition of biologically mediated reactions, such as the rapid oxidation of ferrous iron and sulphide sulphur.

5.1.2 Case study outcomes

The case study used in the study was designed to determine the rate and extent of copper recovery from a low grade ore in a heap leach scenario. Conditions were thus selected to optimise sulphide oxidation, by means of bacterial inoculation, acidic pH values and relatively high flow rates. Nevertheless, the scenario can be correlated with ARD generation from a waste rock pile under worst case conditions i.e. under conditions which promote bacterial activity and acid generation. The case study ore was primarily made up of aluminosilicate minerals with small amounts of chalcopyrite (1.3%) pyrite (0.2%) and calcite (1.4%).

The model developed in this study was implemented using the PHREEQC geochemical code. The model was calibrated with respect to mineral surface areas and precipitating secondary minerals using data from small leach columns, before being validated on the large leach columns in order to assess its predictive capability. Both data sets used in the calibration and validation were derived from the case study. The calibrated mineral surface areas were significantly higher than the values calculated using the geometric method.

This can largely be attributed to the underestimation of the calculated mineral surface areas, mainly due to the large range of particle sizes. Model simulation results indicated that the soluble iron and calcium concentrations were controlled by the precipitation of jarosite and gypsum respectively, with the effluent solutions remaining over-saturated with respect to these secondary minerals throughout the leach period. Jarosite precipitation also resulted in lower pH values and K concentrations. No formation of secondary aluminium precipitates was predicted, with the solution remaining under-saturated with respect to jurbanite, kaolinite and gibbsite.

Generally, there was good correlation between the simulated and the experimental data, due partly to the recycling of leach solution. Since the feed solution composition was predefined in the input file, the difference between the model simulation and the experimental data represented the changes in the feed solution during each irrigation stage. However, discrepancies were observed in the early stages which is attributed to the acid agglomeration of the ore and variations in dissolution rates between fine and coarse particles. In addition to simulating leach profiles and identifying likely secondary precipitating minerals, the model was also able to predict the key main controlling mechanisms and minerals controlling the quality of the effluent solutions, as well as the effects of experimental conditions and parameters on such. According to the model results, dissolved copper was mainly generated from the oxidative dissolution of chalcopyrite by ferric iron. The model predicted that approximately 30.8 % of chalcopyrite had dissolved by the end of the experimental period. Soluble magnesium was attributed to the gradual dissolution of biotite, with approximately 10% dissolution occurring over the leach period. The main source of aluminium was K-feldspar, followed by biotite and, to a lesser extent, albite. Model simulations showed that while calcite was the major neutralising mineral in the early stage of the experiment, following depletion of the calcite after approximately 120 days, the pH was buffered at a value of 2 by the slow dissolution of the aluminosilicate minerals, K-feldspar and biotite. A sensitivity analysis showed that an increase in the pyrite or calcite contents would result in a decrease and increase in the pH values for the first 100 days respectively.

5.2 Concluding remarks

The study has demonstrated that simple modelling approaches can provide reasonably accurate estimates of the time-related concentration profiles of key elements under continuous flow through conditions, as well as identify the controlling geochemical processes and parameters. The additional information obtained from the model with respect to mineral dissolution rates and amounts of undissolved minerals as a function of time are particularly useful in the evaluation of the long term extent of ARD generation.

In addition, this information can be used to interpret laboratory scale results by enabling better understanding to the main controlling mechanisms.

The outcome of this study has identified some of the key limitations of PHREEQC code and conditions under which it can be used for ARD prediction. Due to its limitation to one spatial dimensions and inability to simulate gas and heat transport in the unsaturated media, PHREEQC code is most suitable for fully saturated scenarios or for unsaturated scenarios in which heat and gas transport are not the main influencing processes. In most cases, however, model assumptions and simplifications are likely to result in an overestimation of the time-dependant leachate concentration profiles, and can thus be considered as providing a simulation of the worst-case scenario. Despite these limitations, PHREEQC code can be used as one of the tools for initial screening or evaluation of sulphide waste for potential long term ARD generation, particularly in the early stage project decision making, on the basis of the mineralogy and the physical characteristics of the feed material. This can be coupled with expert knowledge of key reaction mechanism and the typical flow mechanisms and parameters in a disposal scenarios.

On the basis of this work the potential role of PHREEQC code in the overall ARD prediction protocol is illustrated diagrammatically in Figure 33. In accordance with this protocol, level 1 assessment tasks involve analysis of waste coupled with data collection in order to generate information on the relevant physio-chemical parameters required for level 2 assessment. These parameters include mineralogy, physical characteristics of the waste, data pertaining to typical flow rates and saturation levels in waste deposits, mineral reaction rate laws and constants, as well as likely controlling species and mechanisms. Level 2 assessment entails characterisation of the likely ARD generating potential and behaviour of the waste under typical disposal conditions using standard laboratory scale tests and geochemical mass transport models. Standard laboratory scale tests such as the ABA and the NAG tests are used to classify waste in terms of its ARD generating potential while kinetic tests such as the biokinetic test provide information on the relative rates of acid forming and neutralisation reactions. On the other hand, geochemical mass transport models such as PHREEQC code can be used with the information obtained from level 1 assessment to obtain information on the likely controlling mechanisms and the potential pH and concentration profiles in a flow-through scenario. Lastly, level 3 assessment involves the use of long term column leach and lysimeter studies, coupled with advanced predictive modelling, for reliable quantification of site-specific pore water quality over extended time periods. It is recommended that the information obtained from these tests can be combined with that obtained from level 2 assessments as input for carrying out generic and site specific advanced predictive modelling of chemical and physical transport processes under non-ideal flow conditions.

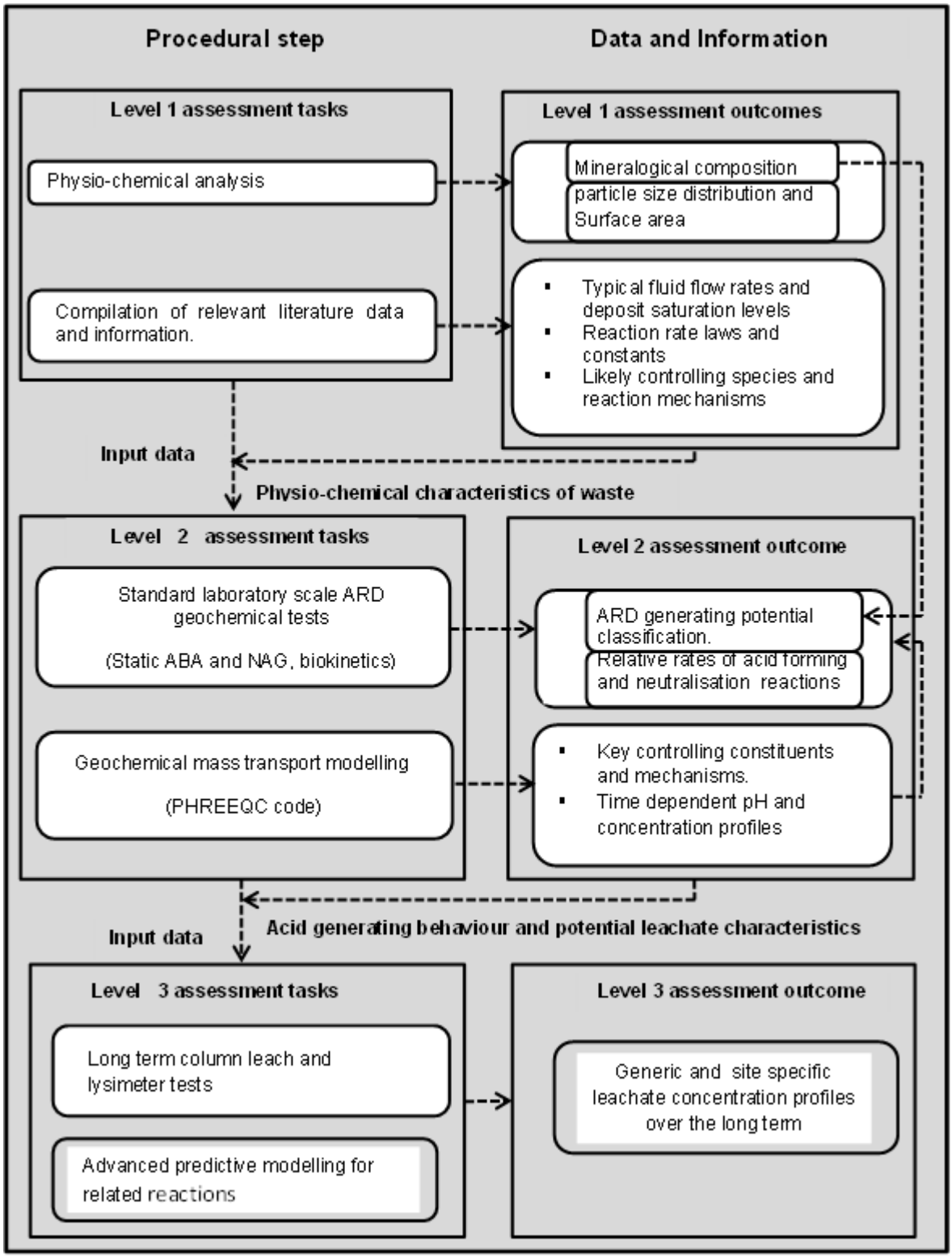

Figure 33: Schematic chart showing the role of PHREEQC code in the overall ARD prediction protocol

5.3 Recommendations for future work

This section makes recommendations on further work in terms of enhancing the reliability and accuracy of the model (sub-section 5.3.1) and extending its application to other feed materials and scenarios (sub-section 5.3.2).

5.3.1 Recommendations for further model development

Future areas of research pertaining to further development and refinement of the PHREEQC-based ARD prediction model are discussed in this sub-section. In the first place, it is recommended that future studies should consider expanding the current model to include other capabilities not considered in this study. Processes to be incorporated should include adsorption/desorption and diffusion processes. In the second place, it is recommended that the level of agreement between a PHREEQC based model and more advanced modelling approaches, which take into account transport in 2-D and unsaturated media, be investigated by running simulations with similar input parameters. This would assess the accuracy of a PHREEQC based model and determine its suitability for assessing the rate and extent of ARD generation under different mitigation options particularly those in which the generation of ARD is kinetically controlled rather than oxygen diffusion controlled. Such a comparison could also be used to assess the ability of the model to assist in preliminary comparisons of the performance of different ARD mitigation options e.g. by comparing options which are designed to limit ingress of oxygen with risk removal options such as desulphurisation and co-disposal.

In the third place, it is recommended that the ability of the model to simulate different column leach scenarios be considered. For instance, it would be interesting to assess the accuracy of the model for an open cycle solution management system i.e. one in which effluent solution is not recycled. This will provide a better indication of the capabilities of the model, under conditions where the model fit to experimental data is not partly aided by the recycled feed solution predefined in the input file. It is also recommended that further efforts are made to improve the quality (both in terms of availability and accuracy) of input data, particularly in terms of mineral surface areas and extent of liberation. This will reduce the uncertainties associated with these parameters and enable a full assessment of the extent of their influence on model output.

5.3.2 Recommendations for further model application

In the light of the outcome of this study, it is recommended that further studies be conducted with a view to extending application of the model to other types of waste (e.g. gold and coal). This will assess the model's reliability and robustness on different waste types.

Secondly, since the model can provide information on the key controlling mechanisms, it would be helpful to use these capabilities in the design, interpretation and optimisation of geochemical test results e.g. biokinetic test.

6 References

Abreham, A.Y., 2007. *Reactivity of alum and black shale in the Oslo region, Norway*. MSc Thesis. Faculty of Mathematics and Natural Sciences, University of Oslo,Norway.

Afewu, K.I., 2009. *Development and testing of a 2D axisymmetric water flow*. PhD Thesis. Vancouver: University of British Columbia.

Africa, C., Harrison, S., Becker, M. & Van Hille, R., 2010. In situ investigation and visualisation of microbial attachment and colonisation in a heap bioleach environment: The novel biofilm reactor. *Mineral Engineering*, 23, pp. 486-491.

Allison, J.D., Brown, D.S. & Novo-Gradac, K.J., 1990. *MINTEQA2/PRODEFA2--A geochemical assessment model for environmental systems-version 3.0 user's manual*. Athens,Georgia: Environmental Research Laboratory, Office of Research and Development, U.S. EPA.

Anbeek, C., 1992. Surface roughness of minerals and implications for dissolution studies. *Geochimica et Cosmochimica Acta*, 56 (4), p.1461–1469.

Andre, B.J., 2009. *Generation of acid mine drainage: Reactive transport models incorporating geochemical and microbial kinetics*. PhD Thesis. Faculty of the Graduate School of the University of Colorado.

Ball, J.W. & Nordstrom, D.K., 1991. *User's manual for WATEQ4F, with revised thermodynamic data base and test cases for calculating speciation of major, trace, and redox elements in natural waters*. Open- File Report 91-183,189p. U.S.Geological Survey.

Banwart, S. A. & Malmstrom, M.E., 2001. Hydrogeochemical modelling for preliminary assessment of mine water pollution. *Journal of geochemical exploration*, 74, pp.73-97.

Benzaazoua, M., Fall, M. & Belem, T., 2004. Contribution to understanding the mechanism of cemented paste backfill hardening. *Mineral Engineering*, 17, pp.141-52.

Bernhard, D., 2005. Basic Concept of Environmental Geochemistry of Sulphide Mine Waste. Lima, Peru, 2005. Society of Economic Geologists.

Bethke, C.M., 2008. *Geochemical and biogeochemical reaction modelling*. 2nd ed. New York: Cambridge university press.

Bigham, JM; Schwertmann, U; Traina, SJ; Winland, RL & Wolf, M., 1996. Schwertmannite and the chemical modeling of iron in acid sulphate waters. *Geochimica et Cosmochimica Acta*, 60(12), pp.2111-21.

Blowes, D.W., Ptacek, C.J., Jambor, J.L. & Weisener, C.G., 2003b. The Geochemistry of Acid Mine Drainage. In H.D. Holland & K.K. Turekian, eds. *9.05 - Treatise on Geochemistry*. Oxford: Elsevier- Pergamon. pp.149-204.

Blowes, D., Ptacek, C. & Jurjovek, J., 2003a. Mill Tailings Hydrogeology and Geochemistry. In J. Jambor, D. Blowes & A. Ritchie, eds. *Environmental Aspects of Mine Wastes*. Mineralogical Association of Canada short course series,Vol. 31. pp.95-116.

Brantley, S.L. & Mellott, N.P., 2000. Surface area and porosity of primary silicate minerals. *American Mineralogist*, 85 (11-12), p.1767–1783.

Brantley, S.L., White, A.F. & Kubicki, J., 2008. Kinetics of Mineral Dissolution. In *Kinetics of Water Rock Interaction*. New York: Springer. pp.151-210.

Broadhurst, J.L., Hansen, Y. & Petrie, J.G., 2007. *Waste characterisation and water related impacts predictions for solid mineral wastes : A new approach.WRC Report No.1550/1/07*. Water Reasearch Commission, South Africa.

Brown, J.G., Glynn, P.D. & Bassett, R.L., 1999. *Geochemistry and reactive transport of metal contaminants in ground water, Pinal Creek Basin, Arizona*. U.S. Geological Survey Water-Resources Investigations Report 99-4018A. Proceedings of the Technical Meeting, Charleston, South Carolina, March 8-12, 1999--Volume 1 of 3--Contamination from Hardrock Mining.

Brunauer, S., Emmet, P. & Teller, E., 1938. Adsorption of gases in multimolecular layers. *Journal of the American Chemical Society*, 60, pp.309-19.

Bryan, G.C., 2006. *A study of the microbiological populations of mine wastes*. PhD Thesis. School of Biological Sciences, University of Wales.

Cheryl , H. E; Stephen , S. A; Jason , S. A; Rose , A & Gary , L., 2005. Modelling the leaching of Pb, Cd, As, and Cr from cementitious waste using PHREEQC. *Journal of Hazardous Materials*, (A125), p.45–61.

Chiume, R; Minnaar, S.H; Ngoma, I.E; Bryan, C.G & Harrison, S.T.L., 2012. Microbial colonisation in heaps for mineral bioleaching and the influence of irrigation rate. *Minerals Engineering*, 39, p.156–164.

Coastech Research, 1991. *Acid rock drainage prediction manual.Energy Mines and Resources, Canada, MEND Project Report 1.16.1b*. [Online] Available at: http://www.mend-nedem.org [Accessed February 2012].

Cordoba, E M; Munoz, J A; Blazquez, M L; Gonzalez, F & Ballester, A., 2008b. Leaching of chalcopyrite with ferric ion. Part II: Effect of redox potential. *Hydrometallurgy*, 93, p.88–96.

Crawford, J., 1999. *Geochemical Modelling – A review of current capabilities and future directions. Swedish Environmental Protection Agency Report*. Royal Institute of Technology (KTH),Stockholm,Sweden.

Croxford, S.J., England , A. & Jarvis, A.P., 2004. Application of the PHREEQC geochemical computer model during the design and operation of UK mine water treatment Schemes: Mine Water 2004 – process, policy and Progress. Newcastle upon Tyne, 2004. International Mine Wate Association Symposium, United Kingdom.

Davis, G.B. & Ritchie, A.I.M., 1986. *A model of oxidation in pyritic mine waste : part 1, Equations and approximate solution*. Sutherland, NSW, 2232, Australia: Australian Atomic Energy Commission, Lucas Heights Research Laboratories.

Department of Water Affairs and Forestry, 2008. *Best Practice Guideline G4: Impact Prediction*. Pretoria, South Africa.

Dorricott, M.G. & Grice, A.G., 2002. Backfill – The Environmentally Friendly Tailings Disposal System. In Green Processing. In *Australian Institute of Mining and Metallurgy*. Melbourne, 2002.

Dutrizac , J.E., 2008. Factors affecting the precipitation of potassium jarosite in sulphate and chloride media. *Metallurgical and Materials Transactions* , 39B, pp.771-83.

Elwood Madden, M.E; Madden, A S; Rimstidt, J D; Zahrai, S; Kendall, M R & Miller, M A., 2012. Jarosite dissolution rates and nanoscale mineralogy. *Geochimica et Cosmochimica Acta*, 91, pp.306-21.

Espana, S.J., 2003. *Acid Mine Drainage in the Iberian Pyrite Belt: An Overview with special emphasis on generation mechanisms,aqueous composition and associated mineral phases*. Madrid, Spain: Geological and mining institute of Spain.

Evangelou, V.P., 1995. *Pyrite oxidation and its control: Solution chemistry, surface chemistry, acid mine drainage(AMD), molecular oxidation mechanisms, microbial role, kinetics, control, ameliorates and limitations, microencapsulation*. New York: CRC press.

Evangelou, V.P. & Zhang, Y.L., 1995. A review: Pyrite oxidation mechanisms and acid mine drainage prevention. *Critical Reviews in Environmental Science and Technology*, 25 (2), pp.141-99.

Fetter, C., 1993. *Contaminant Hydrology*. New York: Macmillan Publishing Company.

Freeze, R.A. & Cherry, J.A., 1979. *Groundwater*. Englewood Cliffs,N J: Prentice-Hall.

Furrer , G., Sollins , P. & Westall, J., 1990. The study of soil chemistry through quasi-steady-state models: II. Acidity of soil solution. *Geochim. cosmochim*, 54, pp.2363 - 2374.

Furrer, G., Westall, J. & Sollins, P., 1989. The study of soil chemistry through quasi-steady-state models: I. Mathematical definition of a problem. *Geochim. cosmochim.*, 53, pp.596 - 601.

Galaction, A.I., Cascaval, D., Oniscu, C. & Tumea, M., 2004. Prediction of oxygen mass transfer coefficients in stirred bioreactors for bacteria, yeasts and fungus broths. *Biochemical Engineering Journal*, 20 (1), p.85–94.

Garcia, C., Ballester, A., Gonzalez, F. & Blazquez, M., 2005. Pyrite behaviour in a tailings pond. *Hydrometallurgy*, 76, p.25–36.

Garcia, C; Ballester, A; Gonzalez, F; Blazquez, M L & Acosta, M., 1996. Chemical and microbiological transformation in a pyritic tailing pond. *Minerals engineering*, 9 (11), pp.1127-42.

Garcia, C; Moreno, D A; Ballester, A; Blazquez, M L & Gonzalez, F., 2001. Bioremediation of industrial acid mine water by metal-tolerant sulphate-reducing bacteria. *Minerals engineering*, 14 (9), pp.997-1008.

Geberetsadike, T.T., 2004. *Modelling reactive transport of acid mine drainage in groundwater: Effect of geochemical processes, spatially variable flow, source location and distribution*. MSc Thesis: Department of Chemical Engineering and Technology, KTH, Stockholm, Sweden.

Gelinas, P; Lefebvre, R; Choquette, M; Isabel, D; Locat, J & Guay, R., 1994. *Monitoring and modeling of acid mine drainage from waste rock dumps—La Mine Doyon case study*. Report GREGI 1994-12 submitted to the MEND prediction commitee. Ottawa, Canada.

Gerke, H.H., Frind, E.O. & Molson, J.W., 1998. Modelling the effect of chemical heterogeneity on acidification and solute leaching in overburden mine spoils. *Journal of Hydrology*, 209, pp.166 - 185.

Ghauri, M.A., Okibe, N. & Johnson, D., 2007. Attachment of acidophilic bacteria to solid surfaces: The significance of species and strain variations. *Hydrometallurgy*, 85, pp.72-80.

Ginn, T.R; Wood, B.D; Nelson, K.E; Scheibe, T. D; Murphy, E. M & Clement, T.P., 2002. Processes in microbial transport in the natural subsurface. *Advances in water resources*, (25), pp.1017-42.

Gitari, W.M., 2006. *Evaluation of the leachate chemistry and contaminants attenuation in Acid Mine Drainage by Fly Ash and its derivatives*. PhD Thesis. University of Western Cape.

Gudbrandsson, S., Wolff-Boenisch, D., Gislason, S.R. & Oelkers, E.H., 2011. An experimental study of crystalline basalt dissolution from 2 ≤ pH ≤ 11 and temperatures from 5 to 75 °C. *Geochimica et Cosmochimica Acta*, 75, p.5496–5509.

Gunsinger, M.R., Ptacek, C.J., Blowes, D.W. & Jambor, J.L., 2006. Evaluation of long-term sulphide oxidation processes within pyrrhotite-rich tailings, Lynn Lake, Manitoba. *Journal of Contaminant Hydrology*, 83 (3-4), p.149– 170.

Hansen, Y., 2004. *Environmental impact assessment of solid waste management in the primary industries - A new approach. PHD thesis dissertation.* University of Sydney, Australia.

Hansen, Y., Broadhurst, J.L. & Petrie, J.G., 2008. Modelling leachate generation and mobility from copper sulphide tailings – An integrated approach to impact assessment. *Minerals Engineering*, (21), p.288–301.

Havik, J.C., 2012. *The fate and transport of nutrients in shallow groundwater and soil of an urban slum area in the city of Kampala, Uganda.* MSc Thesis. Utrecht University, Utrecht, The Netherlands.

Herasymuik, C.M., 1996. *Hydrogeology of a sulphide waste rock dump*. MSc Thesis. Saskatoon,Canada: University of Saskatchewan.

Herbert, B., 1996. *Application of geochemical speciation models for groundwater chemistry modelling and evaluation of remediation technologies*. [Online] Available at: http://geoweb.tamu.edu/Faculty/Herbert/geol641/docs/SpeciationModelingReview.pdf [Accessed 24 October 2013].

Hesketh, A.H., 2010. *An integrated approach to AMD mitigation through sulphide removal from tailings*. MSc thesis. University of Cape Town, South Africa.

Hodson, M.E., Langan, S.J. & Meriau, S., 1998. Determination of mineral surface area in relation to the calculation of weathering rates. *Geoderma* , 83, pp.35-54.

Hodson, M.E., Lee, M.R. & Parsons, I., 1997a. Origins of the surface roughness of fresh and unweathered alkali feldspars grains. *Geochim. Cosmochim. Acta*, 61 (18), p.3885–3896.

Holch, J., 2008. *Thermodynamic and kinetic degradation reactions of organic substances in groundwater modelled with PHREEQC*. MSc Thesis. Baden-Württemberg, Germany: Institute of Hydrology Albert Ludwig University of Freiburg.

Holland , H.D. & Turekian, k.k., 2005. *Environmental Geochemistry: Treatise on Geochemistry, Second Edition, Volume 9*. 1st ed. Oxford: Elsevier.

Hornberger, R.J. & Brady, K.B., 2009. *Kinetic test procedure for the prediction of coal mine drainage quality*. Washington D.C: U.S Environmental Protection Agency.

Horton, J. & Hawkins, R., 1965. Flow path of rain from the soil surface to the water table. *Soil Science*, 6(100), pp.377-83.

INAP, 2009. *The International Network for Acid Prevention (INAP)*. [Online] Global Acid Rock Drainage Guide (GARD Guide). Available at: http://www.gardguide.com/. [Accessed 18 April 2013].

Jamal , A-A; Joy, D. M; Lee, H; Whiteley, H.R & Zelin, S., 1994. Transport of microorganisms through soil. *Water, Air and Soil Pollution*, 75, pp.141-58.

Jambor, J. & Blowes, D., 1998. Theory and applications of mineralogy in environmental studies of sulfide-baring mine waste. In L.J. Cabri & D. Vaughan, eds. *Short Course Handbook on Ore and Environmental Mineralogy.* Mineralogical Association of Canada. pp.367-401.

Jambor, J.L., Dutrizac, J.E. & Raudsepp, M., 2006. Comparison of measured and mineraligically predicted values of the sobek neutralisation potential for intrusive rocks. In Barnhisel, R.I., ed. *7th International Conference on Acid Rock Drainage (ICARD)*. St. Louis MO, 2006. American Society of Mining and Reclamation (ASMR).

Jambor, J.L., Nordstrom, D.K. & Alpers, C.N., 2000. Metal-sulfate salts from sulfide mineral oxidation. In C.N. Alpers, J.L. Jambor & D.K. Nordstrom, eds. *Reviews in Mineralogy and Geochemistry*. pp.303-50.

Jones, D., 1995. The leaching of major and trace elements from coal. In D. Swaine & F. Goodarzi, eds. *Environmental Aspects of Trace Elements in Coal*. Netherlands: Kluwer Academic Publishers. pp.221-62.

Jurjovec, J., Ptacek, C.J. & Blowes, D.W., 2002. Acid neutralization mechanisms and metal release in mine tailings: A laboratory column experiment. *Geochimica et Cosmochimica Acta*, 66(9), p.1511–1523.

Kazadi Mbamba, C., 2011. *Using froth flotation to mitigate acid rock drainage risks while recovering valuable coal from ultrafine colliery wastes. MSc Thesis dissertation*. University of Cape Town, South Africa.

Kedziorek , M.A., Geoffriau , S. & Bourg , A.M., 2008. Organic matter and modeling redox reactions during river bank filtration in an alluvial aquifer of the Lot River, France. *Environmental Science and Technology*, 42, p.2793–2798.

Koptsika, S., Strandb, L. & Clarkeb, N., 2003. On the calculation of the surface area of different soil size fractions. *Applied Geochemistry*, 18, p.629–651.

Kosson, D., Van der Sloot, H., Sanchez, F. & Garrabrants, A., 2002. An Integrated Framework for Evaluating Leaching in Waste Management and Utilization of Secondary Materials. *Environmental Engieering Science*, 19 (3), pp.159-204.

Kung, K.-J., 1990b. Preferential flow in a sandy vadose zone: 2. Mechanism and Implication. *Geoderma*, (46), pp.59-71.

Kuo, E.Y. & Ritchie, A.I., 1999. The impact of convection on the overall oxidation rate in sulfide waste rock dumps, Paper presented at the sulfide waste rock dumps conference. Sudbury, Ontario, Canada, 1999.

Latifi, H., Prasad, S. & Helweg, O., 1994. Air entrapment and water infiltration in two-layered soil column. *Journal of irrigation and Drainage Engineering*, 5(120), pp.871-91.

Lefebvre, R. & Gélinas, P., 1995. Numerical modeling of AMD production in waste rock dumps, Paper presented at the Mining and the Environment conference. Sudbury, Ontario, Canada, 1995.

Lefebvre, R., Hockley, D., Smolensky, J. & Lamontagne, A., 2001a. Multiphase transfer processes in waste rock piles producing acid mine drainage 2. Applications of numerical simulation. *Journal of Contaminant Hydrology*, 52, p.165–186.

Lefebvre, R., Lamontagne, A., Wels, C. & Robertson, A.M., 2002. ARD production and water vapour transport at the Questa Mine, in Proceedings Ninth International Conference

on Tailings and Mine Waste. In *Tailings and Mine Waste*. Fort Collins, Colorado, USA, 2002. A.A Balkema.

Lenk, S. & Wisotzky, F., 2011. Chemical modelling of the groundwater composition in aquifers affected by lignite mine dumps discharge (Surface mine inden, Germany). *Environmental Earth Science*, 62, p.581–591.

Linklater, C.M., Sinclair, D.J. & Brown, P.L., 2005. Coupled chemistry and transport modelling of sulphidic waste rock dumps at the Aitik mine site, Sweden. *Applied Geochemistry*, 20, p.275–293.

Lipson, D.S., McCray, J.E. & Thyne, G.D., 2007. Using PHREEQC to simulate solute transport in fractured bedrock. *Groundwater*, 45(4), p.468–472.

Lottermoser, B.G., 2007. *Mine waste Characterization, Treatment, Environmental Impacts*. 2nd ed. Berlin: Springer.

Luxmoore, R., 1991. On preferential flow and its measurements. In Gish & Shirmohammadi, eds. *Preferential Flow: Proceedings of the National Symposium*. Chicago, Illinois, 1991. American Society of Agriculture Engineers.

Maddocks, G; Newberry, T; Jong, T; Schneider, A & Verburg, R., 2009. *Co-disposal and In-situ Neutralisation of Waste Rock and Tailings: Limiting ARD in Acid Forming Waste Rock, Securing the Future and 8th ICARD, June 22-26,Skelleftea Sweden*. [Online] Skellefteå Available at: www.proceedings-stfandicard-2009.com [Accessed 18 April 2013].

Maest, A.S., Kuipers, J.R., Travers, C.L. & Atkins, D.A., 2005. *Predicting water quality at hardrock mines: Methods and Models, Uncertainties, and State-of-the-Art*.

Mayer, K.U., Benner, S.G. & Blowes, D.W., 1999. The reactive transport model MIN3P: Application to Acid Mine Drainage generation and treatment-Nickel rim mine site, Sudbury, Ontario., 1999. Sudbury 99: Mining and the Environment II Conference Proceedings, Sudbury Ontario.

Mayer, K.U., Benner, S.G. & Blowes, D.W., 2006. Process-based reactive transport modeling of a permeable reactive barrier for the treatment of mine drainage. *Contaminant hydrology*, 85 (3-4), pp.195-211.

Mayer, K.U., Frind, E.O. & Blowes, D.W., 2002. *Multicomponent reactive transport modeling in variably saturated porous media using a generalized formulation for kinetically controlled reactions*. Water resources research, VOL. 38, NO. 9, 1174, doi:10.1029/2001WR000862.

Mayer, K.U., Frind, E.O. & Blowes, D.W., 2003. Advances in reactive-transport modelling of contaminant release and attenuation from mine-waste deposits (Chapter 14). In J.L. Jambor, D.W. Blowes & A.I. Ritchie, eds. *Environmental Aspects of Mine Wastes, Short Course, vol. 31*. Mineralogical Association of Canada. p.283– 302.

Merkel, B.J. & Planer-Friedrich, B., 2008. *Ground water geochemistry, A practical guide to modelling of natural and contaminated aquatic sytems*. 2nd ed. Berlin: Springer.

Molson, J.W., Fala, O. & Bussiere, B., 2005. Numerical simulations of pyrite oxidation and acid mine drainage in unsaturated waste rock piles. *Journal of Contaminant Hydrology*, 78, p.343– 371.

Murad, E. & Rojik, P., 2004. Jarosite, schwertmannite,goethite, ferrihydrite and lepidocrocite: the legacy of coal and sulphide ore mining. In *3rd Australian New Zealand Soils Conference*. University of Sydney, Australia, 2004.

National Research Council, 2007. *Models in Environmental Regulatory Decision Making*. Washington D.C.The National Academies Press

Neuman, S.P., 1990. Universal scaling of hydraulic conductivities and dispersivities in geological media. *Water Resources Research*, 26(8), pp.1749-58.

Newman, L.L., 1999. *Preferential Flow in vertically oriented,unsaturated soil layers*. MSc Thesis. Department of Civil Engineering, University of Saskatchewan,Saskatoon,Saskatchewan,Canada.

Nicholson, R.V., Rinker, M.J., Acott, G. & Venhuis, M.A., 2003. Integration of field data and a geochemical transport model to assess mitigation strategies for an acid-generating mine rock pile at a uranium mine. Proceedings, Sudbury 2003, 2003. Mining and the Environment, CD-ROM.

Nordstrom, D.K., 2005. Modeling low-temperature geochemical processes. In J.I. Drever, ed. *Treatise of Geochemistry: Surface and Ground Water, Weathering, and Soils*. Oxford,UK: Elsevier B.V. pp.37-72.

Nordstrom, D.K., 2009. Acid rock drainage and climate change: Journal of Geochemical Exploration. *Journal of Geochemical Exploration*, 100(2-3), p.97–104.

Nordstrom, D. & Alpers, C., 1999a. Geochemistry of acid mine waters. In G.S. Plumlee & M.J. Logsdon, eds. *The Environmental Geochemistry of Mineral Deposits,Part A. Processes,Techniques,and Health Issues: Society of economic Geologists*. pp.133-56.

Nordstrom, D.K. & Alpers, C.N., 1999b. Geochemistry of ac id mine waters. In G.S. Plumlee & M.J. Logsdon, eds. *In Reviews in Economic Geology, vol. 6A , The Environmental Geochemistry of Mineral De posits. Part A.Processes, Methods and Health Issues*. pp.133-60.

Palandri, J.L. & Kharaka, Y.K., 2004. *A compilation of rate parameters of water-mineral interaction kinetics for application to geochemical modeling*. Menlo Park, California: U.S. GEOLOGICAL SURVEY.

Pantelis, G., 1993. *FIDHELM: Description of model and users guide, Australian Nuclear Science and Technology Organization Report ANSTO/M123*.

Pantelis, G. & Ritchie, A.I., 1991. Macroscopic transport mechanisms as rate-limiting factor in dump leaching of pyritic ores. *Applied mathemitical modelling*, 15, pp.136 - 143.

Parkhurst, D.L., 1995. *User's guide to PHREEQC-A Computer program for speciation, reaction path-path, Advective-transport and inverse geochemical calculations,Water-Resources Investigations Report 95-4227*. [Online] [Accessed February 2012].

Parkhurst, D.L. & Appelo, C.A., 1999. *User's Guide To PHREEQC (VERSION 2): A computer program for Speciation, batch-reaction, One-dimensional transport, and Inverse geochemical calculations*. [Document] U.S. Department of the Interior: USGS Available at: http://wwwbrr.cr.usgs.gov/projects/GWC_coupled/phreeqc/html/final-1.html. [Accessed May 2012].

Perkins, E H; Nesbitt, H W; Gunter, W D; St-Arnaud, L C & Mycroft, J R., 1995. *Critical review of geochemical processes and geochemical models adaptable for prediction of acidic drainage from waste rock*. MEND Report, Mine Environment Neutral Drainage (MEND) Program,Canada.

Petersen, J., 1998. *Assessment and modelling of chromium release in mineral processing waste deposits*. PhD Thesis. Department of Chemical Engineering, University of Cape Town, South Africa.

Petersen, J., 2010a. Determination of oxygen gas–liquid mass transfer rates in heap bioleach reactors. *Minerals Engineering*, 23, p.504–510.

Petersen, J. & Petrie, J.G., 2000. Modelling and assessment of the long-term leachate generation potential in deposits of ferro-chromiun slags., 2000. South Africa Institute of Mining and Metallurgy, South Africa.

Petersen, J., Stewart, M. & Petrie, J., 2000. Management of ferro-alloy wastes. In A. Warhust & L. Noronha, eds. *Environmental Policy in Mining: Corporate Strategy and Planning for Closure*. CRC Press. pp.217-28.

Petrie, J.G. & Broadhurst, J.L., 2005. *Solid mineral waste impacts predictions (WRC K5 /1550) Task 5*. University of Cape Town, South Africa.

Pettena, M., Perrin, J., Pauwels, H. & Ahmed, S., 2013. Simulating fluoride evolution in groundwater using a reactive multicomponent transient transport model: Application to a crystalline aquifer of Southern India. *Applied Geochemistry*, 29, p.102–116.

Pham, V.T.H; Lub, P; Aagaarda, P; Zhub, C & Hellevanga, H.,2011. On the potential of CO2–water–rock interactions for CO2 storage using a modified kinetic model. *International Journal of Greenhouse Gas Control*, 5, p.1002–1015.

Plumlee, G., 1999. The Environmental Geology of Mineral Deposits. In G. Plumlee & M. Logsdon, eds. *The Environmental Geochemistry of Mineral Deposits, Part A: Processes, Techniques and Health Issues,Reviews in Economic Geology Vol. 6A*. Society of Economic Geologists. pp.71-116.

Plummer, L.N., Wigley, T. & Parkhurst, D., 1978. The kinetics of calcite dissolution in CO2-water systems at 5 to 60 °C and 0.0 to 1.0 atm CO2. *American Journal of Science*, 278, pp.179-216.

Price, W.A., 2009. *Prediction manual for drainage chemistry from sulphidic geologic materials*. Canadian MEND Report 1.20.1. Natural Resources Canada.

Rimstidt, D. J., Chermak, J. A. & Gagen, P. M., 1994. Rates of reaction of galena, sphalerite, chalcopyrite, and arsenopyrite with Fe (III) in acidic solutions. In C.N. Alpers & W.D. Blowes, eds. *Environmental Geochemistry of Sulphide Oxidation. ACS Symposium Series*. Washington DC: American chemical society. pp.2-13.

Scharer, J.M., Nicholson, R.V., Halbert, B. & Snodgrass, W.J., 1994. A computer program to assess acid generation in pyritic tailings. In C.N. Alpers & D.W. Blowes, eds. *Environmental Geochemistry of Sulfide Oxidation, ACS Symposium Series 550*. American Chemical Society. pp.132-52.

Schneider, P., Osenbruck, K., Neitzel, P.L. & Nindel, K., 2002. In-situ mitigation of effluent from acid waste rock dumps using reactive surface barriers-a feasibility study. *Mine Water and the Environment*, 21, pp.36-44.

Schwartz, F.W. & Zhang, H., 2003. Fundamentals of Groundwater. John Wiley & Sons, Inc., 592 pp.

Schwertmann, U., 1991. Solubility and dissolution of iron oxides. *Journal of plant and soil*, 130 (1-2), pp.1-25.

Smart , R.S.T.C ; Skinner, W. M; Levay, G; Gerson, A.R; Thomas, J.E; Sobieraj, H; Schumann, R; Weisener, C.G; Weber, P. A; Miller, S.D & Stewart, W. A., 2002. *ARD Test Handbook. AMIRA P387A Project: Prediction and Kinetic Control of Acid Mine Drainage.AMIRA Internationa*. Melbourne,Australia.

Snynder, E.M. & Carline, R.F., 2003. *Resotoration of spawning habitat for trout in big spring creek ,cumberland county pennsylavania*. U.S.G.S. Biological Resources Division.

Steefel, C.I., 2000. New directions in hydrogeochemical transport modelling:Incorporating multiple kinetic and equilibrium reaction pathways. In Bentley, L R; Sykes, J F; Brebbia, C A; Gray, W G; Pinder, G F, eds. *Computational methods in water resources XIII*. Rotterdam,The Netherlands: A.A Balkema. pp.331 - 338.

Stephens, D., 1994. A perspective of diffuse natural rechanrge mechanisms in areas of low precipitation. *Soil Science Society of America Journal*, (58), pp.40-48.

Stewart, W.A., Miller, S.D. & Smart, R., 2006. Advances in Acid Rock Drainage (ARD) Characterisation of Mine Wastes. St. Louis, Missouri, 2006. In Proceedings of the 7th International Conference on Acid Rock Drainage (ICARD).

Stromberg, B. & Banwart, S.A., 1999. Experimental study of acidity-consuming processes in mining waste rock: some influences of mineralogy and particle size. *Applied Geochemistry*, (14), pp.1-16.

Stromberg, B. & Banwart, S., 1994. Kinetic modelling of Kinetic modelling of geochemical processes at the Aitik mining waste rock site in northern Sweden. *Applied geochemistry*, 9, pp.583-95.

Talman, S; Perkins, E; Wigston, A; Ryan, D & Bachu, S., 2013. Geochemical effects of storing CO2 in the Basal Aquifer that underlies the Prairie Region in Canada. *Energy Procedia*, 37, p. 5570–5579.

Tester, J.W; Worley, W. G; Robinson, B. A; Grigseiy, C.O & Feerer, J.L., 1994. Correlating quartz dissolution kinetics in pure water from 25 to 625°C. *Geochimica et Cosmochimica Acta*, 58(11), pp.2407-20.

Tiruta-Barna, L., 2008. Using PHREEQC for modelling and simulation of dynamic leaching tests and scenarios. *Journal of Hazardous Materials*, 157, p.525–533.

US EPA, 1994. *Technical document- Acid mine drainage prediction.* Technical Report EPA/530/R-94/036. Washington, DC: US Environmental Protection Agency, Office of Solid Waste.

Van der Sloot, H.A. & Dijkstra, J.J., 2004. *Development of horizontally standardized leaching tests or construction materials: A material based or release based approach? In Industrial Leaching Mechanisms for Different Materials*. Energy Research Centre of the Netherlands (ECN).

Van Loosdrecht, M., Lyklema, J., Norde, W. & Zehnder, A., 1990. Influence of interfaces on microbial activity. Microbiological Reviews. 54, pp. 75-87.

Van Pham, T.H., Aagaard , P. & Hellevang, , 2012. On the potential for CO2 mineral storage in continental flood basalts – PHREEQC batch and 1D diffusion–reaction simulations. *Geochemical Transactions*, (13.5), pp.1-12.

Vijayan, V. & Noosai, N., 2012. The Study of Geochemical Processes of Selected Technologies for Acid Mine Drainage Treatments. In *MAESC 2012 Conference*. Memphis, Tennessee, 2012.

Warrick, A., Biggar, J. & Nielsen, D., 1971. Simultaneous solute and water transfer for unsaturated soil. *Water Resources Research*, 5(7), pp.1216-25.

Watling, H.R., 2006. *Improving heap bioleaching-Module B1.1 and 2.1 (AMIRA P768A)*. CSIRO Minerals Report.

Wels, C., Lefebvre, R. & Robertson, A.M., 2003. An overview of prediction and control of air flow in acid-generating waste rock dumps. In *Proceedings of the sixth International Conferance on Acid Rock Drainage*. Cains, Queensland, Australia, 2003.

White, W.M., 2011. Reactions kinetics. In *Geochemistry*. pp.156-210.

White, A.F. & Brantley , S.L., 2003. The effect of time on the weathering of silicate minerals: Why do weathering rates differ in the laboratory and field? *Chemical Geology*, (202), p.479–506.

White, A.F. & Peterson, M., 1990. The role of reactive surface areas in chemical weathering. *Chemical Geology*, 84 (1-4), pp.334-36.

Williamson, M.A. & Eary, E.L., 2006. Simulations of the neutralizing capacity of silicate rocks in acid mine drainage environments. 7th International Conference on Acid Rock Drainage (ICARD), March 26-30, 2006, St. Louis MO, 2006. Published by the American Society of Mining and Reclamation (ASMR), 3134 Montavesta Road, Lexington, KY 40502.

Williamson, M.A. & Rimistidt, J.D., 1994. The kinetics and electrochemical rate-determining step of aqueous pyrite oxidation. *Geochim. Cosmochim*, (Acta 58), pp.5443-54.

Wunderly, M. D; Blowes, D. W; Frind, E.O; Ptacek, J.C & Al, T. A., 1995. A multicomponent reactive transport model incorporating kinetically controlled pyrite oxidation. Ontario, 1995. University of waterloo.

Yu, J.-Y., Park, M. & Kim, J., 2001. Solubilities of synthetic schwertmannite and ferrihydrite. *Geochemical journal*, 36, pp.119-32.

Zheng, C. & Bennett, G.D., 2002. *Applied Contaminant Transport Modeling*. 2nd ed. NY: J. Wiley and Sons.

7 Appendices

List of appendices

Appendix A: Case study experimental set up

Table A 1: Initial columns set up and operating conditions (Watling, 2006)

	Large Column	**Small columns**
Ore	chalcopyrite ore as supplied, conditioned with the equivalent of 20 Kg sulphuric acid /tonne ore	chalcopyrite ore as supplied, conditioned with the equivalent of 20 Kg sulphuric acid /tonne ore
Solution Feed	Total volume 20 L (about 18 L in reservoir, 2L hold up)	Total volume 4 L
pH	1.5	1.5
Air flow	500 mL per minute	200
Irrigation	1.7 mL/minute (2.45 L/day)	1.02 mL/min (10L/m2/hr
Inoculum	1L containing 2.10E+08 cells per mL, mixed inoculum containing equal numbers of each of the project selected strains (mesophiles, moderates and thermophiles).	
Mass of ore (kg)	36.42	4.18
Microbial cells/kg	5.77E+08	2.10 E +08 cells/mL,5.0 E+06 cells/kg ore
Temperature	40ºC	40ºC
Column diameter (mm)	150	100
Column height (mm)[1]	1280	360

[1] Column heights does not include beads

Table A 2: Column leach solutions terminologies

Terminology	**Description**
Column discharge	Column Discharge is the sample from the bottom of the column. The difference between the composition of the column feed and the column discharge reflects changes that have occurred as the solution passes once through the ore bed.
Column effluent	Column Effluent is the total solution that has been collected from the bottom of the column since the previous sampling event.
Bulk solution	Bulk solution is the column effluent combined with the usually small amount of remaining solution in the feed reservoir. It represents the cumulative solution composition and is recycled to the top of the column after the pH is adjusted. Thus Bulk solution is recycled to become the Feed solution to the top of the column.

APPENDIX B: Case study experimental results

Table B 1: Results for small column leach test

	Exit Solution		Acid Added (mL)		Bulk solution (mg/L)							
days	pH	Eh (mV)	cumulative	step	Cu in 4L	Fe in 4L	Fe(II) in 4L	S in 4L	Al in 4L	K in 4L	Na in 4L	Mg in 4L
0	2.55	618	3	3	1	999	500					
3	2.92	563	5	2	280	63	1	3429	639	75	37	1148
7	3.33	526	5	0	327	435	1	4453	849	99	35	1360
10	2.08	558	7	2	318	529	12	4456	845	86	36	1296
15	2.04	556	9	2	361	494	3	4902	892	114	37	1388
17	1.92	559	13	4	388	649	4	5433	970	144	38	1485
21	1.88	586	16	3	391	649	4	5191	935	153	35	1408
24	1.98	572	16	0	436	670	6	5562	1009	159	37	1529
27	1.99	568	25	10	478	627	33	5845	1058	165	38	1676
30	1.84	661	27	2	500	711	1	6187	1138	173	38	1743
35	1.88	681	28	1	530	726	9	6760	1206	202	38	1841
38	1.87	676	33	5	557	775	16	6793	1256	207	38	1902
44	1.79	689	39	7	613	746	8	6897	1311	222	39	2055
51	1.84	658	47	8	653	693	1	7235	1377	181	37	2146
58	1.82	641	51	4	704	712	8	7435	1509	257	39	2256
65	1.84	635	58	7	744	820	4	7822	1562	224	37	2410
72	1.83	636	63	5	779	935	1	8607	1690	271	38	2578
79	1.78	643	66	3	849	1094	1	9710	1863	325	43	2724

days	Cu %	Mg %
0	0.0	0
3	5.6	3.9
7	6.6	4.6
10	6.4	4.4
15	7.2	4.7
17	7.8	5.0
21	7.8	4.7
24	8.7	5.2
27	9.6	5.6
30	10.0	5.9
35	10.6	6.2
38	11.2	6.4
44	12.3	6.9
51	13.1	7.2
58	14.1	7.6
65	14.9	8.1
72	15.6	8.7
79	17.0	9.2

Table B 2: Results for large column leach test

	Column Discharge			Column Effluent				Column bulk solution (before the pH is adjusted with acid)			Acid Added				
days	pH	Eh mV	Fe2+ mg/L	pH	Eh mV	Fe^{2+} mg/L	Free Acid g/L	pH	Eh mV	Fe2+ mg/L	Daily mL	Daily g	Cumulative g	Cumulative kg/ton ore	kg/kg Cu
0							N/A	1.50	473	500	399	734	734	20	91770
1	2.20	378	12579				N/A				0	0	734	20	#DIV/0!
3				2.55	371	11049	N/A				0	0	734	20	388
7	4.61	512	1				N/A								
9	4.85	407	1	2.98	374	2270	N/A	2.32	401	1878	37	68	802	22	389
17	3.96	462	1	3.93	500	1	0.3	1.53	427	419	35	64	867	24	202
25	3.87	468	1	3.91	456	1	0.4	2.05	441	113	25	46	913	25	136
32	3.84	516	1	3.17	548	1	0.4	1.73	603	1	10	18	931	26	117
39	3.53	532	5	3.46	536	8	1.4	2.10	579	18	30	55	986	27	81
46	3.19	534	1	2.55	593	14	1.7	2.04	581	1	30	55	1041	29	93
53	3.03	588	1	2.97	597	1	1.1	1.90	615	1	30	55	1097	30	79
60	3.02	577	1	2.97	591	1	1.9	1.78	591	1	25	46	1143	31	78
67	3.04	566	1	2.80	578	1	2.6	1.67	601	1	25	46	1189	33	75
74	2.50	611	4	2.63	610	3	1.9	2.37	616	3	30	55	1244	34	62
81	2.44	624	1	2.44	605	1	0.8	2.14	608	1	20	37	1281	35	58
88	2.43	608	3	2.41	595	1	1.2	2.03	613	2	30	55	1336	37	57
94	2.40	611	1	2.46	607	1	2	1.78	618	1	15	28	1363	37	55
101	2.13	644	1	2.31	604	8	2.5	2.33	607	5	45	83	1446	40	52
107	2.17	639	1	2.17	640	1	2.2	1.91	618	1	30	55	1501	41	47
112	2.11	646	1	2.14	653	3	4.4	1.99	648	1	35	64	1566	43	47
113	2.10	645						1.45	643	1	0	0	1566	43	44
116	2.13	640	10	2.13	643	14	7.7	1.61	643	13	10	18	1584	43	48
123	2.17	635	2	2.15	633	1	2.7	1.56	632	2	20	37	1621	45	50
130	2.29	602	1	2.24	604	1	2.7	1.94	609	2	35	64	1685	46	38
133	2.06	630	5	2.24	637	6	2.7	1.62	634	7	20	37	1722	47	36
137	2.02	639	1	2.10	643	1	2.7	1.63	652	2	35	64	1787	49	40
147	2.08	627	1	2.11	630	1	3.8	1.92	628	4	0	0	1787	49	40
158	2.26	580	1	2.21	574	2	4.4	2.19	598	1	30	55	1842	51	38
170	2.21	580	2	2.22		12	3.8	1.64		11	25	46	1888	52	38
183	2.24	623	1	2.26	630	1	3.3	2.06	632	1	40	74	1961	54	38
193	2.20	632	9	2.24	643	9	4.4	1.77	648	4	70	129	2090	57	41
205	2.10	621	14	2.10	654	10	4.4	1.72	658	22	54	99	2190	60	41
217	2.07	641	1	1.92	653	2	4.4	1.64	671	1	54	99	2289	63	43
221	2.03	613	1	2.06	634	1	4.4	1.39	660	1	20	37	2326	64	44
233	2.03	638	1	2.02	663	1	7.1	1.68	665	3	65	120	2445	67	45
242	1.81	656	5	1.91	658	7	3.3	1.48	683	8	25	46	2491	68	45
252	1.91	663	8	1.89	675	3	3.3	1.82	679	3	80	147	2639	72	48
262	1.81	652	8	2	667	6		1.70	663	3	70	129			
273	1.78	630	3	2	667	1		1.72	672	1	100	184			

days	Cu mg/L	Fe mg/L	S mg/L	Mg mg/L	Al mg/L	Si mg/L	K mg/L	Ca mg/L	Na mg/L	Cu %	Mg %	pH	Log[Fe]
0													
1													
3													
7													
9	107	2212	7511	2373	1407	45	494	346	60	1.12	4.20	2.32	3.34
17	180	689	5932	1603	688	70	1589	508	41	1.76	3.54	1.53	2.84
25	367	202	4731	1787	772	96	135	507	46	3.31	3.87	2.05	2.31
32	655	56	4640	1820	788	113	49	528	45	5.42	3.92	1.73	1.75
39	897	24	5143	2009	852	118	30	535	45	7.29	4.26	2.10	1.38
46	1240	15	5462	2116	907	127	15	523	47	9.83	4.45	2.04	1.17
53	1499	16	5811	2157	953	138	10	542	41	11.45	4.52	1.90	1.19
60	2243	21	5792	2287	1016	142	7	534	44	16.92	4.64	1.78	1.32
67	2416	22	6986	2617	1175	131	9	527	47	18.70	5.23	1.67	1.34
74	3235	28	6227	2659	1204	155	21	531	41	24.08	5.57	2.37	1.44
81	4190	25	6745	2809	1281	152	16	550	45	23.71	5.84	2.14	1.40
88	4206	22	6965	2732	1265	150	17	538	43	26.70	6.00	2.03	1.33
94	4176	23	8262	2974	1452	146	21	548	50	33.03	6.73	1.78	1.37
101	4141	38	7879	3277	1685	163	19	535	46	32.61	7.27	2.33	1.58
107	4190	66	8592	3429	1818	155	35	545	48	32.90	7.54	1.91	1.82
112	4353	107	8999	3777	2017	154	38	560	50	33.85	8.15	1.99	2.03
113	3797	111	9545	3270	1701	100	47	480	41	32.13	7.26	1.45	2.04
116	3958	111	10057	3976	2074	136	46	465	39	33.85	8.51	1.61	2.04
123	4053	101	9639	3837	2006	164	59	514	48	34.05	8.26	1.56	2.00
130	4558	89	9551	4023	2044	159	63	546	48	37.64	8.24	1.94	1.95
133	4486	82	10673	4302	2117	141	88	555	49	37.10	8.74	1.62	1.91
137	4303	85	11285	4246	2107	106	81	475	54	37.14	8.64	1.63	1.93
147	4363	100	11595	4588	2314	128	75	487	54	37.66	9.24	1.92	2.00
158	4513	93	11661	4702	2411	143	82	510	55	38.74	9.44	2.19	1.97
170	4623	92	11818	4886	2544	142	97	540	55	39.81	9.77	1.64	1.96
183	4537	127	12671	5018	2558	135	144	490	53	40.07	10.00	2.06	2.10
193	4716	131	14405	6075	2932	164	152	547	62	42.32	11.87	1.77	2.12
205	4807	141	13885	5996	3034	160	140	573	61	42.83	11.73	1.72	2.15
217	5008	233	15224	6198	3409	168	186	572	64	44.46	12.09	1.64	2.37
221	5147	259	16343	6369	3592	182	248	567	60	45.04	12.39	1.39	2.41
233	5221	281	17861	6492	3734	212	282	610	63	45.91	12.61	1.68	2.45
242	5782	290	18012	6689	4099	190	384	617	67	49.48	11.67	1.48	2.46
252	5619	416	16811	6450	3825	157	425	597	60	50.03	13.49	1.82	2.62
262	5573	368	16192	6367	3631	172	486	616	61	50.28	13.34	1.70	2.57
273	5615	390	18469	6992	4109	176	515	604	59			1.72	2.59

APPENDIX C: Calculation of model input parameters

Table C 1: Calculation of rock density and minerals volume fractions in particles

Mineral	Wt. %	Mineral density (g/cm3)	Mass of mineral per cm^3 of rock*	Mineral mass (g) (M_i)	Mineral volume (V_i)	Mineral volumetric fraction (X_i)
Pyrite	0.2	5.01	0.01	0.00539	0.00108	0.00113
Chalcopyrite	1.3	4.19	0.0545	0.0350	0.00836	0.00878
Calcite	1.4	2.71	0.03794	0.0377	0.0139	0.0146
Biotite	21.4	3.09	0.661	0.577	0.187	0.196
Chlorite	3.3	3.00	0.099	0.089	0.0297	0.0311
Plagioclase	8.7	2.68	0.233	0.235	0.0875	0.0919
Orthoclase	39.6	2.58	1.0217	1.068	0.414	0.434
Kaolinite	1.9	2.6	0.0494	0.051	0.0197	0.0207
Magnetite	0.3	5.15	0.0155	0.008	0.00157	0.00165
Quartz	17.9	2.66	0.476	0.483	0.181	0.19
Rutile	0.2	4.25	0.0085	0.005	0.00127	0.00133
Apatite	0.9	3.19	0.0287	0.024	0.00761	0.00798
Total	100	M_T = 2.696		2.618	0.953	1

*If one cm^3 of waste rock is assumed, the contribution of mineral *i* towards total mass (M_T) of rock is calculated as;

$$M_T = \sum_i \text{wt.}\,\% \times \rho_i$$

Where $\text{wt.}\,\%$ is the weight percent of mineral *i* in the waste rock and ρ_i is the specific density of mineral *i.* The mass of each mineral (g) per cm^3 of rock is calculated as;

$$M_i = \text{wt.}\,\% \times M_T$$

The volume of mineral *i* (cm^3) is calculated as;

$$V_i = \frac{M_i}{\rho_i}$$

Where M_i is the mass of mineral i per cm^3 of waste rock and ρ_i is the specific density of mineral *i.* The volumetric fraction of mineral *i* is calculated as;

$$X_i = \frac{V_i}{V_T}$$

Where V_T is the total volume of all minerals and V_i is the volume of mineral i.

For one cm^3 waste rock, the density is calculated as 2.696g/cm^3 or 2696 kg/m^3

Table C 2: Calculation of surface area of 1 kg sample

Particle size range		Average diameter (m)	Volume of one Particle (m^3)	Number of particle (n_i)	Surface area of Particle ($A_{i,p}$)	Surface area of class ($A_{i,t}$)
Size classes (mm)	Wt. %					
-20 + 13.5	38.6	0.01654	0.000002369	60	0.00086	0.052
-13.5 + 9.5	21.5	0.01132	0.00000076	105	0.00040	0.042
-9.5 + 6.7	10.7	0.00798	0.000000266	149	0.0002	0.030
-6.7 + 3.35	10.5	0.00474	0.000000056	698	0.000071	0.049
-3.35+ 1.18	6.9	0.00199	0.000000004	6203	0.000012	0.077
-1.18	11.9	0.00059	0.000000000108	410461	0.00000109	0.449
Total						0.699

The volume of one particle in class *i* was calculated as;

$$\mathrm{V_i} = \frac{4}{3}\pi\left(\frac{\mathrm{d_i}}{2}\right)^3$$

Where d_i is the average diameter (geometric mean) calculated from the minimum (d_{min}) and the maximum diameters (d_{max}) in the size class ($d_{min} < d_i < d_{max}$).The number of particles in one size class is calculated as;

$$\mathrm{n_i} = \frac{\mathrm{W_i} \times \mathrm{M_t}}{\mathrm{V_i} \times \rho}$$

Where $\mathrm{M_t}$ is the total mass of the sample (kg), $\mathrm{W_i}$ is the mass fraction in size class *i,* ρ is the density of the rock (kg/m^3) and $\mathrm{V_i}$ is the volume of one particle in size class *i.* The surface area of one particle in size class *i* was calculated as;

$$\mathrm{A_{i,p}} = 4\pi\left(\frac{\mathrm{d_i}}{2}\right)^2$$

The total surface area in class *i* was calculated as

$$\mathrm{A_{i,t}} = \mathrm{n_i} \times \mathrm{A_{i,p}}$$

The total surface area of one kg sample was calculated as 0.7 m^2 (0.0007m^2/g) using the equation below;

$$\mathrm{A_{total}} = \sum_{\mathrm{i}} \mathrm{A_{i,t}}$$

Where the total surface area is the sum of the surface areas in size classes.

Table C 3: Calculations of amounts of reactants

Mineral	Amounts (mol dm^{-3})
Pyrite	0.3
Chalcopyrite	1.27
Calcite	2.51
Biotite	7.57
Chlorite	1.07
Plagioclase	4.73
Orthoclase	25.54
Kaolinite	2.98
Magnetite	0.23
Quartz	53.41
Rutile	0.45
Apatite	0.30

The amounts of solid reactants are calculated using the Equation below;

$$\text{mineral moles per cubic decimeter (m)} = \frac{(1-\phi)\rho W_i}{100 M_i \phi_w}$$

Where W_i, M_i, ρ, ϕ and ϕ_w represent the mineral weight percentage, molar mass (g/mole), rock density (g dm^{-3}), total porosity (0.4) and water filled porosity (0.09), respectively.

Table C 4: Calculated minerals surface areas

Mineral	Volumetric fraction	Mineral surface area (m^2 dm^{-3})
Pyrite	0.001129763	0.000425
Chalcopyrite	0.008780602	0.0215
Calcite	0.014620213	0.0385
Biotite	0.195997374	9.10
Chlorite	0.031130611	0.193
Plagioclase	0.091871206	1.50
Orthoclase	0.434380619	32.41
Kaolinite	0.020681175	0.167
Magnetite	0.001648576	0.000929
Quartz	0.190443587	6.41
Rutile	0.001331791	0.000503
Apatite	0.007984483	0.013

The mineral were assumed to be uniformly distributed in the waste rock and their surface areas were assumed to be equivalent to their volumetric fraction in the waste rock. The surface area of mineral *i* was calculated as;

$$A_i = A_{geo} X_i M_i m_i \gamma$$

Where A_{geo}, X_i, M_i m_i and γ are specific geometric surface area (m^2/g), volumetric fraction, molar mass (g/mole), amounts of reactants (mole/dm^3) and surface roughness factor. A surface roughness factor of 15 was used in all the calculations.

Table C 5: Calculation of transport parameters

Parameters	Small column	Large column	Parameter	Small column	Large column
Column height (m)	0.47	1.28	Longitudinal dispersivity	0.0058	0.025
Column diameter	0.1	0.15	Time step (s)	5541	24200
Flow rate (mL/min)	1.02	1.7	Shifts	1232	975
Bed porosity	0.4	0.4	Number of cells[1]	3	3
Bed saturation	0.09	0.09	Cell length	0.16	0.43
Simulation Time (days)	79	273	Pore volumes	411	325
Weight of ore in column (kg)	4.18	36.42	Boundary conditions	Flux flux	Flux flux

[1]The flow path in each column was divided into three equal cells or boxes

The cell length was calculated as;

$$\text{Cell length} = \frac{\text{Column height}}{\text{number of cells}}$$

The longitudinal dispersivity was calculated as;

$$\propto_x = 0.0175\text{L}^{1.46}$$

Where L is the flow path or column height (m)

The advective time step was calculated from bed pore volume and irrigation rate as;

$$(\Delta t)_A = \frac{PV}{Q}$$

Where PV is the pore volume (m^3) and Q is the solution volumetric flow (m^3/s).

The numbers of shifts were calculated from the time step and the total simulation time as;

$$\text{Shifts} = \frac{t}{(\Delta t)_A}$$

Where t is the total simulation time.

$$\text{Pore volumes} = \frac{\text{shifts}}{\text{number of cells}}$$